Synthesis of Functional Microporous Polymers for Catalytic and Electronic Applications

vorgelegt von

M.Sc. Hakan Bildirir

aus Istanbul, Türkei

von der Fakultät II – Mathematik und Naturwissenschaften

der Technischen Universität Berlin

zur Erlangung des akademischen Grades

Doktor der Naturwissenschaften

- Dr. rer. nat. -

genehmigte Dissertation

Promotionsausschuss:

Vorsizender: Prof. Dr. Regine von Klitzing

Gutachter: Prof. Dr. Arne Thomas

Gutachter: Prof. Dr. Ullrich Scherf

Tag der wissenschaftlichen Aussprache: 13.05.2015

Berlin 2015

D83

The work presented herein was carried out in the research group of Prof. Dr. Arne Thomas (functional materials group) at the department of chemistry at Technical University of Berlin, Germany, in the time between June 2011 and March 2015.

Acknowledgements

I would like to express my gratitude to the people who have been really helpful to overcome difficulties during preparation of this PhD thesis;

I would like to thank;

to Prof. Dr. Arne Thomas for giving me the opportunity to work in his group and his support,

to Prof. Dr. Ullrich Scherf and Prof. Dr. Regine von Klitzig for sparing their precious time to evaluate this thesis,

to Dr. Jerome Roeser and Dr. Robin J. White for not only their scientific support, but also being a mentor during the time I spent in Berlin,

to Dr. Kamalakannan Kailasam and Dr. Johannes Schmidt for their introduction of this new field when I started in Thomas Group,

also to all (former)members of the Thomas group; Christina Eichenauer, Daniel Becker, Dr. Elham Bektash, Dr. Jens P. Paraknowitsch, Dr. Kerstin Thiel, Maria Unterweger, Matthias Trunk, Dr. Michael J. Bojdys, Miriam Klapproth, Dr. Phisan Katekomol, Dr. Robert Dawson, Dr. Sabrina Fischer, Sophie Kücken, Dr. Xiao Xie, Daniel Hagemeyer, Miriam Klapproth, Ha Vu Le, Amitava Acharjya, Dr. Ali Yassin, Nicolas Chaoui and especially to our secretary, Anne Sobotta for her patience and help with all bureaucratic paper works.

additionally, to my friends Dr. Bahadir Gacal, Hakan Kaygusuz, Serdar Okcu, Zuleyha Yenice, Dr. Alev Tuzun, Dr. Ipek Osken, Dr. Tim Fellinger, Dr. Anett Döring, Claudia Voigt, Dorothee Marecki for their moral support…

finally, to my family, for everything that I have…

ABSTRACT

Porous materials have been a topic of interest in materials chemistry because of their high potential for various applications such as heterogeneous catalysis and gas storage. Beside the common porous materials, such as zeolites or activated carbons, some novel "soft" porous materials, namely organic microporous polymers, have been a focus of recent research, as the covalently bonded organic backbone enables high chemical and thermal stability with wide range specific functionalities while such properties are difficult to combine in inorganic or organic-inorganic hybrid systems. Thus, the introduction of suitable functionality into the porous backbone with high surface area is considered as one of the main targets in the field of porous polymers with the aim to develop properties for specific applications.

In this context, organic porous networks based on electron rich building-blocks can extend the applicability of such materials to organic electronics or light driven catalytic systems. The present work focuses on the synthesis of novel porous polymers based on sulphur containing, π-conjugated functional monomers and is divided into two main topics according to the targeted applications:

1. Synthesis of functional polymer networks for organic electronic applications;

   In this work, investigations related to the introduction of strong electron donors such as tetrathiafulvalene (TTF) and dithienothiophene (DTT) into conjugated microporous polymer (CMP) backbone will be presented. The subsequent formation of corresponding charge-transfer salts after iodine exposure of these electron rich moieties will be discussed. Furthermore, electrochemical polymerisation of DTT monomer will be examined for comparison of the (opto)electronic behaviours in bulk and film in addition to investigations related to the chemical and electrochemical redox properties of those DTT based CMPs.

   Along with the preparation of novel electron donor systems, this section will also contain discussions related to the mechanism of network formation for Sonogashira-Hagihara cross-coupling derived CMPs considering the influence of regarding reaction media and monomer ratios for.

2. Synthesis of functional polymer networks for light driven heterogeneous catalysis;

In this part the incorporation of a frequently used photoinitiator compound for photopolymerisation process, namely thioxanthone, into different microporous polymer backbones *via* two different polycondensation reactions will be presented. Applications on heterogeneous sustainable initiation of photopolymerisations of methyl methacrylate and cyclohexene oxide either under artificial light source or sunlight will be introduced.

ZUSAMMENFASSUNG

Poröse Materialien zeichnen sich durch ihre vielfältigen Anwendungsmöglichkeiten in Bereichen wie der heterogenen Katalyse oder der Gastrennung und –Speicherung aus. Neben den anorganischen Materialien wie Zeolithen und porösen Kohlenstoffen rücken auch immer mehr organische Materialien, wie z.B. mikroporöse Polymere, in den Fokus der Forschung. Diese Netzwerke bestehen aus kovalent verbundenen, organischen Bausteinen. Daher lassen sich durch die Variation der Bausteine Netzwerke unterschiedlichster Funktionalitäten synthetisieren und so Materialien mit hoher chemischer und thermischer Stabilität erhalten. Diese Variabilität ist mit rein anorganischen oder Hybridmaterialien schwer zu erreichen. Daher ist die Entwicklung von Materialien für spezifische Anwendungen durch gezieltes Einbringen von funktionellen Gruppen eines der Hauptziele in der Synthese von porösen Materialien.

Durch den Einsatz von elektronenreichen, organischen Molekülen in der Synthese von porösen Netzwerken können diese für Anwendungen im Bereich der organischen Elektronik oder Photokatalyse genutzt werden. Die vorliegende Arbeit beschreibt die Synthese von neuartigen, porösen Polymeren basierend auf schwefelhaltigen, π-konjugierten Monomeren und ist thematisch in zwei Teile bezüglich deren Anwendungsmöglichkeiten unterteilt:

1. Synthese von funktionalisierten Polymernetzwerken für die organische Elektronik;

   In diesem Teil werden Untersuchungen zum Einbau von starken Elektronendonatoren wie Tetrathiafulvalene (TTF) und Dithienothiophene (DTT) in konjugierte mikroporöse Polymere (CMP) vorgestellt. Die sich ausbildenden Charge-Transfer Verbindungen, welche durch die Exposition von Iod entstehen, werden genauer untersucht und beschrieben. Zusätzlich wird die elektrochemische Polymerisation von DTT untersucht und Vergleiche zum chemisch hergestellten Material im Bezug auf chemisch und elektrochemische Redoxeigenschaften sowie deren (opto)elektronischen Eigenschaften untersucht.

   Neben der Synthese der neuartigen Elektronendonatoren wird auch der Reaktionsmechanismus, welcher dem Aufbau dieser Netzwerke durch Sonogashira-Hagihara Kreuzkupplung zugrunde liegt untersucht wobei das Hauptaugenmerk auf dem Verhältnis der Monomere sowie dem Einfluss des Reaktionsmediums liegt.

2. Synthese von funktionalisierten Polymernetzwerken für die Photokatalyse;

   In diesem Teil der Arbeit wird der Einbau eines häufig verwendeten Photoninitiators für die Photopolymerisation, Thioxanthone, in mikroporöse Polymere durch zwei verschiedene Polykondensationen vorgestellt. Diese Netzwerke werden als Photoinitiatoren in der heterogenen Initiierung der Polymerisation von Methylmetacrylat und Cyclohexenoxid, sowohl unter künstlichem als auch Tageslicht genutzt.

TABLE OF CONTENT

A. INTRODUCTION

A.1. POROUS MATERIALS

Since the discovery of the beneficial size selective porosity of Zeolites research has focused on the development of further functionality, textural porosity, morphology as a general theme, the chemistry of porous materials have been aimed to ultimately produce increasingly efficient heterogeneous catalysts.[1-3] Other major usage areas for porous materials are sensing, gas separation and storage.[4-6] Energy and electronic device applications can be highlighted as increasingly topical and developing areas as a consequence of advanced research on organic-based structures.[7-10] Additionally, applications in drug delivery have also been studied.[11]

The classification of porous materials is typically performed based on pore sizes or building blocks. Regarding porous features, materials can be classed into three groups, namely macro-, meso- and microporous, reflective of three different pore size regimes (Figure A.1.1).

	Macroporous Materials	Mesoporous Materials	Microporous Materials
Pore size	> 50 nm	2-50 nm	< 2 nm
Surface area	<10 m²/g	100-1000 m²/g	> 1000 m²/g
	(Polymer) foams, Membranes, Aerogels, Photonic crystals....	Mesoporous silicas (MCM, SBA...), metal oxides, mesoporous carbon (CMK)	Zeolites, activated carbon, MOFs

Figure A.1.1: Classification of porous materials depending on the pore size.

Secondly, porous materials are categorised as inorganic, organic-inorganic hybrid, and fully organic depending on their constituent building blocks.[12]

Inorganic porous materials are mainly based on metal oxides and carbons. For the metal oxides, the first important family is the Zeolites as a consequence of their high internal surface area and various industrial applications; e.g. water softeners, highly size selective heterogeneous catalysts in petro-refineries, *etc.*.[1, 13] Furthermore, it is always hard to tune and add functionalities to inorganic porous materials without using harsh conditions (acid leaching, high temperature (800°C<) steaming etc.).[12, 14, 15] Besides Zeolites, other examples in this class (mesoporous metal oxides) that have been applied in artificial photo- or electro- catalytic oxygen evolution from water.[16, 17]

Additionally, carbon-based structures are as also classified as inorganic porous materials. Whilst classical microporous or activated carbons have been employed as water purification media and as catalysts supports. Besides being an adsorbent/support, these materials are also used commonly electrochemically induced catalytic reactions and energetic applications.[7, 8]

Following interest in conventionally microporous Zeolites, researchers (e.g. at Mobil Corp.)[18, 19] intended to produce mesoporous materials featuring the beneficial properties of crystalline Zeolites. Although the generation of crystalline materials were initially unsuccessful, this research led to the synthesis of a range of mesoporous inorganic materials (e.g. MCM-41, SBA-15) that are featuring ordered mesopore structuring via templating.[20-22] These materials have found a variety of applications including, perhaps the most popular, the preparation of supported catalysts (i.e. metal nanoparticles) for various reactions.[23, 24]

A similar class of materials in this field are the periodic mesoporous organosilanes (PMOs) which are the organic structures are not only the templates but further functionalities.[25] Condensation of precursors such as $(EtO)_3Si\text{-}R\text{-}Si(OEt)_3$ with the free hydroxyl groups over the pores ($\sim XO_n\text{-}Si\text{-}OH_{(4-n)}$, where X is the rest of the structure) in presence of templating surfactants, results the desired organic-inorganic hybrid structure.[25, 26] The organic functionalizations are mainly targeted to enhance the properties for the applications of the mesoporous silicas such as in organic electronics and drug delivery besides the commonly used fields such as gas sorption and catalysis.[11, 26-28]

With the aim of introducing useful and applicable functionality to the structures of classical metal or siliceous-based inorganic porous materials, researchers have investigated the synthesis of metal containing networks featuring functional organic components.[12, 14] At the time of writing, metal-organic frameworks (MOFs) are dominating this area with their exceptionally high surface areas (up to 7140 m^2g^{-1} Figure A.1.2) and "easy to build" functionalities with various organic counterparts.[29, 30] MOFs are formed from the reaction of multidentate ligands and metal salts; thus, these materials are also called as coordination polymers.[31] The term MOF first appeared in 1995 after a publication describing the coordination of benzene-1,3,5-tricarboxylic acid (also known as trimesic acid - TMA) with a cobalt salt in presence of pyridine (Py) by Yaghi *et al*., and in 1999 HKUST-1 was published by Chui *et al*., which was formed from the reaction of TMA with a copper (II) nitrate trihydrate.[32, 33] HKUST-1 become one of the mostly used MOF with the original paper[33] receiving 2458 citations (Web of Science 11.12.2014). Demonstrating the success of this one single material system, a review related solely to the gas sorption properties of HKUST-1 has been published.[34]

MOF-5 is the other important member of the family that was built out of 1,4-benzenedicarboxylate (BDC) and Zn^{2+} (proposed total formula=$Zn_4O(BDC)_3{\cdot}(DMF)_8(C_6H_5Cl)$) which have been used widely (original paper cited 3007 times, Web of Science 11.12.2014).[35-37] MOFs are used in various areas

from organic electronics to drug delivery, but their predominant use lies as sorbents in sorption/separation applications.[31, 37-39]

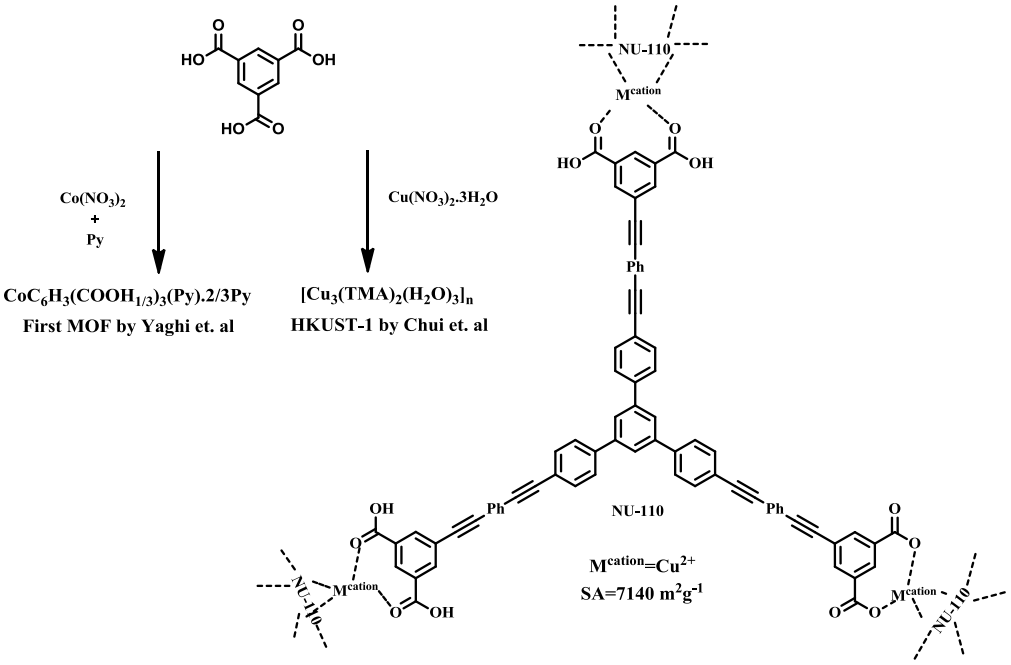

Figure A.1.2: Structures and formulas of the MOFs named above.[29, 32, 33]

The last group of the porous materials based on a building block categorisation are the Porous Organic Polymers (POPs), which are composed solely of organic components as the name suggests.[12] To produce such materials, it is necessary to have non-flexible monomers with angles, which can be termed as structure directing motives, tectons or crosslinkers, within the structure that forms permanent porosity (Figure A.1.3). If it is desired to use linear monomers to form porous organic polymers, a co-polymer of the original monomer with a suitable crosslinker is a reasonable synthetic pathway to achieve this aim.

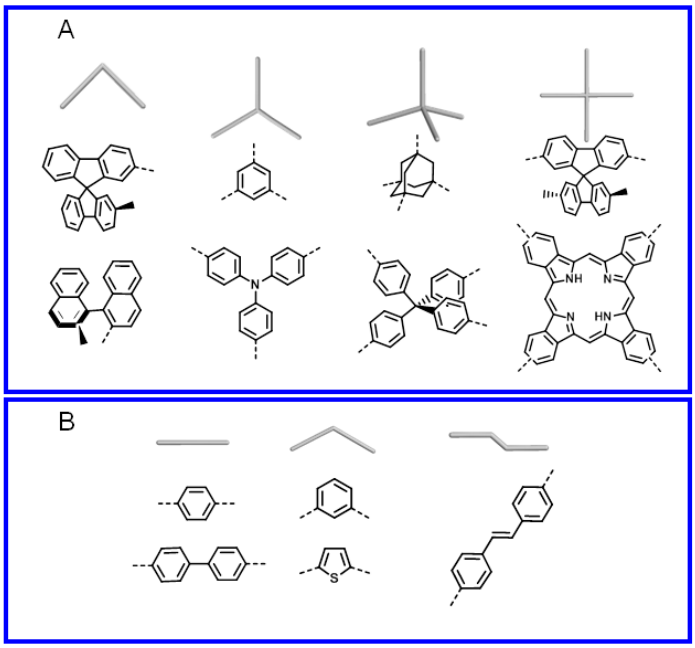

Figure A.1.3: Selected structure directing motives used in syntheses of POPs.

The sub-divisions of the parent POP class are determined by structure, crosslinker, and the bonding nature of the monomers within the polymers.[40] Several sub-classes of POPs have been identified including hypercrosslinked polymers (HCPs),[41, 42] polymers of intrinsic microporosity (PIMs),[43, 44] covalent organic frameworks (COFs),[45, 46] covalent triazine frameworks (CTFs),[47, 48] and conjugated microporous polymers (CMPs).[49, 50] These porous polymers can be obtained via wide range of reaction types from variety of simple metal-free reactions to complicated carbon-carbon crosscouplings.[40, 51, 52]

Hypercrosslinked polymers can be ascribed as the first member of POPs that was published in early 1970 which applications were mostly focused on gel properties (i.e. swelling in different solvents).[53] The idea was introducing further crosslinking to linear polymers such as polystyrene to obtain a new type of polymer network.[53-55] These polymers mostly carry secondary sp^3 carbons on their skeletons, whereas other common porous polymers are based sp^2/sp hybridised 3° or 4° carbons which keep the porosity permanent as a consequence of rigidity.[41, 56] As it can be understood from the sub-class name, hypercrosslinking induces permanent porosity.[57] For example, if the crosslinker is benzene, six carbons of the ring can be connected with other monomer that makes rotation around sp^3 carbons nearly impossible (Figure A.1.4).[58] Nevertheless, the porous properties of such materials are more dependent on the synthesis media (i.e. swelling in a solvent, ambient conditions, or under high pressure) than with respect to sp^2/sp hybridised rigid porous polymers.[59-61]

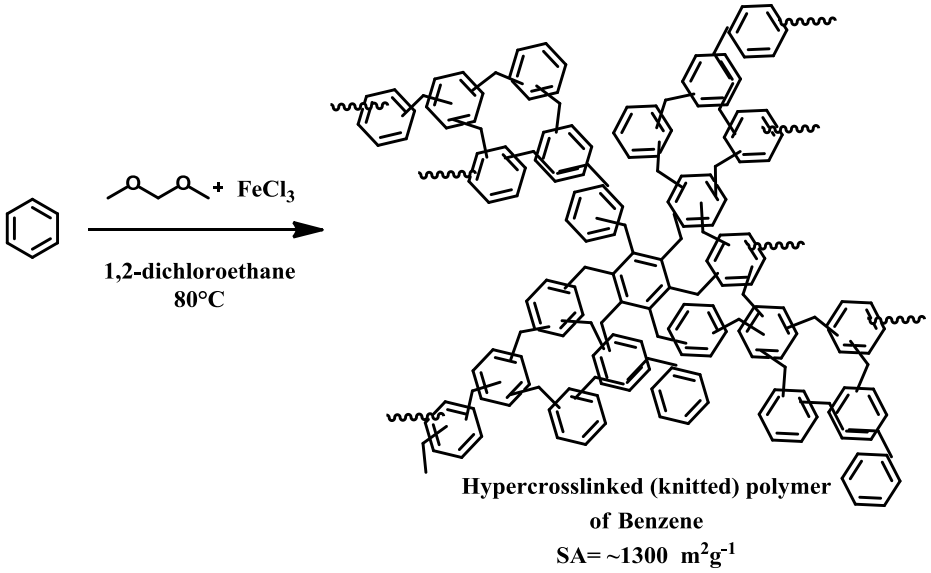

Figure A.1.4: Homo-hypercrosslinked polymer of benzene via Friedel-Crafts acylation.[58]

PIMs are mostly formed via basic substitution reactions between alkoxides and halogenes where one of the monomers should be angled to provide the intrinsic permanent porosity (note that PIMs are typically constructed from spiro compounds that also carry sp^3 carbons with the bicyclic nature of these quaternary carbons inducing backbone rigidity, Figure A.1.5).[43, 44, 62]

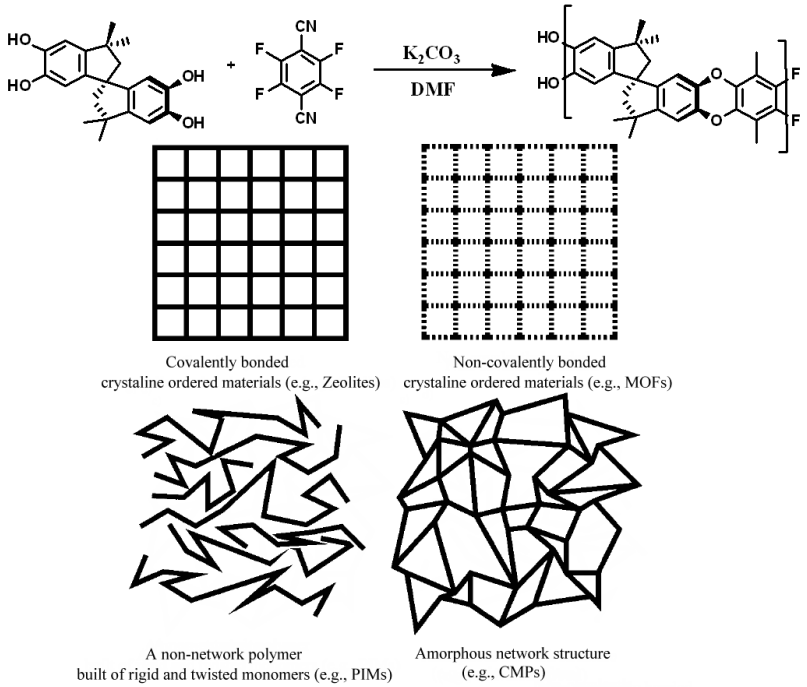

Figure A.1.5: Synthetic scheme of PIM-1.[62] Below illustration[44] explains how the pores are formed in different morphologies and geometries.

Besides non-soluble network PIMs, this POP member is known as the only example of the porous polymeric materials (molecular compounds like porous cages[63, 64] and hydrogen bonded porous

structures[65] will not be discussed) that can be soluble.[43, 44, 66, 67] The solvated polymers in conventional solvents like THF or DMF can be precipitated in an anti-solvent like chloroform or methanol to obtain a permanent porous solid.[43, 44]

Another group of material in POPs are COFs which are conventionally formed via a condensation reaction of an organo-boronic acid and alcohol or imine bonding of a carbonyl group (typically aldehyde) and a primary amine (Figure A.1.6).[45, 68]

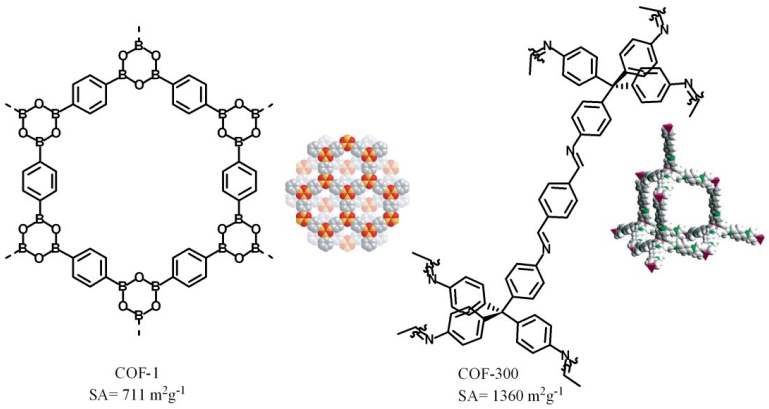

Figure A.1.6: Examples for boronic acid (condensation of benzene-1,4-diboronic acid and hexahydroxytriphenylene) and imine (condensation of tetra-(4-anilyl)methane and terephthaldehyde) COFs.[45, 68]

CTFs (covalent triazine frameworks) have a similar design with COFs but boron and oxygen species were replaced with carbon and nitrogen, respectively (Figure A.1.7).[47] The remarkable benefit of CTFs with respect to COFs is their stability due to strong covalent bonding instead of comparatively unstable boronic esters (Imine-based COFs are relatively more stable than boron-based systems but still have low stability to ambient conditions[69] for further applications).

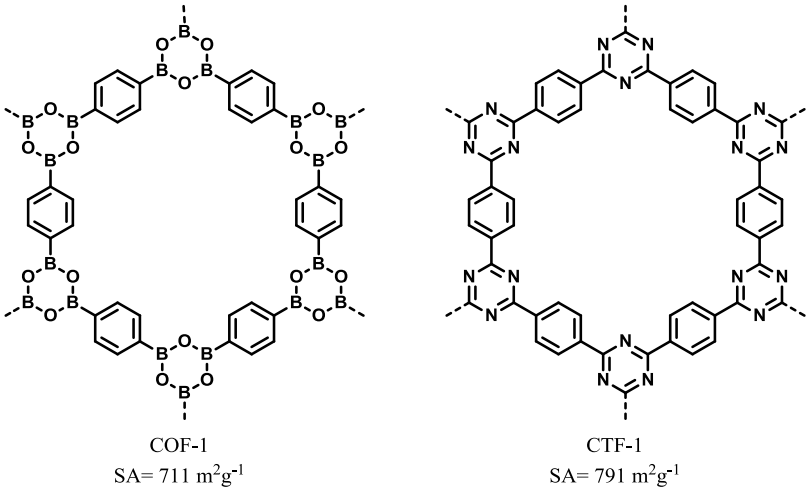

Figure A.1.7: Model structures for COF-1 and CTF-1.[45, 47]

Porous aromatic frameworks (PAFs) are a class of porous polymers which lies between hypercrosslinked polymers and conjugated microporous polymers (CMPs). PAFs arise due to limiting

conjugation through the backbone, typically broken by the introduction of an sp^3 carbon in the crosslinker (e.g. tetraphenyl methane).[70, 71] The highest surface area thus far reported is for PAF-1 (Figure A.1.8), a homopolymer of tetrakis(4-bromophenyl)methane synthesised via Yamamoto Coupling (SA ~ 5600 m^2g^{-1}).[70]

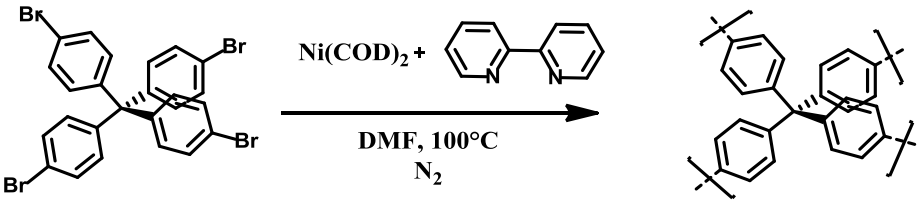

Figure A.1.8: Reaction scheme for PAF-1 (COD = cyclooctadiene).[70]

CMPs, as first published by the Cooper et al. and have found successful application in a variety of fields.[49, 61, 72-79] CMPs feature conjugation throughout the network generating an electron rich, rigid backbone as a consequence.[12] The first CMP was produced from Sonogashira-Hagihara reaction)[49] and in following years most of the typically C-C bond formation reactions such as Suzuki Coupling, Yamamoto Coupling, oxidative polymerization, etc. (Figure A.1.9).[50, 80, 81]

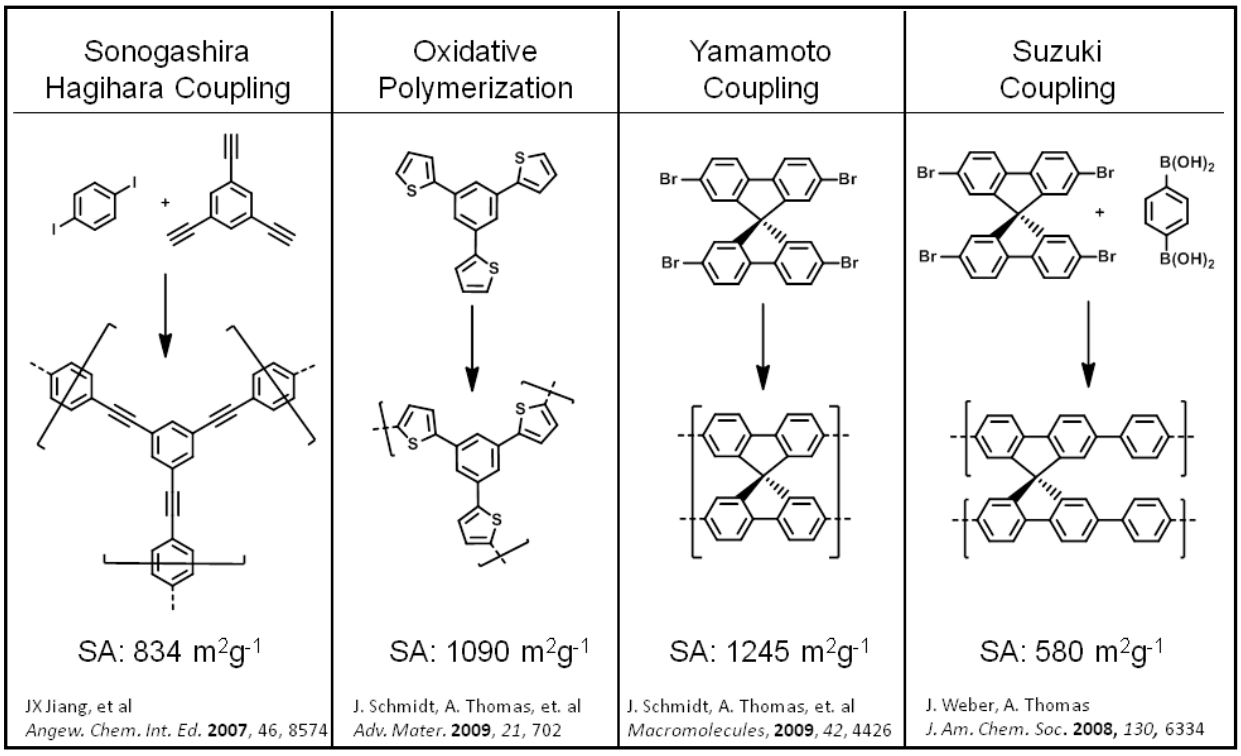

Figure A.1.9: Varios methods to build CMPs (note that 3rd and 4th example has spirofluorenes as tectons which have sp^3 carbons. Unlike PAFs, conjugation is not broken over the chains; electron flow can go through the phenyl rings).

A.2. APPLICATIONS OF POROUS ORGANIC POLYMERS

A.2.1. Heterogeneous Catalysis

Heterogeneous catalysis is one of the main application field of POPs due to their insoluble nature in common organic solvents and water and accessibility of the pore structure / active sites by target compounds in such conditions.[2, 82] The biggest advantage of this non-solubility is reusability which in most cases allows separation of the POP catalyst via simple filtration (see Figure A.2.1 for the selected examples).[2, 82]

One of the most important issues in today's world is the search for sustainable alternative sources to conventional fossil fuels. Producing hydrogen from water is one of the opportunities considered to achieve this purpose. In this context, CTF and its analogues have been investigated and demonstrated to be capable of proudcing hydrogen from water.[83, 84] CTFs have been used also to remove the effects of fossil fuels from the environment and convert such pollutants into useful compounds for the chemical industry. As an example, the green house gas, CO_2, was converted to cyclic carbonates under high pressure in autoclave in the presence of CTF-1 and epoxide derivative.[85]

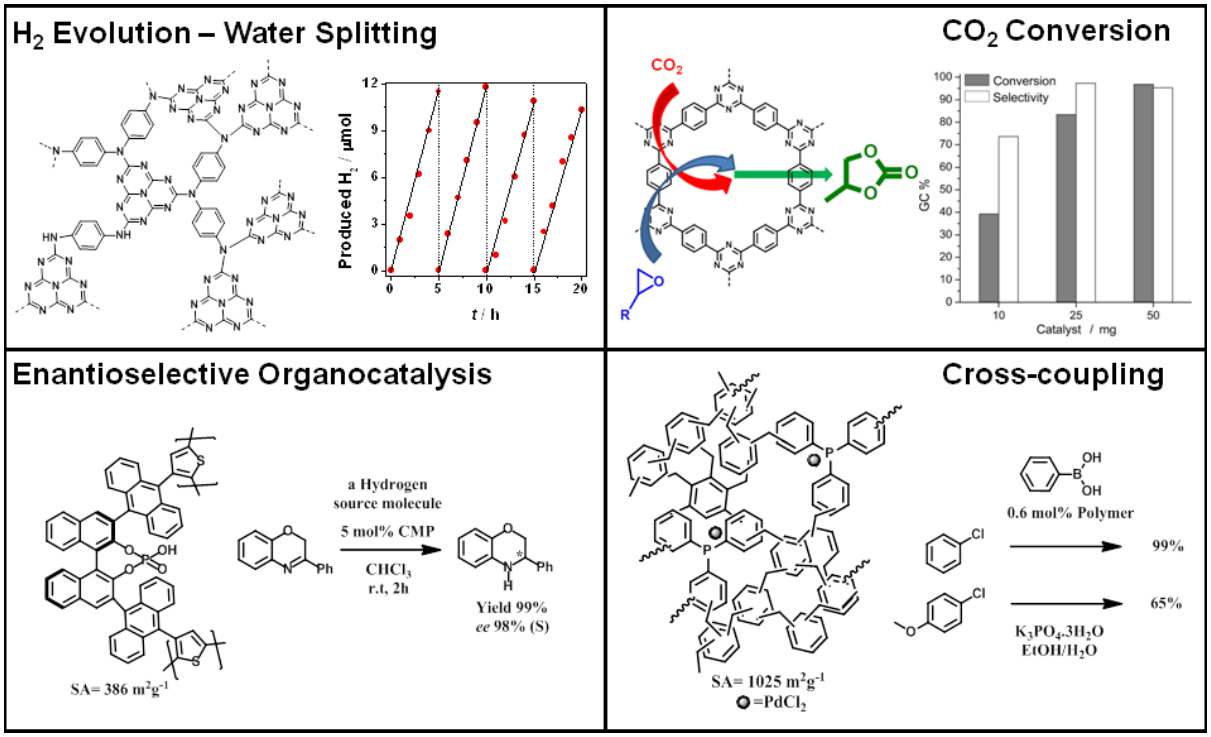

Figure A.2.1: Materials that were mentioned in the Heterogenous Catalyse section section (see references[84-87], graph for CO_2 conversion was taken from ref[85] and modified).

Another important example relates to the use of POPs in enantioselective synthesis. This has recently been demonstrated using a POPs based on binol units which are commonly used catalyst for asymmetric syntheses in molecular form.[86, 88] For instance, in literature,[86] asymmetric hydrogenation

of 3-phenyl-2H-1,4-benzoxazine was performed via a binol-based POP and 99% conversion in 98% enantiomeric excess was achieved.

The last example in this sub-section is related to catalyzing carbon-carbon cross-coupling reactions. It has been shown that the stabilisation / immobilisation of Pd nanoparticles within a knitted triphenylphosphine network worked as well as molecular standards and gave good conversions (between 65-99%) in a classical coupling reaction (e.g. phenyl-boronic acid and chlorobenzene).[87]

A.2.2. Gas Storage and Separation

The other main area of interest for POP materials is in the field of gas storage and separation.[40, 89] With these applications in mind, the polymer backbone can be tailored depending on which gas is desired to be stored and/or separated.[6, 90] A good example from literature would be post-synthetically sulfonation of PAF-1 (or PPN-6) and monitoring the increased uptake/selectivity for CO_2 (Figure A.2.2).[91] Pristine PPN-6 has a CO_2 uptake of 5.1 wt % at 295 K and 1 bar (~1.4 mmol g^{-1}), whereas sulfonated PPN-6 13.1% and PPN-6-SO_3Li 13.5 wt % (equivalent to 3.6 and 3.7 mmol g^{-1}, respectively).[91]

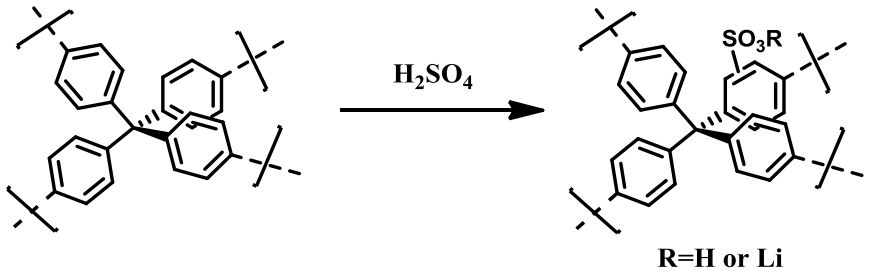

Figure A.2.2: Postsynthetic modification of PAF-1 (or PPN-6) network to tune gas seperation selectivity and increasing CO_2 uptake.[91]

To give an interesting and topical example regarding separation, a CO_2/N_2 gas mixture can be selectively separated via an increase in aniline co-monomer content in the knitting co-polymerisation with benzene (Figure A.2.3).[58] Increasing the amine content via increasing the ratio of aniline resulted in a change in the CO_2**:**N_2 selectivity from 15.9**:**1 to 49.2**:**1.

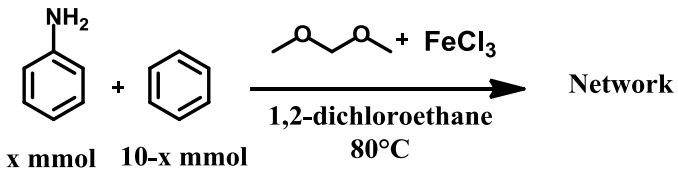

Figure A.2.3: General reaction equation for aniline and benzene knitted co-polymer for comparison of side groups in gas selectivity.[58]

A.2.3. Sensing

Since POP materials are commonly electron rich, they can be used for sensing applications.[73, 75, 92-94] For this purpose, a luminescence change is often monitored depending on the target product to be sensed. For example, the introduction of electron accepting nitrobenzene and relatively electron donating toluene to the pore structure of a carbozole-based CMP resulted a luminescence quenching or enhancement respectively (Figure A.2.4).[73] Sensing of these small molecules takes place within the pores which does not significantly occur in linear analogues of the investigated polymer (i.e. a non-porous variant).[73]

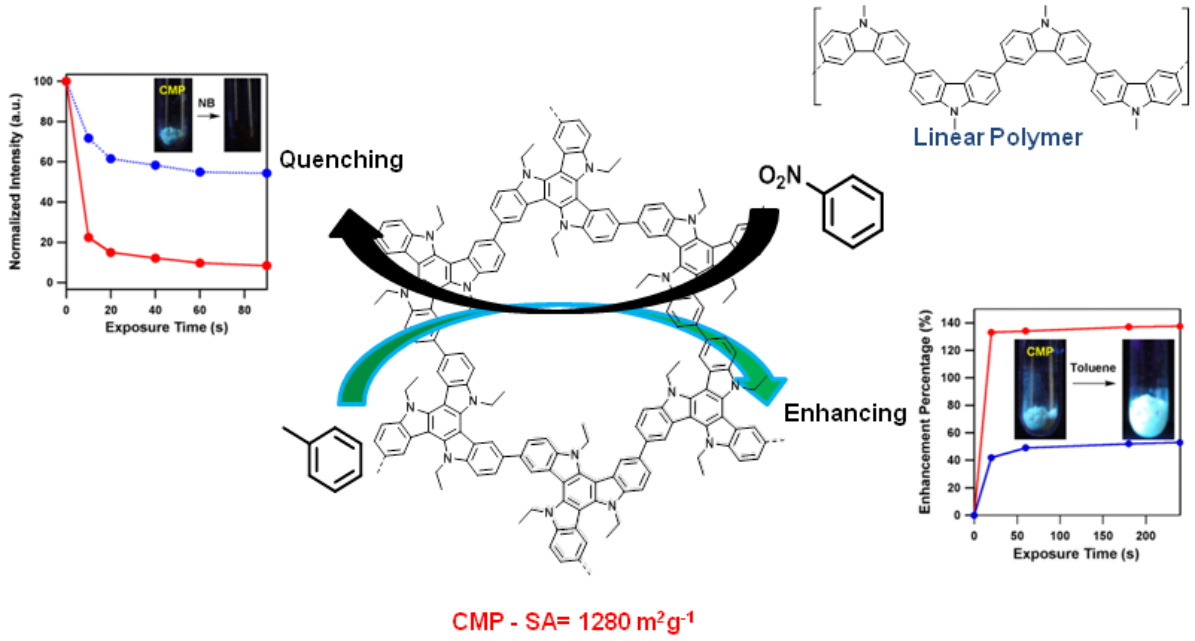

Figure A.2.4: Carbazole based CMP in luminescene on/off switching (blue lines on the graphs belong to linear polymer and red lines to CMP, NB=nitrobenzene, graphs were taken from ref[73]).

A.2.4. Organic Electronics

Electron rich materials (e.g. carbazole, tetrathiafulvalene and thiophene) are commonly used in the production of organic electronic devices including solar cells (or photovoltaic devices-PVs), organic field effect transistors (OFETs) and organic light emitting diodes (OLEDs).[95, 96] Enhanced electron density and conjugation within the structure particularly important for solar cells as a result of the good absorption properties, which perfectly fits the working principle for the solar cells which collect light to produce electricity.[97] Particularly, polymers prepared out of heteroatom rich materials are applied to bulk-heterojuction type solar cells as the donor component, and their charge transfer complexes with electron poor moieties (i.e. fullerenes) provides suitable electronic band gaps to absorb light in order to move electrons through the holes, and desired electrical potential is produced via this movement between two electrodes. The comparison parameter for solar cells is termed *power*

conversion efficiency (PCE), derived from the current when there is 0 potential through the device (*short-circuit current* – I_{SC}) and the potential when there is no current through the device (*open-circuit voltage* – V_{OC}).[98]

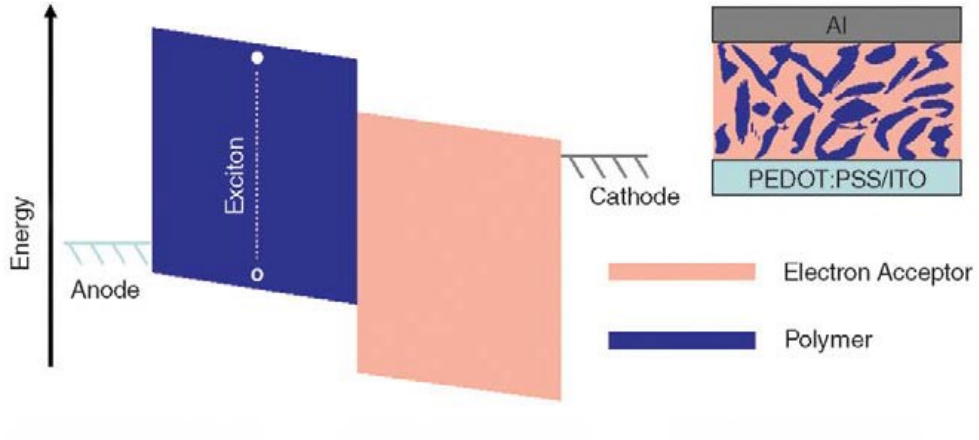

Figure A.2.5: Illustration of electron transfers in bulk-heterojunction solar cells (picture taken from ref[97]).

Besides solar cells, usage area in OFETs is breakthrough as well, due to the electron rich and well-packing nature of such sulphur rich materials.[99] OFETs can be described simply like the transistors that are built out of organic semiconductor which is more flexible with respect to inorganic based transistors.[99] The general comparison parameter for different OFET devices is the hole (μ_h) or electron (μ_e) carrier mobility that are the values for *p*-channel or *n*-channel devices, respectively, whereas some materials can have ambipolar behaviour.[100] In a related manner, studies on OLEDs in electronics are also challenging especially for growing industrial interest on lighter/flexible plastic displays which are produced of OFETs as transistors instead of silicon.[99] Suitable materials for this application must have good electroluminescence properties at suitable potentials and quantum efficiencies (e.g. oxidized thiophene derivatives).[101] The intriguing issues with OLEDs are brightness and the colour of the emitted light (i.e. white).[102]

In recent perspective articles, changing dimensionality from 1D to 2D is discussed widely, and benefits of improved properties listed such as enhanced π–π stacking.[103, 104] Authors of these articles also mention limited experimental results on 3D structures prevents a thorough assessment of the applicability in electronics, but calculations provide promising results including lower band gaps in infinite molecular weights.[103, 104]

As a consequence of the non-soluble nature of POPs (excluding PIMs), the construction of electronic devices from these polymer systems remains a challenge. Therefore, there are only a few examples regarding the use of POPs in organic electronics. Chronologically, a carbazole derivative of tetraphenylmethane as an interlayer (i.e. the *hole transporting material* which is aimed to balance/reduce the difference of the band gaps between electrodes and active layer) has been used in a

solar cell and a light emitting diode (Figure A.2.6).[105] In the former example, a CMP film was prepared via electrochemical polymerisation and several modifications (e.g. doping with ClO_4^- to improve hole transport), resulting in the solar cell having an efficiency (photo conversion efficiency = PCE) of 7.56% compared to the efficiency of the same device without the CMP interlayer of 5.68%.[105] However, devices with undoped films gave poorer performances than without CMP interlayer.[105] Furthermore, the use of the a CMP in light emitting diodes also led to better efficiencies and improved light brightness than the same device prepared without the use of the polymer.[105]

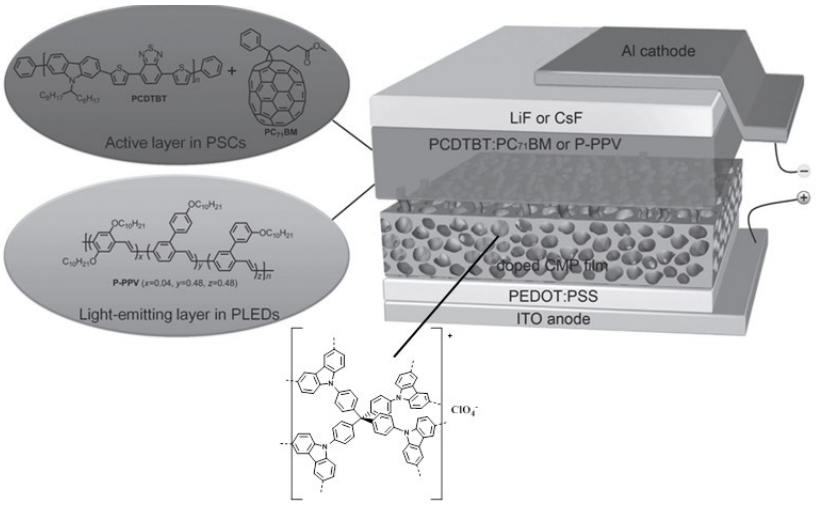

Figure A.2.6: Illustration of OLED and solar cell device structures which are prepared out of carbazole based POPs as hole transporting layer (Figure A.2.s were taken from[105]).

Another published example of the use of POPs in solar cells was based on the use of a thienothiophene-based COF (Figure A.2.7) leading to a poor PCE (0.053%).[106] Nevertheless, the importance of this work relates to the first porous organic material as an active layer in photovoltaic applications.

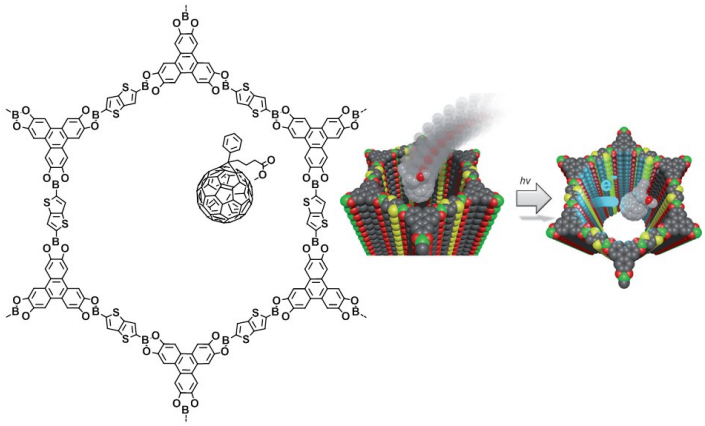

Figure A.2.7: Thienothiophene-COF based photovoltaic device (Figure A.2.s were taken from ref[106]).

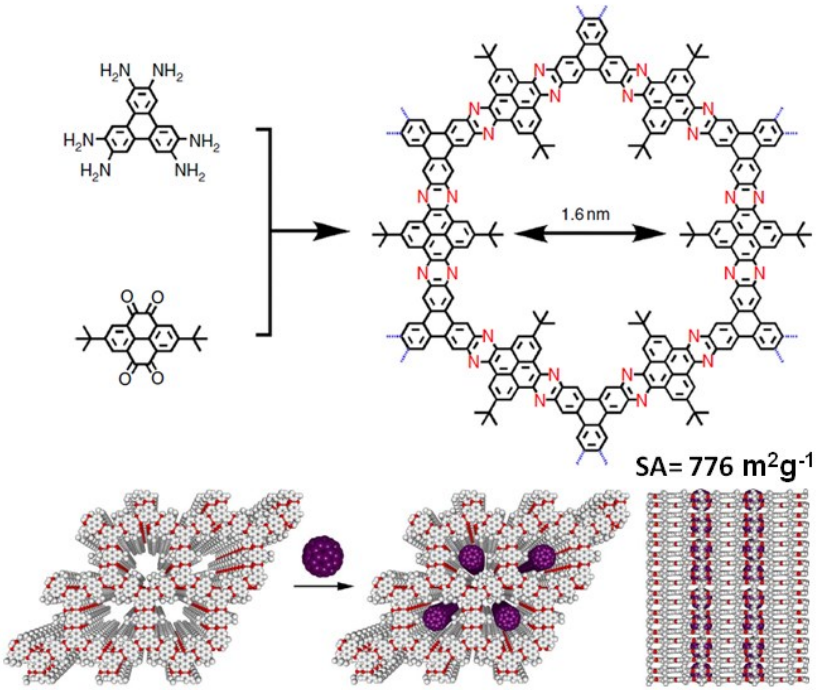

Figure A.2.8: Imine COF that was used for conductivity measurement and solar cell device. After infiltration of C_{60} (purple structure) through pores, surface area drops from 776 m^2g^{-1} to 291 m^2g^{-1} (Figures were taken from ref[10]).

One of the most recent examples of POP use in organoelectronic devices is this elegant work reported by Guo *et al*. Here the authors reported the use of an imine-based COF in the measurement of conductivity and the construction of a solar cell (Figure A.2.8).[10] The conductivity measurement was found to be 4.2 $cm^2V^{-1}S^{-1}$ which is comparable with state-of-the-art semiconductors (note that different methods to measure conductivity may give different results, 4.2 $cm^2V^{-1}S^{-1}$ was recorded via *time-of-flight* method but *flash photolysis time-resolved microwave conductivity* method gave 0.5 $cm^2V^{-1}S^{-1}$ for the same polymer. For further information on conductivity measuring techniques, see Ref. [107]).[10] The solar cell built from the described COF gave 0.9% power conversion efficiency (PCE) which is considered a reasonable performance.[10]

The most recent and interesting example in this field relates to CTFs that was claimed to have the closest structure as predicted for graphitic carbon nitride (g-C_3N_4) so far.[108] The application of the material to microchip technology showed comparable properties with respect to silicon.[108]

A.3. OUTLOOK AND MOTIVATION

As the outlook of this chapter, porous materials have been briefly classified with a specific focus on organic-based polymeric systems and some of their important applications have been addressed. Organic-based porous materials were discussed in terms of the wide scope of functionalisation and feasible applicability to recent needs. As the most important thing related to porous materials was pointed as the accessible surface area which is important in heterogeneous catalysis and gas storage/separation (in general). Additionally, how to improve these capabilities via functionalisation/co-polymerisation was highlighted. Finally, growing interest on electronic device production has been discussed and concluded as electron rich 2D/3D nature of such porous organic materials have shown promising results even in micro-chip technology as probably the most challenging area of electronics.

From this point of view, the synthesis of conjugated porous polymers with electron rich heteroatom containing counterparts is the primary aim of this doctoral research. Thus in this thesis, examples of microporous polymers built on tetrathiafulvalene, dithienothiophene, and thioxanthone backbones will be described. Depending on the published studies (in the following chapter, there will be short introduction to these organic compounds related to their synthetic procedures and applications in molecular or linear polymer cases), these molecules are expected to form porous materials that are promising for organic (opto)electronics. Besides organic electronics, the three described counterparts allow the production of local charges/radicals within the materials via (electro)chemical or light inducement that make their co-polymers useful in catalytic applications in the context of mimicking classical inorganic Zeolite behaviour.

B. METHODS AND MATERIALS

B.1. METHODS

B.1.1. Gas Physisorption: A Method for Surface Area Calculation

Gas sorption analysis can be employed to enable the specific surface area and indeed porosity of a material. This technique in its simplest description can be viewed as a controlled addition of a probe gas molecule or "adsorbate gas" (e.g. N_2, Ar, Kr) on the material regulated pressure (e.g. from vacuum to higher pressures, i.e. *relative pressure* = P/P_0) (see Figure B.1.1 for illustration of gases over the pores). Thus the amount of gas applied to the pores can be used to provide a quantitative description of the surface area, pore size, and pore volume of a material.[109] If the interaction between adsorbate and adsorbent is strong (chemical bonding), the process is called "chemisorption"; if the interactions are week (e.g. via Van der Waals interactions), the process is called "physisorption".[109]

The two most common methods to calculate the specific surface area are the Langmuir and Brunauer-Emmett-Teller (BET) equations.[110, 111] The surface areas given in recent publications are typically calculated via the BET model as conventional Langmuir theory assumes that only a monolayer of gas molecules form within the pores during sorption; an assumption that is not generally accurate.[112]

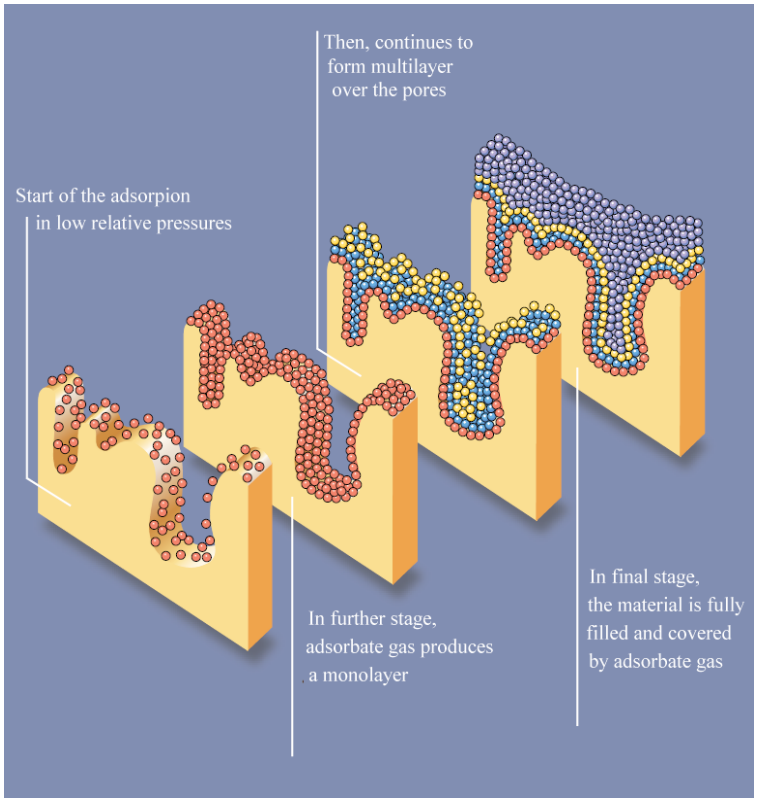

Figure B.1.1: Illustration gas sorption over the pores (the picture was taken from ref[113]).

Derivation of a linearised form of the BET equation (Equation B.1.1) is omitted here since it is out of scope of the thesis. The BET model uses the following equation to interpret the multilayer region of the adsorption isotherm, and allows for the calculation of the adsorbate monolayer capacity:

Equation B.1.1: Linearised form of the BET equation for determination of the monolayer capacity on a given adsorbent material.

$$\frac{P}{v_a\left(P_o - P\right)} = \frac{1}{v_m.C} + \frac{(C-1).P}{v_m.C.P_o}$$

where v_a is the number of moles absorbed per gram absorbent at a given pressure P; v_m is the monolayer capacity of the surface (i.e. the number of moles of gas per gram of adsorbent required to form the monolayer); P_o is the saturation pressure and C is the BET constant which is a function of the heat of adsorption. Utilising the monolayer capacity, the specific surface area (S_{BET}) in metres squared per gram can be calculated (Equation B.1.2).

Equation B.1.2: Calculation of the specific BET surface area of a given solid.

$$S_{BET} = v_m.a_m.N_A.10^{-20}$$

where N_A is Avogadro's number (6.02 x 10^{23} molecules per mol); a_m is the molecular cross-sectional area of the gas molecule (0.162 nm^2 for N_2). The calculation of the specific surface area is important, and may give an indication of the formation of a porous structure, but it is important to note that it does not provide a quantitative measure of pore size distribution or pore volume.

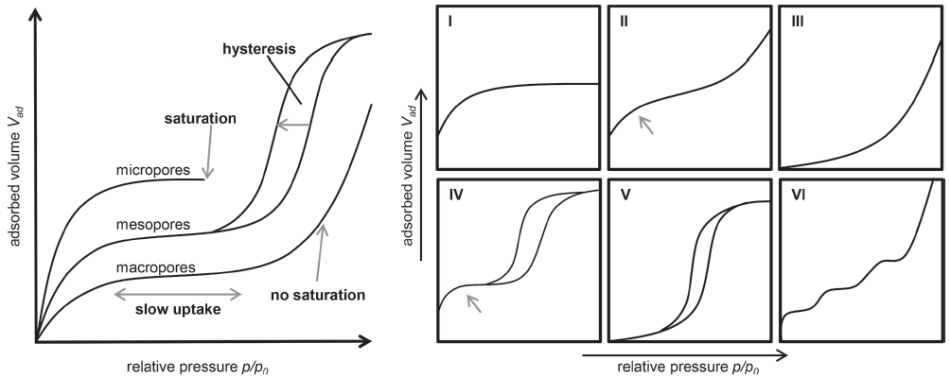

Figure B.1.2: Isotherm categorization depending on pore characters of the materials (picture was taken from ref[114]).

The isotherms constructed based on the quantity of gas adsorbed as a function of relative pressure can provide a basic insight into the corresponding pore structure of the material under investigation. The *International Union of Pure & Applied Chemistry* (IUPAC) have provided a standard classification of

physisorption isotherm profiles based on adsorption / desorption behaviour, representing five main experimentally-observed profiles, with a sixth presenting a theoretical curiosity (Figure B.1.2).[114, 115]

Uptake at low relative pressure (P/P_0) occurs in micropores (i.e. where D < 2 nm), whilst in the intermediate relative pressures, the mesoporous domains are increasingly filled, with a continuous uptake to be reflective of the presence of pores with D > 50 nm; i.e. macroporous behaviour or outer surface adsorption. Type III, V, and VI isotherms are not typically observed and result mostly non-porous materials.[115] Type I isotherms are typical of microporous materials which have a small outer surface, as can be monitored by diffusion of gas molecules through small pores at relatively low pressures. Since the outer surface is small, nearly no uptake can be observed at higher relative pressures.[115] Type II isotherms are common for non-porous and macroporous materials (which mostly exhibits small surface areas) as can be expected from the adsorption behaviour that increases linearly with relative pressure.[115] Type IV isotherms, typically associated with mesoporous materials, behave like Type I and Type II profiles. However, a difference between adsorption and desorption in a critical relative pressure range results in a hysteresis (generally between $0.2 < P/P_0 < 0.8$). This non-reversibility of the sorption process in the same relative pressures is the result of the capillarity effect of the (meso)pore shape that causes a delay in desorption of the condensed gas.[115, 116] It is important to note that this hysteresis behaviour depends not only on the material pore structure but also on the measurement conditions (e.g. adsorbent gas, temperature).[117],[118]

B.1.2. Diffuse Reflectance Spectroscopy (Solid-State UV)

Except for PIMs, it was mentioned in the previous chapter that POPs are non-soluble materials. Therefore, they have to be characterised in the solid state. In this context, since sample beam is perpendicularly sent to the material from light source in classical absorption spectroscopy, there are possibilities of diffractions/reflections from material powders. Thus classical UV measurements are not particularly suited to record the UV/Vis absorption spectra for solid powders.

A technique called *diffuse reflectance spectroscopy* was developed to overcome this problem and basically involves the mounting of a special apparatus (integrating sphere) to the instrument that makes it possible to collect reflected light from the powder. In this set-up, the sample beam is directed through the *integrating sphere* where *diffuse reflection* of non-absorbed light is collected inside (Figure B.1.3). The collected reflectance evaluated with the reference beam and absorption can be calculated to draw the spectrum.

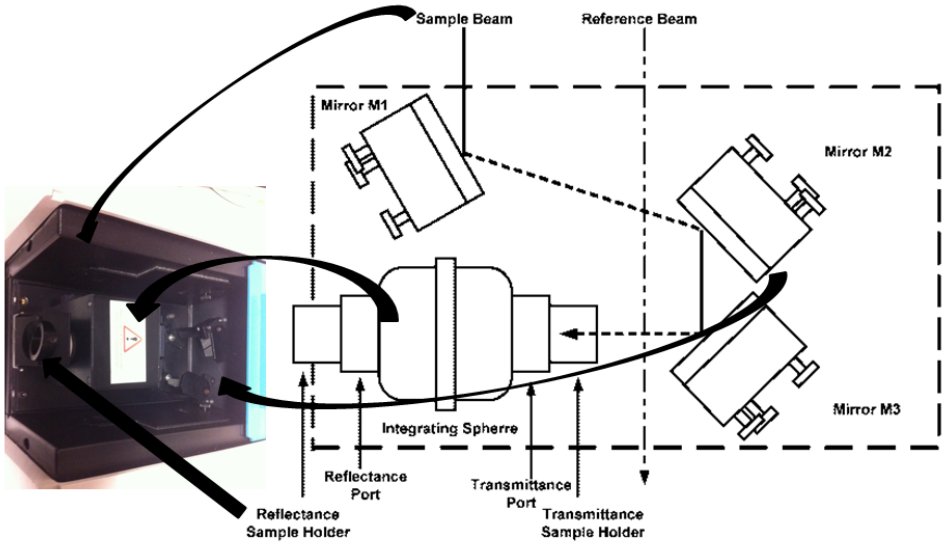

Figure B.1.3: General view of the technique for diffuse reflectance UV/Vis measurements (sketch was taken from ref[119]).

B.1.3. Cross Polarisation Magic-Angle Spinning Nuclear Magnetic Resonance Spectroscopy (CP-MAS NMR/Solid State NMR)

Nuclear magnetic resonance (NMR) is a powerful method for fundamental structural characterisation in chemistry. This method involves the application of an external magnetic field to create degenerate levels in nuclei and recording the signal of electromagnetic radiation for the transition between these artificially created energy levels. Furthermore, every individual atom has a characteristic resonance frequency depending on the environment (i.e. media, neighbouring atoms) which makes the method more useful to characterise the structural arrangements and geometry of the molecule. The conventional sample preparation method for soluble materials is the dissolution of molecules in a suitable solvent. To record a ^{1}H-NMR spectra, deuterated solvents are conventionally used, since the total resonance of this isotope of hydrogen is zero in the applied magnetic field.

When it comes to solid state (e.g. for non-soluble materials), formation of discrete degenerate levels are harder than solvated materials. The reason for the limitation is related to the restricted ability of molecular motion in the solid state which is required for efficient activation (degenerate level formation) in the applied magnetic field.[120, 121] To overcome this, *Cross-Polarization* (CP) and *Magic Angle Spinning* (MAS) methods are employed and typically combined. CP helps to improve signal quality/intensity via polarising high abundant nuclei over the material skeleton and transfer of this polarisation to the low abundant targeted nuclei. For example, detection of carbons over the structure is hard even in liquid state NMR due to the low abundance of ^{13}C nuclei (NMR active carbon isotope, 1.1%) and requires more than 1000 scans to record a spectrum in a conventional NMR instrument while ^{1}H core has high abundance (99.98%) and 16 scans are enough for a standard measurement.

Using the CP technique, it is possible to polarise hydrogens over the structure and transfer this polarisation to ^{13}C nuclei. Thus, the other common name of this method is *proton enhanced nuclear induction*.[122, 123] Besides abundance, there is another benefit of this polarisation transfer as the parameter called *spin relaxation times* (i.e. the transition time between thermally stable state and magnetically degenerated state; this parameter will not be discussed in detail) in which ^{1}H nuclei have a more suitable property with respect to ^{13}C. If it is considered *spin relaxation times* are longer in the solid state due to limited motion, transferring polarisation from easily activated ^{1}H to ^{13}C helps to work in reasonable (not very high) magnetic fields.[122] The MAS method refers to the angle between the spinning sample and applied magnetic field, used to reduce couplings (neighbouring effect) and the production of narrower signals.[121] The basic concept behind the discovery of MAS is the determination of the angle between the *interaction vector of neighbours* (considered as a line between two atoms) and *direction of the applied magnetic field* that makes the equation zero (the factor in the equation $(1-3\cos^2\theta) = 0$ where θ is the magic angle ~ 54°).[121]

B.2. MATERIALS

Key information will be given in this section regarding the functional monomers that were used in the synthesis of microporous polymers described in this thesis. Besides synthetic approaches for the presented monomers, short introductions describing their use will also be presented.

B.2.1. Tetrathiafulvalenes (TTFs)

Tetrathiafulvalene (TTF) and its derivatives are probably the best organic donor molecules in material science and have been studied intensively after the discovery of TTF's stable radical cation formation by Wudl in 1970.[124, 125] Since then, application fields of TTF derivatives varied from catalysing radical reactions to organic electronics (see Figure B.2.1).[126, 127]

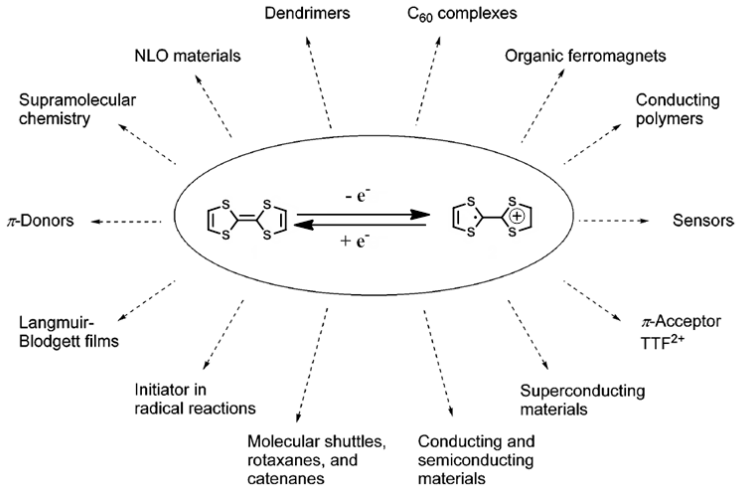

Figure B.2.1: Basic application areas of TTF derivatives (scheme was taken from ref[127]).

TTF's 14-π electron/non-aromatic nature helps it to be tuned geometrically or electronically via oxidation to its radical cation ($TTF^{\cdot+}$) or dication (TTF^{2+}), with both cationic structures having aromatic character (see Figure B.2.2).[127-129]

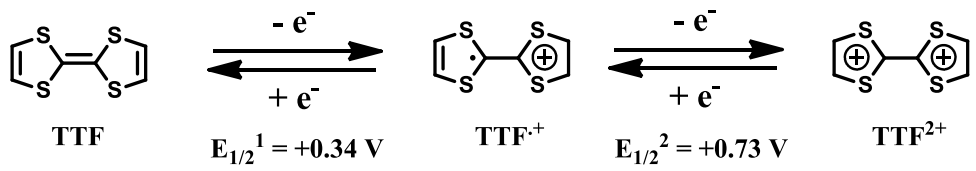

Figure B.2.2: Formation of radical cation ($TTF^{\cdot+}$) and dication (TTF^{2+}) of TTFs in cyclic voltammetry against Ag/AgCl in acetonitrile.[127]

The oxidation of TTFs may take place electrochemically or chemically. Electrochemical oxidation of TTF is typically reversible with some rare exceptions such as the formation of a stable charge-transfer complex with a side group of the TTF derivative or poor of solubility of the material that results in

precipitation of the oxidized state (see Figure B.2.3 for effect of solubility in spectroelectrochemical measurements). Chemical oxidation may also take place in presence of organic or inorganic electron acceptors which commonly results in the formation of permanent radical cationic state that is irreversible due to high stability.[124, 130]

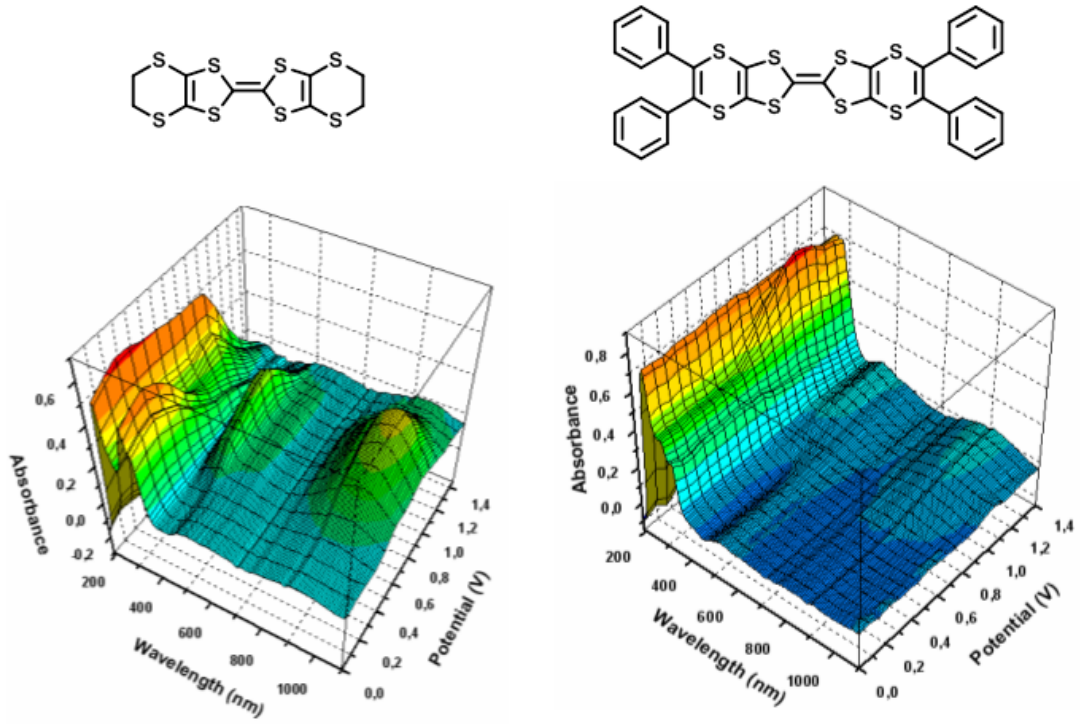

Figure B.2.3: in-situ spectro-electrochemical 3D graphics of bis(ethylenedithio) tetrathiafulvalene (BEDT-TTF / on left) and its unsaturated tetraphenyl analogue (on the right) in 0.1 M TBABF4/CH2Cl2 against Ag/AgCl reference electrode. After second oxidation, it is observed BEDT-TTF is precipitating while its analogue is still soluble due to tetraphenyl functionalization (for further information see ref[131]).

The intriguing issue for inorganic charge transfer salts of TTF derivatives is superconductivity that can be reached at relatively high temperatures (the $(BEDT\text{-}TTF)_2Cu[N(CN)_2]Cl$ salts shows superconductivity at 12.5 K).[132, 133]

Since it is challenging to produce electronic devices fully in plastics, charge transfer salts/complexes of TTF derivatives have been a great interest after the discovery of the metallic character of mixture of TTF and tetracyanoquinodimethane (TCNQ), and this remains the preferred option for many applications of donor-acceptor type semiconducting structures in organic electronics.[134-136]

There are numerous synthetic strategies employed to obtain TTFs and its derivatives. The most commonly employed approach employs the coupling of two 1,3-dithiol-2-one derivatives in presence of triethyl phosphite ($P(OEt)_3$) (Figure B.2.4).[124, 137-140]

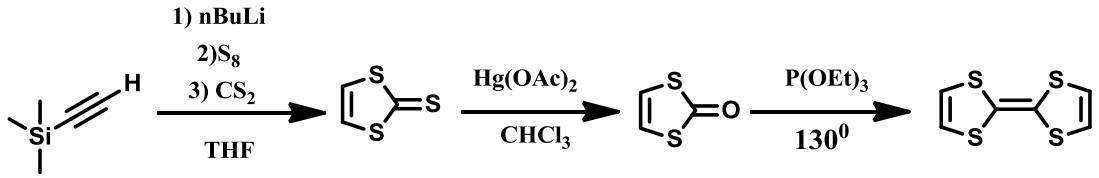

Figure B.2.4: An easy approach for synthesis of TTF.[139] First 1,3-dithiole-2-thione is formed from trimethylsilisum protected acetylene. Then, thion converted to ketone, and finally coupling can be performed.

Functionalization of TTFs can go under two ways; starting the synthesis from pre-functionalized counterparts (i.e. from functionalized 1,3-dithiol-2-one) or abstracting hydrogen from TTF's dithiole ring via a strong base (i.e. lithium diisopropylamide (LDA), see Figure B.2.5).[141-143]

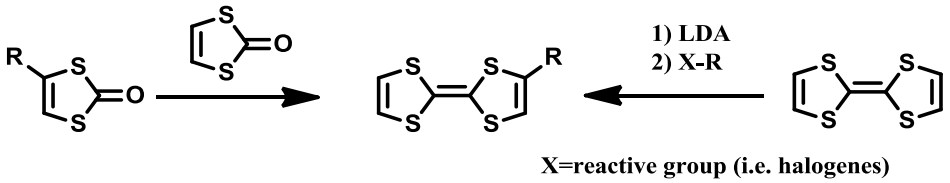

Figure B.2.5: Two main pathway for functionalisation of TTFs.

After TTF, one of the most studied derivatives is BEDT-TTF (Figure B.2.3). Functionalizing BEDT-TTF is a more complicated than TTF.[144] For the synthesis of the desired BEDT-TTF derivative, functionalized reactants should be used during the dithane ring formation since post-functionalization after ring formation via hydrogen abstraction is limited by decomposition of dithiane ring (see Figure B.2.6 for convensional synthetic path for BEDT-TTF).[144] Ring closure is mostly conducted via simple substitution reactions,[144] although other methods including Diels-Alder addition can also be used.[144, 145]

Regarding current research on synthetic TTF chemistry, obtaining neat TTF or BEDT-TTF is not challenging since these molecules are commercially available and intensively studied. The challenging issue for those compounds is to functionalize them to introduce donor and acceptor moieties on the same single molecule. Besides obtaining donor-acceptor structure in one single molecule, functionalization is mostly conducted to obtain attaching some groups that lead these materials to co-polymerisation with other (mostly acceptor) molecules. For this purpose, derivatisation (e.g. via halogenation) is the main pathway to generate good leaving groups over TTFs which most of the condensation reactions require.[146] Post-synthetic formation of TTF moieties over the polymers is an alternative way to prevent limitations that TTF may have.[147]

Since TTF derivatives are electron rich active materials, this efficiency leads some limitations in TTF chemistry.[148] First of all, as a consequence of electron rich backbone which results narrow electronic band gaps, compounds functionalised with active groups may undergo oxidation from ambient oxygen.[149, 150] Additionally, derivatives like BEDT-TTF are decomposed in harsh conditions like lithiation for further functionalization.[144]

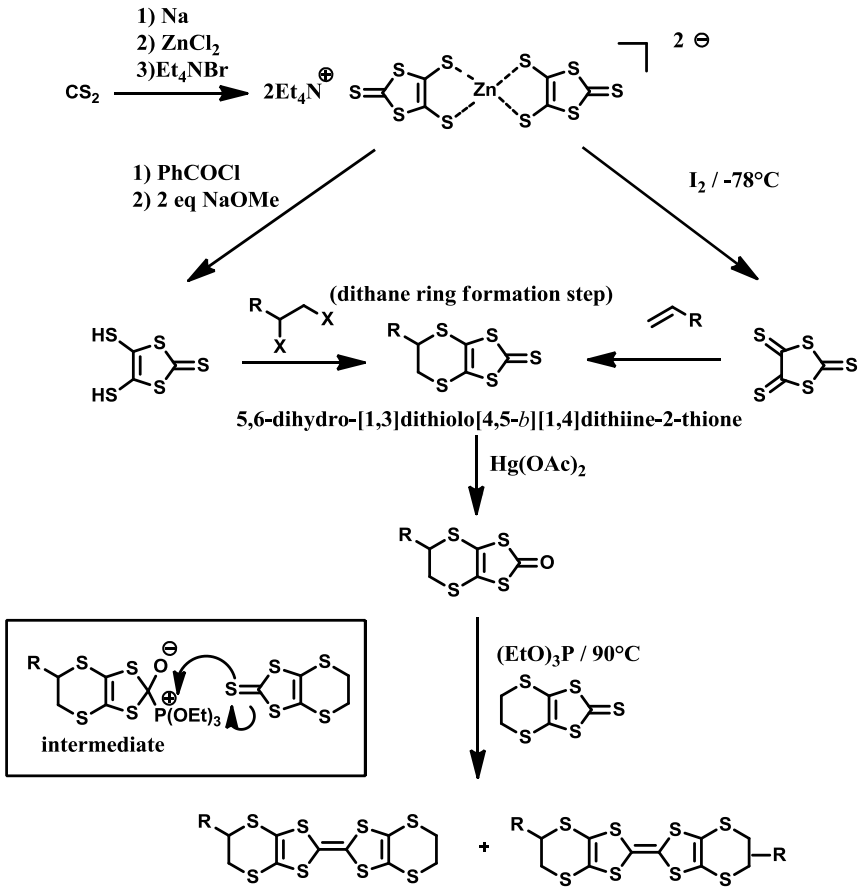

Figure B.2.6: Conventional synthesis of (functionalised) BEDT-TTFs.[144] If a cross-coupling is desired in the final step, studies showed that mixture of thione (5,6-dihydro-[1,3]dithiolo[4,5-b][1,4]dithiine-2-thione) and ketone (5,6-dihydro-[1,3]dithiolo[4,5-b][1,4]dithiin-2-one) half units should be used since oxygen of the ketone reacts with $P(OEt)_3$ to form intermediate while sulfur of thione has a better nucleophlic nature to attack electron poor moieties. Thus, homocoupling of ketone half units will be minority.

Moreover, TTFs can be considered very important donor molecules in electronic devices. The attachment of electrochemically polymerisible moieties (i.e. thiophene) to TTFs to form electrochemical TTF polymer film-based electrodes has been extensively studied. A substantial hindrance in this context, is the resistance of TTFs to undergo electropolymerisation due to lower first oxidation potential as compared to most of the electropolymerisable groups.[151] For example, most thiophene-derived TTFs cannot undergo electropolymerisation as TTF counterparts trap the radicals formed over the thiophenes which these radicals are supposed to lead polymerisation.[152-155] To overcome this, two main strategies can be followed; 1) adding alkyl chains (sp^3 hybridised side groups) between thiophene and TTF counterparts to prevent intramolecular charge transfer, 2) inserting a combination of materials that have lower first oxidation potentials (i.e. bithiophene, ethylenedioxythiophene (EDOT)) (see Figure B.2.7).[151, 156, 157] Note that, it was highlighted also introducing solvents that have electron affinity (e.g. nitrobenzene) to electrolyte solution may aid the

electrochemical polymerisation of TTFs in some cases via the formation of temporary charge-transfer complexes which can block the interaction of the TTF radical cation with thiophenic moieties.[156]

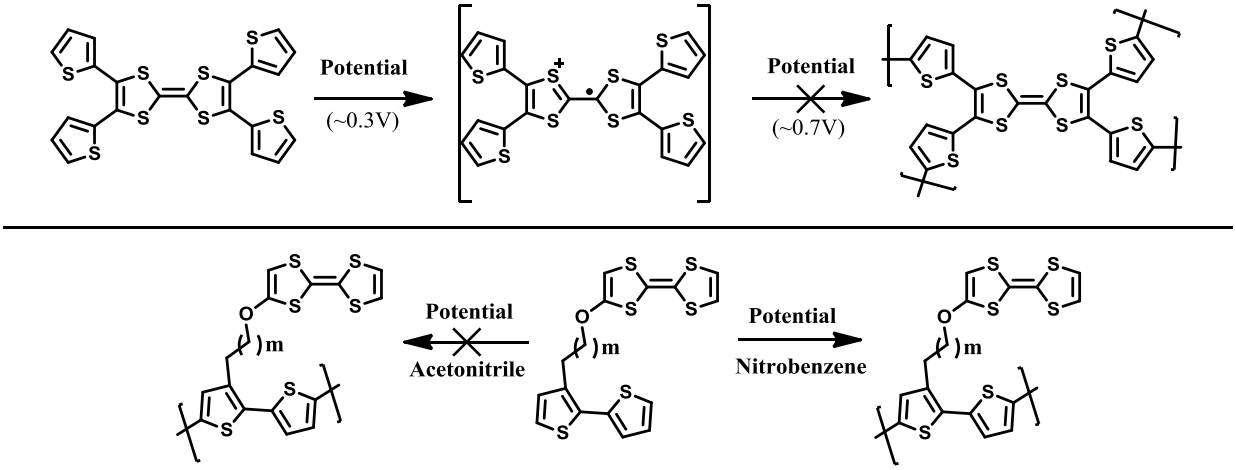

Figure B.2.7: Selected examples for thiophene derived TTFs.[152, 156] First scheme shows a TTF derivative that cannot be electro-polymerised after radical cationic moieties are formed.[152] Second example is related introducing alkyl chain to block intramolecular radical trapping.[156] Additionally, in the same work bithiophene was used which has lower first oxidation potential than thiophene and nitrobenzene was inside the electrolyte solution to form temporary charge transfer complex with TTF core.[156]

As described earlier, there is a wide application area of TTF derivatives in organic electronics. Since TTFs have electron rich, heteroatom containing, non-aromatic structure, they are generally preferred in OFETs, and additionally solar cell applications are favourable due to their suitable band gap and high tendency to form donor-acceptor couples.[140, 158, 159] Moreover, TTFs are poorly luminescent and thus OLED applications are rare for such materials. Applications of TTFs in OFETs are the main interest due to its strong electron donor character which provides the required high mobilities.[158] It is known that a good-packing is important for OFET applications. One remarkable example in this context is the case of α-TTF and β-TTF which differ highly in mobilities due to their different packing style (Figure B.2.8). α-TTF shows 1.2 $cm^2V^{-1}s^{-1}$ while β-TTF has 0.23 $cm^2V^{-1}s^{-1}$, explained by strong π–π and *S*-*S* interactions in the case of α-TTF.

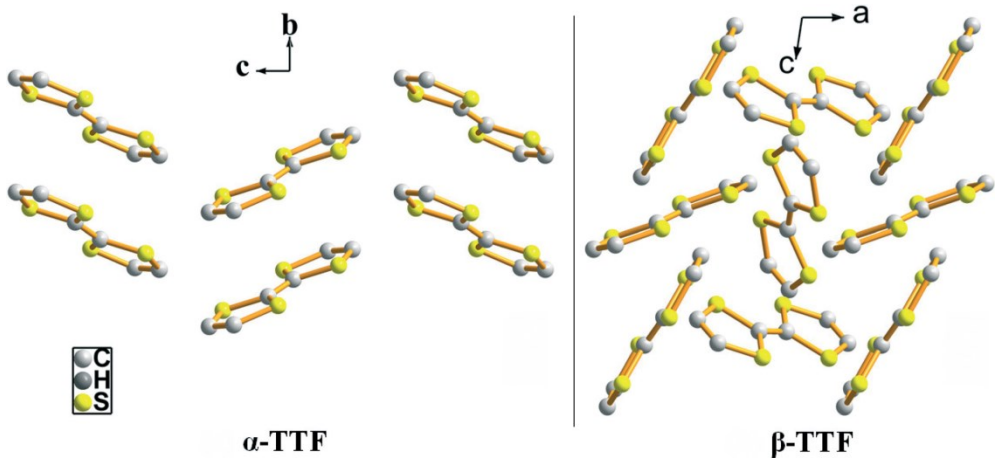

Figure B.2.8: The two different packing styles of TTF molecules that leads different mobilities indicates the importance of morphology (ref[160]).

The highest mobility reached by TTFs was recorded in a single crystal-based device (see Figure B.2.9 for the materials used) that reached 10 $cm^2V^{-1}s^{-1}$.[161] In this device, electrodes were modified with TTF/TCNQ thin films to render the *working function* suitable.[161-164] Thus, TTFs function not only as the semiconducting materials in OFETs, but can also be used as performance enhancing components.[161]

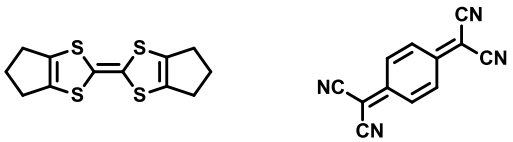

Figure B.2.9: The derivative that is used in single crystal OFET fabrication[161] (left) and TCNQ (right).

Use of TTFs in solar cells is based on their excellent donor character which allows heterojunction formation with electron acceptors (i.e. fullerenes).[159] Recent literature reports describe TTF derivative (the compound on left in Figure B.2.10) based dye-sensitized solar cell having a ~6.5% PCE (J_{sc} = 13.76 mA cm^{-2}, V_{oc} = 617 mV, fill factor (FF) = 0.75).[165] Besides as an active layer component, TTFs are also used as hole transporting materials thanks to their electron rich semiconducting nature.[149] In a recent example, a TTF derivative (the compound on right in Figure B.2.10) replaced the conventional doped spirofluorene (spiro-OMeTAD) hole transport layer and exhibit comparable efficiency (11.03%) with respect to spiro-OMeTAD based devices, but better performance/stability.[166]

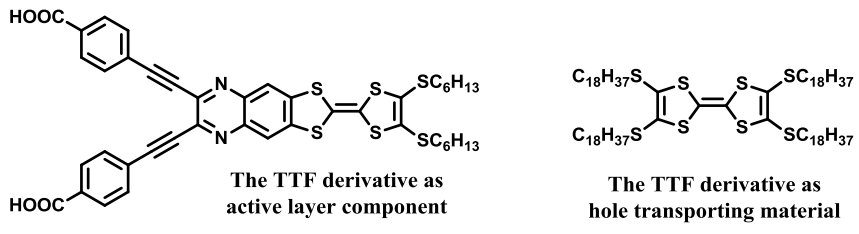

Figure B.2.10: TTF derivatives used in solar cells. [165, 166]

B.2.2. Dithienothiophenes

Thiophene and its derivatives are some of the most important heterocyclic aromatic compounds currently are used in organic and materials chemistry especially due to their ease of functionalisation, and low cost.[167, 168] Particular interest on thiophene derivatives arose after the discovery of conductivity in organic polymers (polyacetylene) as a consequence of the ability to tune their electronical configuration in various ways based chain length, side groups, and co-polymerisation with electron rich/deficient materials.[169-175] The most typically used thiophene derivatives (and their homo-/co-polymers) in lab or industrial scale are ethylenedioxythiophene (EDOT) and 3-hexyl thiophene (3HT) due to their low band gaps which is crucial in organic electronics (Figure B.2.11). The transparency of polymeric EDOT (pEDOT) makes it particularly useful in the devices related to light absorption/emission (e.g. solar cells and OLEDs).[176]

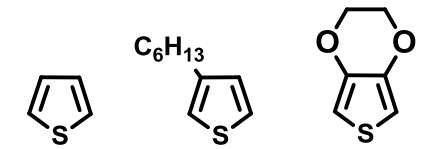

Thiophene **3HT** **EDOT**

Figure B.2.11: Structures of thiophene, 3-hexylthiophene, and EDOT.

The most commonly used fused analogues of thiophenes are formed from 2 (thienothiophenes, TTs) and 3 (dithienothiophenes, DTTs) fused rings because of complex synthetic procedures and poor solubility in further number of fused units.[177-179] Use of 'fused thiophenes' have been extensively studied via various synthetic methods to obtain advanced properties in organic electronics.[177, 180-183] The favourable benefits of such compounds can be listed for electronic devices (i.e. OFETs, PV cells, OLEDs) including stiff/well-packed/ordered structures to enhance electron mobility,[179, 184-187] low band gap structures as a consequence of increased conjugation through the rings,[188-190] efficient luminescence properties of compounds.[191, 192]

Thienothiophene molecules are composed of two fused thiophene units (Figure B.2.12). These molecules have a relatively better solubility, and simpler synthetic procedures with respect to higher numbered fused analogues.[190]

thieno[3,2-*b*]thiophene **thieno[2,3-*b*]thiophene** **thieno[3,4-*b*]thiophene** **thieno[3,4-*c*]thiophene**

Figure B.2.12: Isomers of TTs.[182]

This analogue of fused thiophenes are typically preferred in OFET and solar cell application due to higher mobility and lower HOMO level.[193, 194] The most famous example of TTs in OFET was published in 2006 demonstrating a field effect mobility at 0.6 cm^2 V^{-1} s^{-1} which is close to the range of amorphous silicon (0.5 $cm^2V^{-1}s^{-1}$).[195] Furthermore, studies of TTs in photovoltaic cell applications demonstrated the highest power-conversion efficiencies so far for polymer-based devices (7.4% and 7.9%, respectively in references).[196, 197]

DTTs are analogues of thiophenes constructed from three fused thiophene rings. Six structural isomers of DTTs are possible depending on synthetic strategy (Figure B.2.13). The mostly studied isomer is the Dithieno[3,2-*b*;2'.3'-*d*]thiophene (DTT) as result of its beneficial cross-conjugation of fused rings.

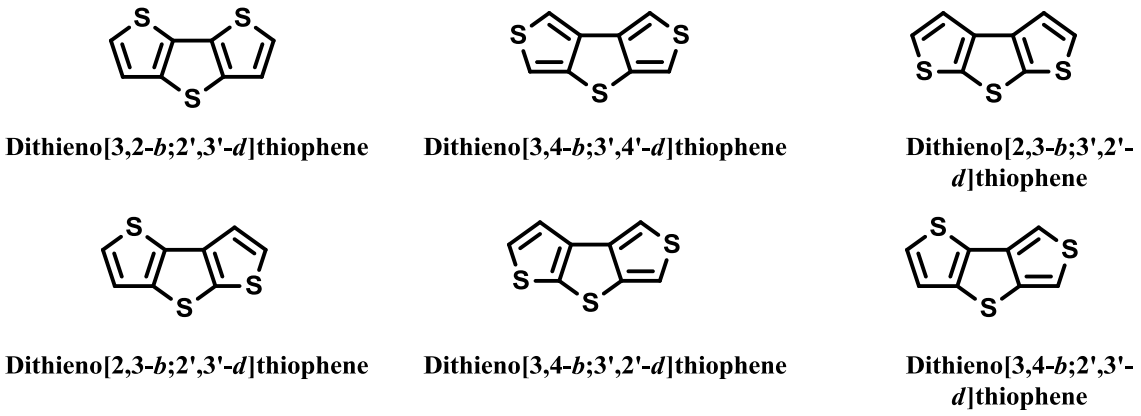

Figure B.2.13: Isomers of DTTs

There are a couple of important synthetic approaches to obtain DTTs.[181, 198-203]

The first fully characterised method was developed by Janssen and Jong based on the relatively cheap 3-bromothiophene, and ring closure of the sulphur bridged intermediate (Figure B.2.14).[204]

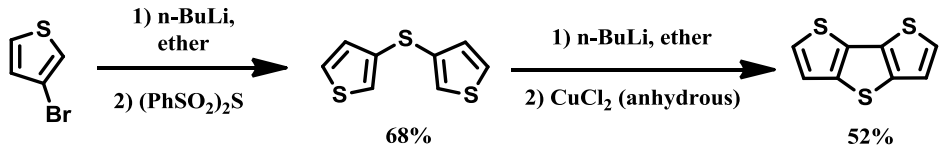

Figure B.2.14: The first fully characterized method to form DTTs

Another reported approach is based on tetrabromothiophene, with the first step resulting in the synthesis of 3,4-dibromo-2,5-diformylthiophene in 80% yield (Figure B.2.15). After this step, ethylmercaptoacetate was added and subsequent substitution and addition reactions gave a 2,2′ diester DTT (71%). The esters were transformed to the acid by LiOH, and after decarboxilation, DTT was yielded in 87%.[202]

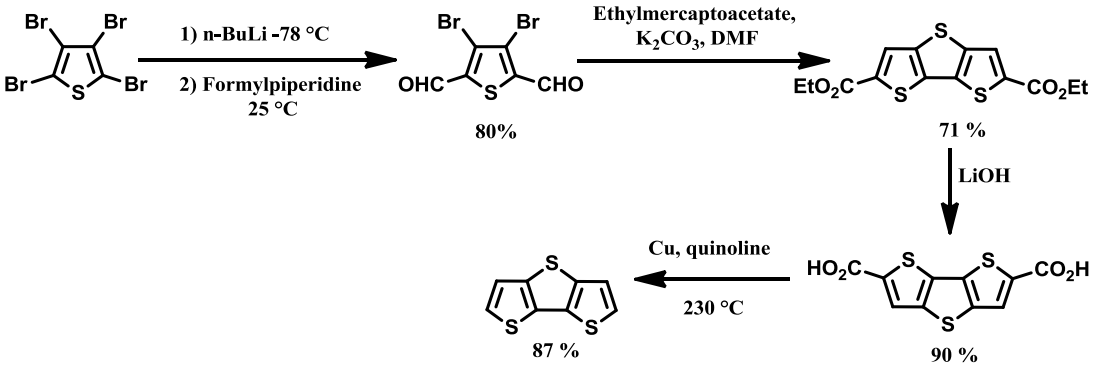

Figure B.2.15: Easy synthesis of DTTs *via* ethylmercaptoacetate in high yields.

Another relative simple and high yielding approach to DTT was published by Allared *et al.*[199] 2,3-dibromothiophene was used as starting material and a bithiophenic precursor was formed after coupling from 2 positions (79%) (Figure B.2.16). Afterwards, this material was lithiated via n-BuLi and the middle ring was formed after insertion of $(PhSO2)_2S$ as the sulphur source (70%).

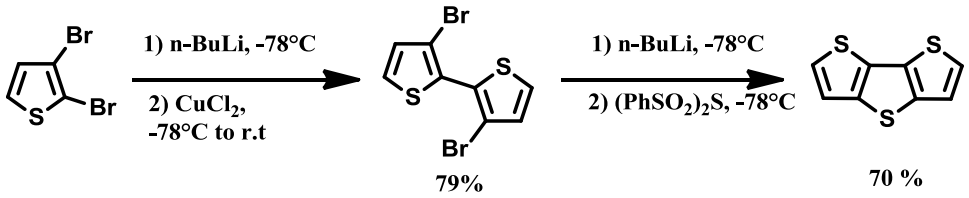

Figure B.2.16: Improving the method from ref[198] for synthesis of DTTs.

In 2004, the Ozturk group published a new ring closure method for synthesis of DTTs.[203] This method is convenient for synthesis of directly functionalized DTTs from 3,3′ positions (Figure B.2.17).

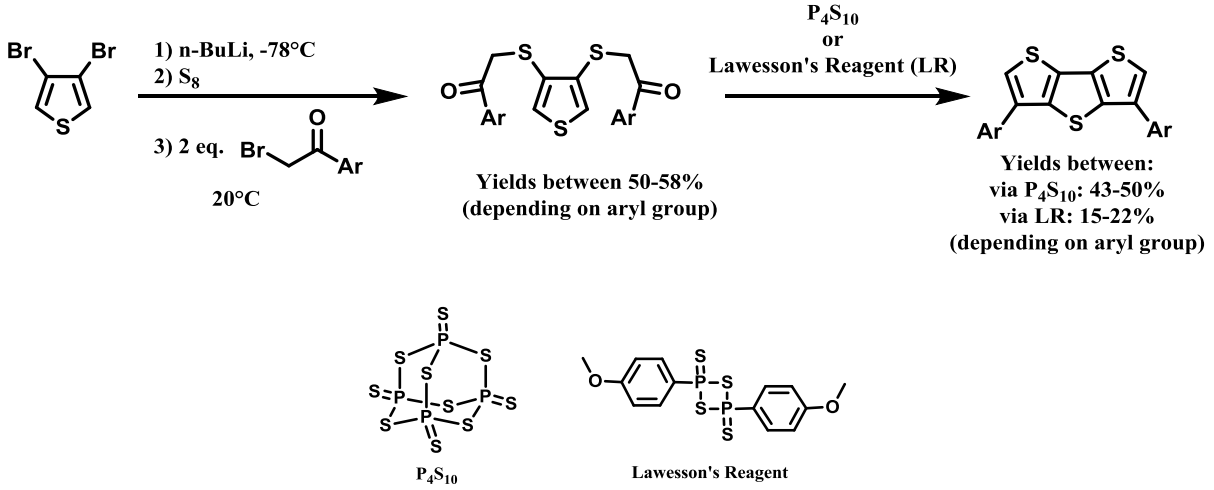

Figure B.2.17: Synthesis of DTT via P_4S_{10} or Lawesson's Reagent.

The same group later discovered that an EDOT analogue is also formed during this method; the synthetic route has been upgraded in 2012 by adding *p*-toluenesulfonic acid (pTSA) or $NaHCO_3$ to direct the reaction to DTTs or to the analogue of EDOT (vinylenedithiathiophene (VDTT)), subsequently (Figure B.2.18).[170] Additionally, in this work tert-BuLi was preferred instead of n-BuLi due to increase the yield of 1,8-diketone. Besides the higher reactivity of tert-BuLi, the authors claim that the linear carbanion formed from reacted n-BuLi attacks the halogene of the α-bromoketone and leads to lower yields.

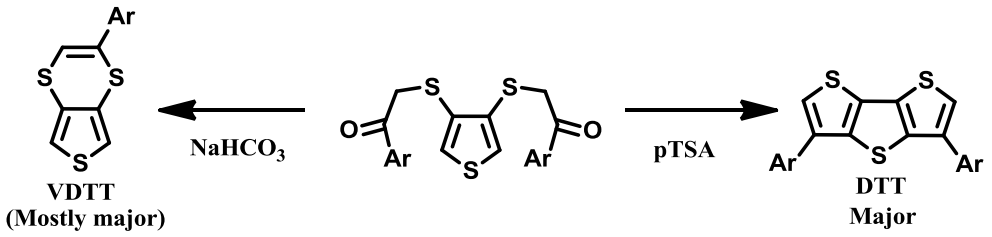

Yields;
Ar = -OMe / DTT 12% // VDTT 26%
Ar = -H / DTT — // VDTT 30%
Ar = -Br / DTT 22% // VDTT 13%
Ar = -NO_2 / DTT — // VDTT 56%

Yields;
Ar = -OMe / DTT 75% // VDTT n.a
Ar = -H / DTT 87% // VDTT n.a
Ar = -Br / DTT 95% // VDTT n.a
Ar = -NO_2 / DTT 53% // VDTT 5%

Figure B.2.18: Modification of the route in ref[203] and tuning conditions for shifting yields to DTTs or VDTTs via acid or base addition (all results above from the reaction with P_4S_{10} in toluene).[170]

DTTs have been used in solar cells due to good visible light adsorption properties,[205-207] and in OFETs due to beneficial conjugation and packing of fused rings.[96, 208-211] However, a number of examples have demonstrated shown that these application areas are not the best fields for DTTs as such molecules have good electroluminescent properties especially after the middle ring is oxidized.[173, 191, 192, 212, 213] Thus, examples of DTTs applied in OLEDs are more common with respect to solar cells and OFETs.

From a recent example of DTT-*S,S*-dioxide – flourene based co-polymer, it has shown that changing the ratios of the materials and geometry of the polymer lead to different colours (Figure B.2.19).[192] In that paper, it is stated that linearly conjugated polymers have a bathochromic shift in fluorescence and absorption spectrums while V shaped (denoted as P3; Figure B.2.19 and Figure B.2.20) polymers have hypsochromic shifts probably due to extended cross-conjugation of linear polymer whereas the V shaped material diverts the conjugation and withdraws the electrons from DTTs to phenyl rings.[192]

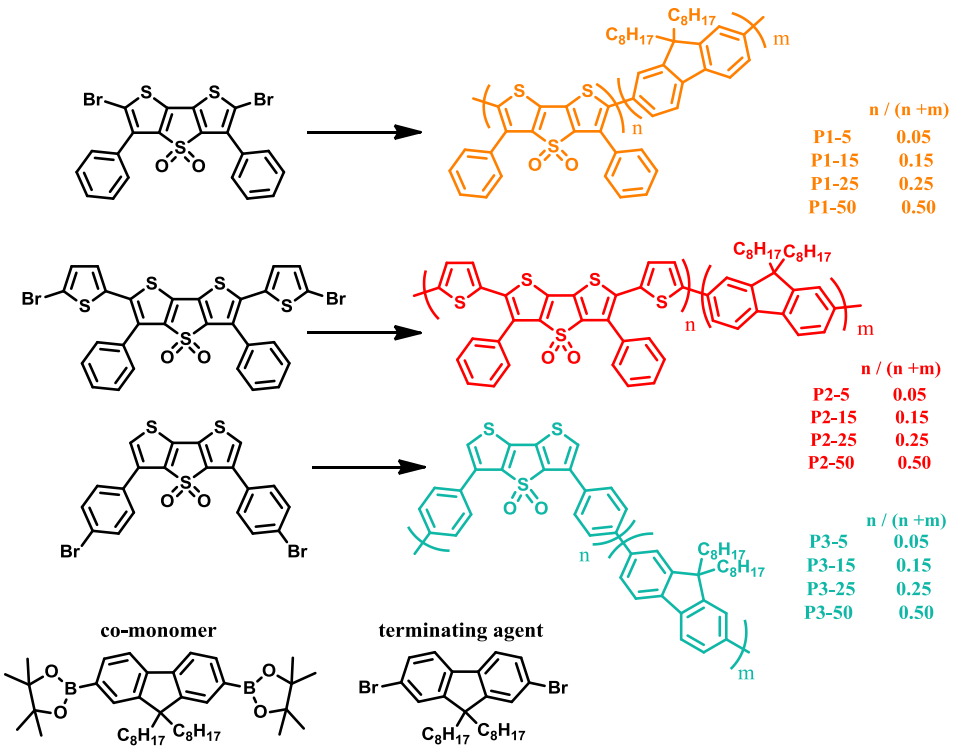

Figure B.2.19: DTT *S,S*-dioxyde-fluorene co-polymers in different ratios.[192]

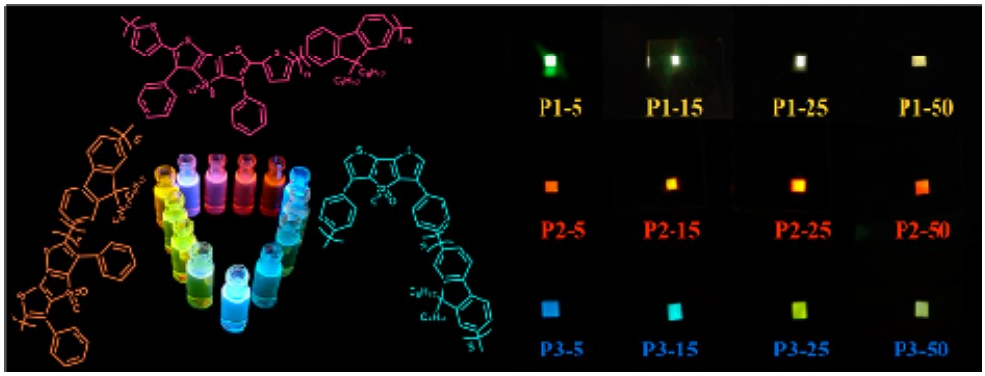

Figure B.2.20: Photos of the liquid luminescence and the devices that was built in different ratios of the DTT *S,S*-dioxyde-fluorene co-polymer. Different ratios and different geometries resulted different colours (from ref[192]).

In the literature, one can be see that oxidation is not the only way to tune electronic properties of DTTs.[214] Adding electron deficient boron moieties into the structure can also lead to an increase luminescence efficiency of the material (Figure B.2.21).[214] A study from Mazzeo *et al*. showed introducing boron species to the DTT structure lead to bright white emission.[215] In this study, it is compared with and without *S,S*-dioxyde-functionalised DTT and the compound that was not oxidized has shown better efficiency.[215] This behaviour was considered to the result of introducing both of electron the withdrawing groups (oxide and boron) which caused interference of each other's dipole moment.

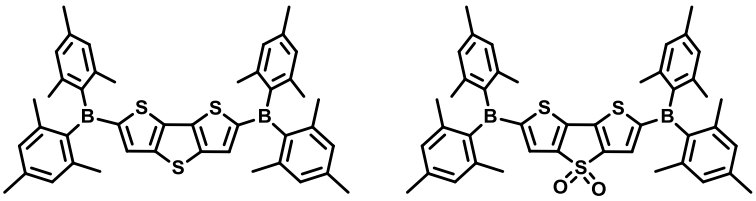

Figure B.2.21: Boron functionalized DTTs.

Besides organic electronics, DTTs were used as photoinitiator in light induced polymerisations.[216-218] Producing radicalic moieties over DTTs after light irradiation initiates free radical or cationic polymerisations which will be main application of following material namely thioxanthone.

B.2.3. Thioxanthones (TXs)

Thioxanthone (TX) and its derivatives are probably the most studied photoinitators in photo-induced polymerisation systems as a result of their excellent absorption behaviour in near UV range which enables the formation of stable triplet state radicals suitable for further initiation (see Figure B.2.22 for the illustration of photopolymerisation).[219, 220]

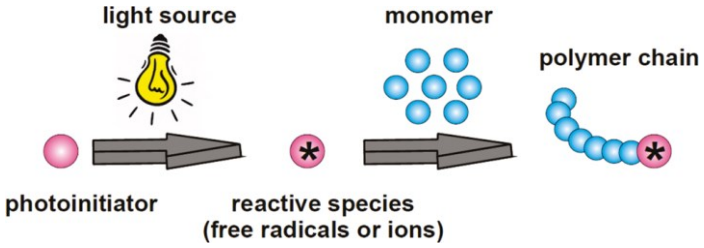

Figure B.2.22: Basic illustration of photopolymerisation.[219]

To understand use of TX, it is necessary to discuss the two main photoinitiation mechanisms which are triggered by *Type I* and *Type II* initiators in photo-induced reactions (Figure B.2.23).[219] *Type I* (also known as α-cleavage) mechanism undergoes after cleaving a bond to form radicals.[219] *Type II* photoinitiators requires a co-initiator that has acidic hydrogen (H-donor, i.e. triethylamine) or the compounds can cleave to form radical species (i.e. iodonium salts ($Ph_2I^+PF6^-$).

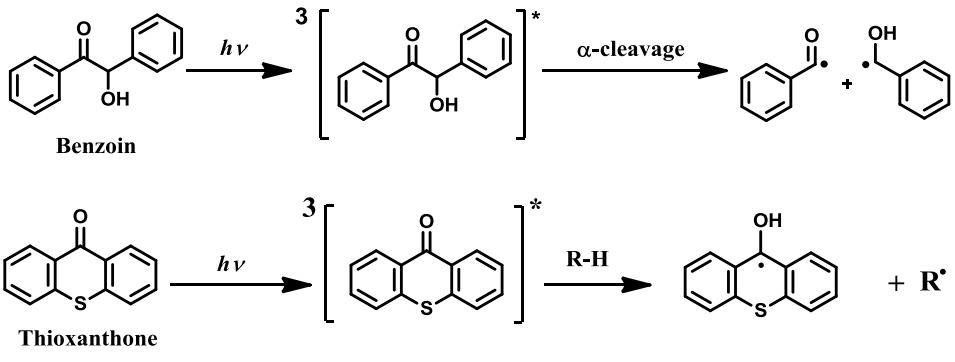

Figure B.2.23: Benzoin's *Type I* and TX's *Type II* photoinitiation mechanisms.

As one of the most important *Type II* photoinitiators, TX has been deeply studied and many derivatives have been synthesised to achieve improved properties such as putting co-initiation ability on TX via the introduction of an acidic hydrogen carrier group (e.g. thiol,[221] carboxylic acid,[222, 223] or carbazol[224] units; Figure B.2.24).[219] Additionally, the anthracene derivative of TX can initiate polymerisation without a co-initiator using ambient oxygen.[225]

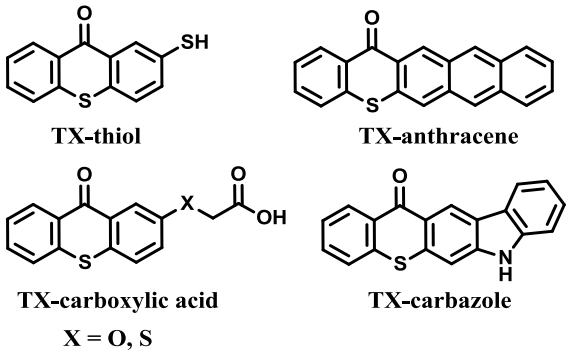

Figure B.2.24: TX derivatives mentioned in the text.

Mainly studied reactions in chemistry of *Type II* initiators are free radical and cationic polymerisations (Figure B.2.25).[219, 226] In free radical polymerisation, for example with a co-initiation of a H-donor, after H abstraction is complete, the co-initiator directly reacts with monomer (e.g. styrene, methyl methacrylate (MMA)) and forms the polymer chains.[227]

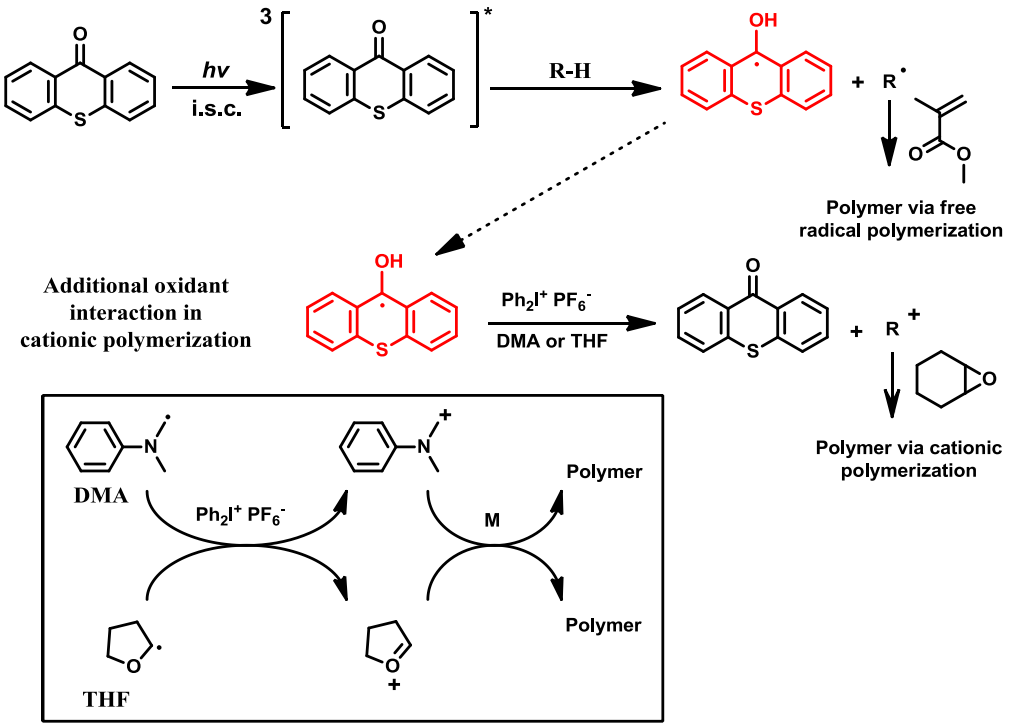

Figure B.2.25: Polymer initiation mechanisms of free radical and cationic polymerisation.

In cationic polymerisation, additional oxidants (e.g. silver hexafluorophosphate ($Ag^+PF_6^-$), diphenyliodonium hexafluorophosphate ($Ph_2I^+PF_6^-$)) are used with co-initiator, and either the H donor cation or the H^+ that is formed after interaction with the salt may initiate the polymer formation.[228]

C. RESULTS AND DISCUSSIONS

C.1. TETRATHIAFULVALENE BASED CONJUGATED MICROPOROUS POLYMERS (TTFCMPS)

As discussed in Chapter 1, besides the more common applications of microporous polymers in gas storage and separation or catalysis, especially conjugated microporous polymers are promising materials for emerging applications in organic electronics.[2, 6, 40] In this aspect, incorporation of heteroatom rich conjugated monomers (i.e. thiophene, carbazole) in such microporous polymer networks are starting to be frequently studied in order to elaborate electron rich functional CMPs that fulfil the requirements for such organic electronic applications.[105, 106, 229] Furthermore, the formation of intermolecular interactions between electron donating structures and relatively electron deficient counterparts in conventional π-conjugated polymers has been reported to be an interesting approach for optoelectronic applications.[193, 230-232] Among the most studied compounds in this field, tetrathiafulvalene (TTF) and its derivatives have received increasing interest due to their exceptional π-electron donating structure.[124, 125, 127, 140, 159, 233] Following the same tendency as in molecular or polymer chemistry, a growing interest in the field of TTF based porous materials has been recently witnessed as exemplified from the recent work on TTF-COFs and TTF-MOFs, where studies were mainly focused on altered conductivity responses upon chemical/electrochemical oxidation of TTF moieties (i.e. comparison of pristine vs. doped material).[234-238] Hence, our motivation was to synthesise a TTF based CMP and investigate its structural and electronic properties upon formation of its charge transfer salts with iodides.

The first step in the elaboration of the desired TTF based microporous polymer was to obtain a suitable functional, i.e. polymerisable, TTF monomer. In this respect, a diiodo-TTF was synthesised by hydrogen abstraction *via* a strong base (lithiation *via* lithium diisopropylamide (LDA)) to produce dicarbanions on TTF followed by a subsequent elimination of iodine from perfluorohexyl iodide (TTF-I_2, Figure C.1.1).

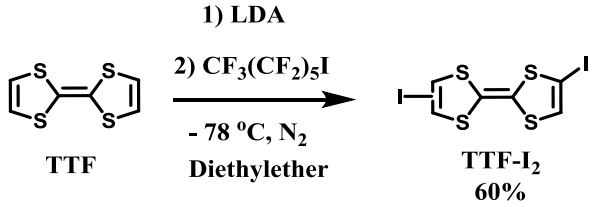

Figure C.1.1: Diiodination of TTF.

Analytically pure (E,Z)-4,4'-diiodo-2,2'-bi(1,3-dithiolylidene) was obtained as an orange-red powder in 60 % yield and ^{1}H NMR in $CDCl_3$ showed only one peak as expected at = 6.30 ppm, and ^{13}C NMR

in $CDCl_3$ revealed three peaks at = 121.2 (***C***-H), 113.7 (***C***=***C***), 63.6 (***C***-I) ppm which was the same as the reported values in literature (detailed information can be found in experimental part).[142]

After the successful synthesis of TTF-I_2, polymerisation and network formation was achieved *via* a Sonogashira-Hagihara cross-coupling reaction with 1,3,5-triethynylbenzene (Figure C.1.2).

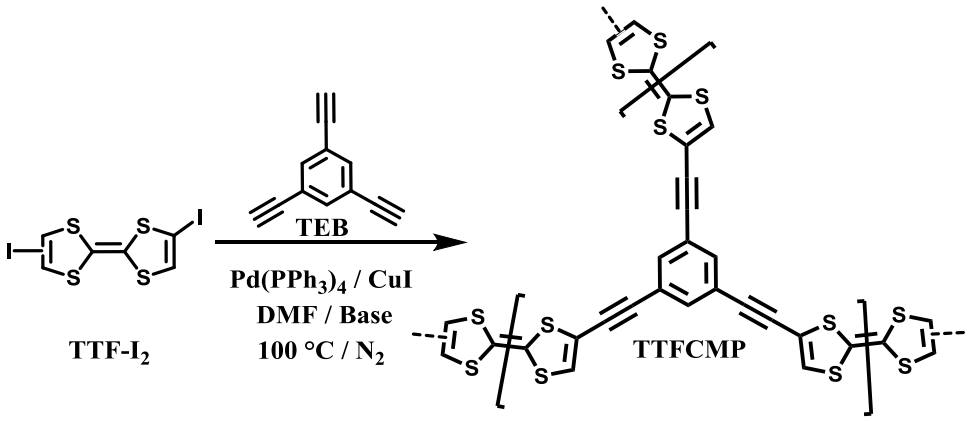

Figure C.1.2: Formation of TTFCMP via Sonogashira-Hagihara cross-coupling.

In a first attempt the synthetic procedure reported in the first paper on CMPs[49] was followed in as it was reported that a maximum BET surface area could be reached when an excess ratio of the acetylene to the halogen compound was used[239] and that 100 °C in DMF appeared to be a temperature and solvent of choice for CMP synthesis.[240] Polymerization of TTF-I_2 under these conditions (Figure C.1.2) yielded an insoluble brown powder after extensive washing and Soxhlet extraction, denoted as TTFCMP. The porous properties of the network were evaluated by nitrogen sorption measurements at 77 K and the apparent Brunauer-Emmett-Teller (BET) surface area (*SA*) was evaluated to be 180 m^2g^{-1}. [*NB: all apparent surface areas presented in this manuscript were calculated via the BET equation).* The surface area was relatively low in comparison to predominantly carbon-based CMPs which typically have SAs in the range of 500 to 1000 m^2g^{-1}.[74] Various reasons, may cause a lower surface area, especially for heteroatom containing monomers, like e.g. a lower reactivity, poor solubility, their relatively higher molecular weight etc.[74, 241]

An optimisation of the reaction conditions was then attempted with the aim to obtain polymer networks with higher SAs. It has been reported that the replacement of triethylamine (TEA) with a stronger base, such as diisopropylamine (DIA), improves polymerisation yields and kinetics of the Sonogashira-Hagihara cross-couplings due to enhanced acetylene deprotonation.[242-247] In this case, using DIA as base during the Sonogashira coupling indeed resulted in TTF-based networks with a slightly higher SA of ~ 264 m^2g^{-1}.

To further optimize the reaction conditions, we aimed at preventing early stage precipitation during the coupling procedure in order to reach higher polycondensation degrees, which should supposedly yield polymers with higher surface areas.[248] Therefore, attempts to optimise the DMF/DIA solvent mixture

were studied since alkylamines (in this case DIA) may act as an anti-solvent to poorly soluble TTF oligomers. Indeed, reducing the amount of DIA to catalytic quantities (i.e. from 15 to 0.6 mL) gave rise to a network with a SA of 413 m^2g^{-1}.

Finally, the influence of using an excess molar ratio of acetylene to halogen functionalities was evaluated and reactions with an equimolar acetylene to halogen ratio were tested.[49, 74, 239, 249] In the case of TTFCMP network, reducing the TEB ratio did not result in a significant change, as the surface area only slightly changed and was measured to be 434 m^2g^{-1} in that case (vs. 413 m^2g^{-1} for a 1.5 molar ratio of functional groups). It thus seems that in the case of TTF, an excess amount of acetylene is not necessary to increase the SA. Additionally, the use of an excess of acetylene compared to halogen groups may lead to side reactions such as the homocouplings of acetylene groups.[249] This matter will be discussed in more details in the following section.[249]

Table C.1.1: Various reaction conditions for the synthesis of TTFCMP and the surface area of the resulting networks.

$TTFI_2$eq.	(TEB)	Solvent	T, °C	Time, h	Yield, %	SA, m^2g^{-1}
1	1	DMF/TEA (15/15 mL)	100	72	110	180
1	1	DMF/DIA (15/15 mL)	100	72	90	264
1	1	DMF/DIA (25/0.6mL)	100	72	105	413
3	2	DMF/DIA (25/0.6 mL)	100	72	85	434*
1	1	DMF/TEA (25/0.75 mL)	100	72	107	130
3	2	DMF/TEA (25/0.5 mL)	100	72	99.5	99
3	2	DMF/TEA (5/5 mL)	100	72	97	54

**Isotherms were derived from Autosorb-1-MP whilst other measurements were performed using a Quadrasorb SI instrument.*

The polymers were characterized by ^{13}C cross-polarization magic-angle spinning (CP-MAS) NMR spectroscopy (Figure C.1.3). The spectrum of TTFCMP shows five peaks at δ = 131, 121, 113, 90, and 80 ppm that can be ascribed to the aromatic and acetylene carbons within the structure. Notably the peaks at δ = 121 and 113 ppm, which can be assigned to the outer and inner carbons (bridging carbons between 1,3-dithiole rings) of TTFs, respectively, proved the successful incorporation of TTF moieties into the polymer backbone. Moreover, NMR analysis gave additional evidence on the origin of the decreased surface area observed when a high amount of alkylamine was used. In that case, the NMR

spectra seems to indicate a lower cross-linking degree, as the peak at δ = 65 ppm corresponding to the C-I carbon is clearly visible for the network synthesised in presence of a high amount of base. The presence of this peak indicates a high amount of terminal groups and therefore is a proof of a lower polymerisation degree, which explains the low surface areas observed.

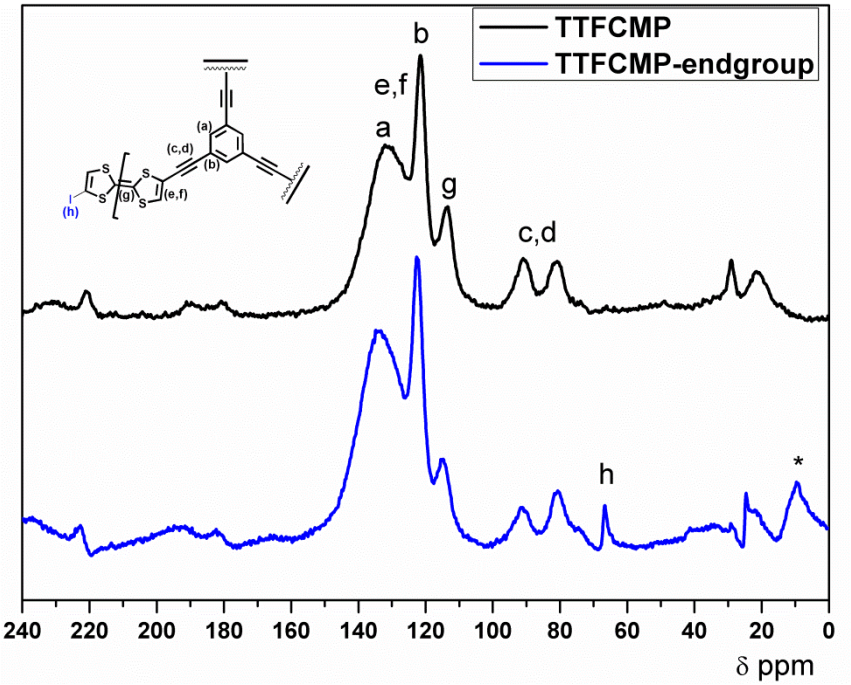

Figure C.1.3: ^{13}C CP-MAS NMR spectra of low (blue curve, 180 m^2g^{-1}) and high (black curve, 434 m^2g^{-1}) surface area TTFCMPs. All unassigned peaks are spinning side bands, the marked peak at around 9 ppm originates from entrapped TEA.

After obtaining TTFCMP with a relatively high surface area, the possibility to introduce local charges within the structure was studied, to investigate the potential of TTFCMP in organic electronic applications. Iodine was chosen as a suitable oxidant owing to its relatively small size with respect to other common dopants such as tetracyanoquinodimethane (TCNQ), which should favour its diffusion through the microporous structure of the network. The comparison of I_2 *vs*. TCNQ as dopants in case of a TTF based COF was recently investigated.[236] It was shown that the conductivity increase of the pristine TTF-COF was ~10^3 after doping with I_2 whereas it was only ~10 times for TCNQ.[236] Additionally, oxidation with iodine is a controlled process for which the oxidation stops after the formation of the radical cations[250] whereas another frequently used oxidant, $Fe(ClO_4)_3$, is known to further oxidize TTFs to dicationic states.[251-255] Since the oxidation takes place heterogeneously, it would be hard to control the reaction with $Fe(ClO_4)_3$ which would possible give rise to a mixture of neutral, radical cationic and dicationic states of TTF within the structure. Moreover, $Fe(ClO_4)_3$ could

further cause a network decomposition due to the sensitivity/reactivity of acetylenes to iron species.[256]

In order to form charge transfer complexes within the network, TTFCMP was dispersed and stirred in a solution of ethanol (EtOH) containing an excess of iodine (Figure C.1.4). The resulting powder indicated a clear colour change of the pristine powder sample from dark brown to black. Nevertheless, the reaction was allowed to stir longer in order to reach equilibrium and after 7 days, the mixture was centrifuged and the precipitate was washed/centrifuged with EtOH for several times until the washing solution became colourless. Finally, the doped network powder ($TTFCMP^{\cdot+}$-I_n^-) was dried in vacuo at 40 °C in order to remove remaining iodines species and solvent.

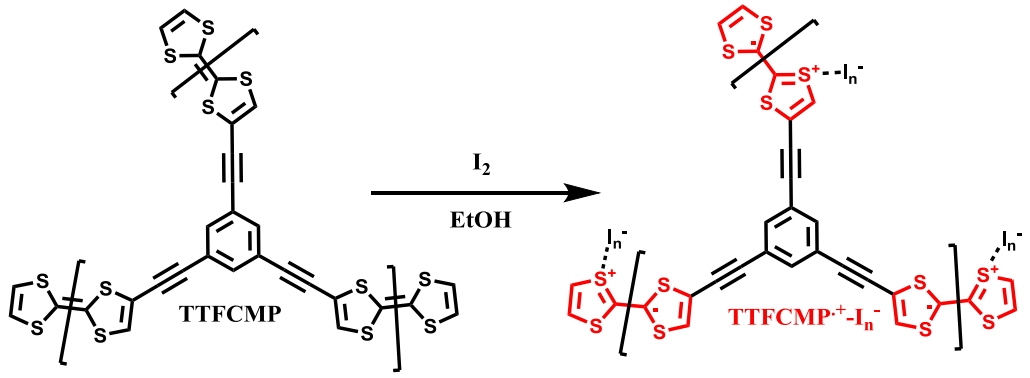

Figure C.1.4: Charge transfer salt formation over TTF moieties.

Due to the difficulties of the precise recovery of all doped network after work-up based on decantation, we decided to measure the gravimetric TTF/iodide molar ratio from gas phase iodine exposure experiments. For this purpose, an open vial containing only TTFCMP polymer was placed in a bigger vial that was filled with excess of iodine crystals (see Figure C.1.5). After sealing of the reaction setup, diffusion of I_2 through the pores of TTFCMP was directly evidenced by a rapid colour change from dark brown to black after a couple of minutes. The exposure was carried out for 7 days in order to ensure maximum functionalisation, and after 7 days the small vial with doped network was removed and put in a vacuum oven at 40°C for the removal of unreacted iodines. The weight increase after I_2 exposure was then measured and a molar ratio of 1.38 of iodide to (theoretical) TTF moieties within the network was calculated (Table C.1.2). According to this calculated value, the proposed nature of the counter anion within the network can be assumed to be a mixture of monoiodides (I^-) and triiodides (I_3^-).[250] Nevertheless, possible pore blockage after the formation of charge transfer complexes on outer TTF moieties would possibly lead to an incomplete charge transfer salt formation due to limited diffusion of I_2 through the whole amorphous network. Thus, it can fairly be postulated that I_3^- are the major counter anion formed as reported for other similar charge-transfer complexes.[250, 257-259] Note that further measurements on $TTFCMP^{\cdot+}$-I_n^- were performed on the networks doped in

I_2/EtOH mixture since the effect of pore blockage are assumed to be reduced due to favorable solvent-swelling effects.[249]

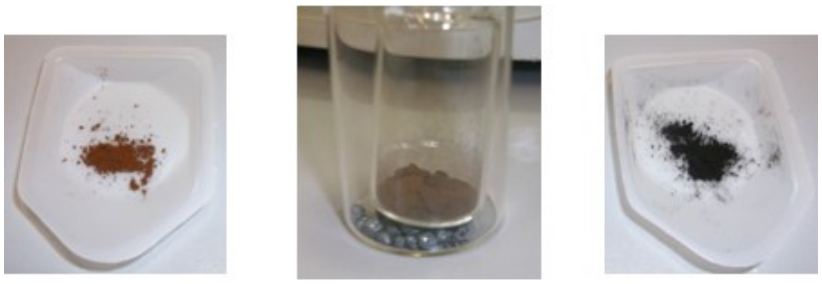

Figure C.1.5: Pictures of TTFCMP (left), TTFCMP treated by I_2 vapor diffusion (middle) and iodine treated sample TTFCMP$^{\cdot+}$-I_n- (right).

Table C.1.2: Values for sublimation of I_2 through TTFCMP.

TTFCMP (g)	TTF in polymer* (g)	TEB in polymer* (g)	Iodine uptake (g)	TTF in polymer* (mmole)	Iodine uptake (mmole)	Ratio	Weight Ratio % I_n^-/TTFCMP-I_n^-
0.0514	0.0346	0.0168	0.0296	0.17	0.23	TTFCMP-$I_{1.38}^-$	36.5

**theoretical values assuming formation of an ideal network.*

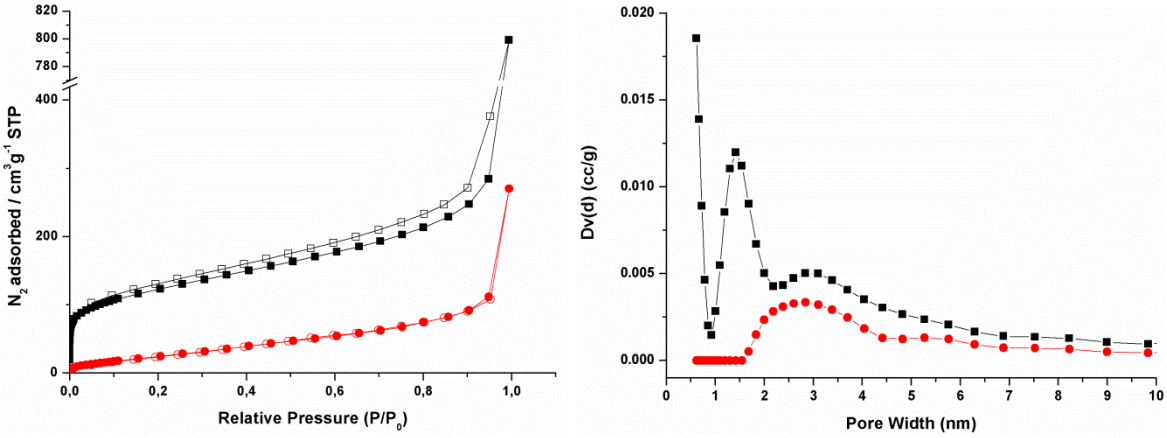

Figure C.1.6: N_2 sorption isotherms and corresponding NL-DFT pore size distributions for TTFCMP (black) and TTFCMP$^{\cdot+}$-I_n^- (red).

After iodine treatment of the polymers, the changes in gas sorption isotherms and pore size distributions also point to incorporation of I_n^- species in the structure. The surface area of the iodine doped TTFCMP (in EtOH, TTFCMP @434 m^2g^{-1}) decreased to 108 m^2g^{-1}, which can be explained by the overall increase of the molecular weight of the repeating units of the polymer networks and also by the considerable size of iodide, probably blocking the pores of the network. This can be especially seen in the decreased microporosity of the samples indicated by the lower uptake at low relative

pressures (P/P_o < 0.2, Figure C.1.6) and by the NL-DFT pore size distribution analysis showing that the pores with a 1.4 nm diameter where blocked during the process.

The structural changes of the doped TTFCMP network were also evaluated by solid state ^{13}C CP-MAS NMR as the response of the TTF carbons to the magnetic field are expected to change dramatically (see Figure C.1.7, note that detailed ^{13}C NMR discussions were made for pristine network, previously, below Figure C.1.3). Indeed, the non-aromatic (14-π) electron system of TTF turns to a partially aromatic system after radical cation formation and the 1,3-dithiolium cation shows a thiophenic character with a 6-π electron system. The π-electrons of the ethylene carbons in TTF were cleaved in order to form aromaticity over the oxidized ring, and the double bond between the two dithiole rings was converted as a consequence to a single bond. This behaviour was observed experimentally as the significant increase in the intensity of the broad peak at δ = 131 ppm showed that the concerned bridging carbons adopt an aromatic character due to the deshielding effect on the 1,3-dithiole rings, yielding a shift to lower fields, that is, in the region of thiophene-like aromatic carbons (Figure C.1.7). Similar changes were observed in ^{13}C CP-MAS NMR spectrum of molecular TTF iodide salts.[260]

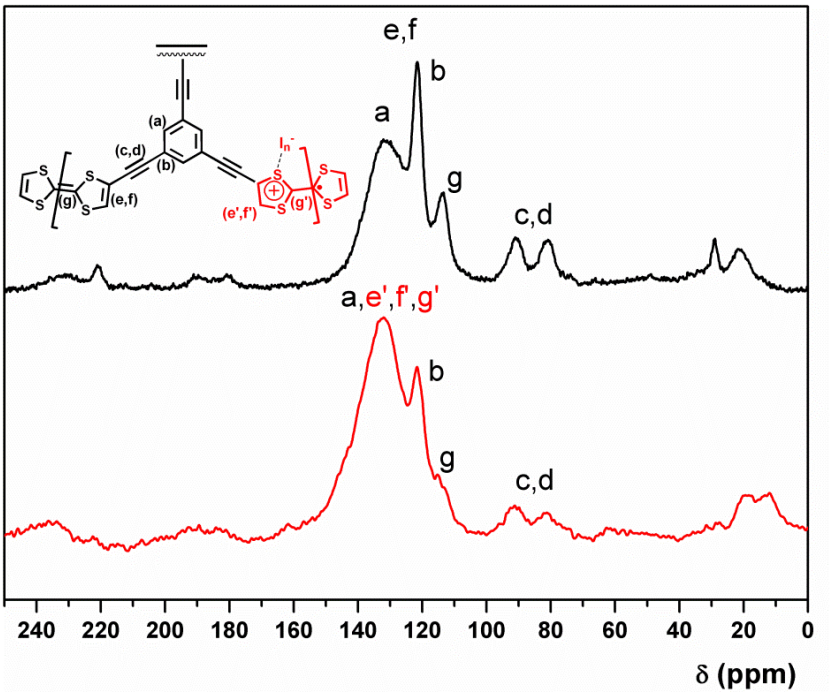

Figure C.1.7: Comparison of solid state ^{13}C CP-MAS NMR spectra of TTFCMP (black) and TTFCMP$^{\cdot+}$-I_n^- (red).

Fourier transform infrared spectroscopy (FT-IR) is another key measurement for the structural analysis of charge transfer complexes/salts of such sulphur containing, π-electron rich heterocyclic structures, especially due to the expected shifts in the range of the carbon-sulphur-double bond stretching modes between 1050-1200 cm^{-1} (Figure C.1.8).[261-263]. Thus, the FT-IR spectra of both TTFCMP and TTFCMP$^{\cdot+}$-I_n^- were recorded and indicated the formation of charge transfer salts over TTF moieties as the shift of the sharp peak from 1053 to 1094 cm^{-1} and the appearance of a high intensity band at 1194 cm^{-1} point to the formation of a radical cation. Additionally, a low intensity band at 720 cm^{-1}

further shows the formation of a thiophenic out-of-plane deformation of the C-H bond in the structure of TTFCMP$^{\cdot+}$-I_n^- indicating the transformation of 1,3-dithiole rings to a thiophene-like structure.

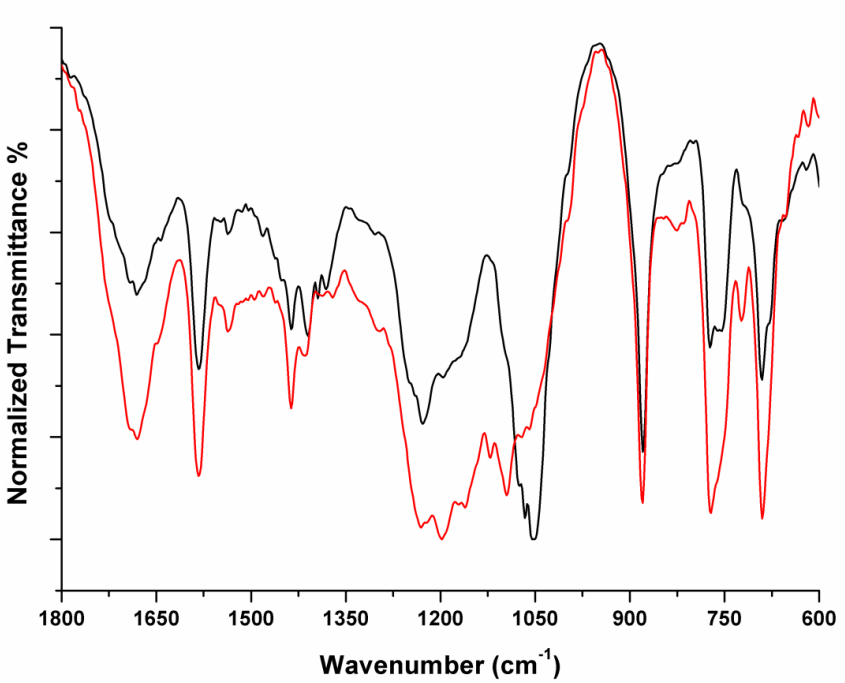

Figure C.1.8: FT-IR spectra of TTFCMP (black) and TTFCMP$^{\cdot+}$-I_n^- (red).

To further corroborate this information, solid state diffuse reflectance UV-Vis (DRUVS) and electron paramagnetic resonance (EPR) measurements were performed (Figure C.1.9-A). For molecular TTF derivatives, the main characteristic absorption bands associated with a radical cation formation have been reported to appear at λ = 580, 620 and 1200 nm.[130, 252, 257, 264] DRUVS analysis of the synthesised networks showed the expected bands at λ = 580 and 620 nm as partially visible shoulders within a broad absorption feature typically observed for such 3D amorphous networks.[61] The band at 1200 nm could unfortunately not be investigated due to instrument limitation (accessible scanning range only up to 800 nm).

As one of the main goals of this work focuses on the formation of radical cations over TTF moieties, it was obligatory to perform EPR measurements since this technique is frequently applied in the determination of radical species for both organic and inorganic compounds (Figure C.1.9-B).[265, 266] Particularly for compounds like TTF, which are widely used in charge-transfer complexes, the observation of a characteristic *g*-factor (the parameter that is used in EPR terminology that is derived from the *applied frequency/absorbed magnetic field*) helps to address if the radical cationic states are formed over the expected species.[267] During EPR measurements of the TTF based networks, a typical *g*-factor between 2.007-2.008 for the iodine doped material[267] and no response in the magnetic field for the pristine TTFCMP were expected. However, pristine TTFCMP had a *g*-factor 2.0072 at 150 K with a similar EPR line shape as seen for TTFCMP$^{\cdot+}$-I_n^-, that indicated a *g*-factor 2.0078 at 150 K. The situation would be surprising for monomers although there are some examples of intramolecular

charge transfer complexes that were observed for some TTF derivatives (TTF radical cations are possible to form even with the ambient oxygen).[236, 267-269] Since the structure of the polymer networks issued here is amorphous and 3D with an extended conjugation, the observation of stable radicals over the pristine TTFCMP can be understood, even more as also for other microporous polymers with weaker electron donors incorporated, have shown stable radicals on EPR without any further doping.[72, 236, 270, 271]

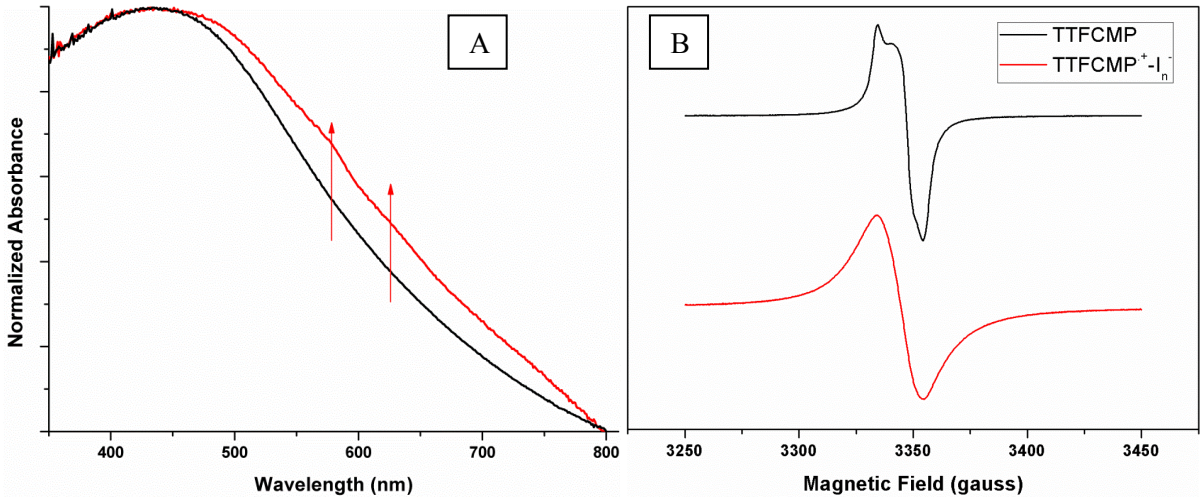

Figure C.1.9: Solid-state diffuse reflectance UV-Vis (A) and EPR (B) spectra of TTFCMP (black) and TTFCMP$^{\bullet+}$-I_n^- (red).

Investigation of the chemical composition in the synthesised materials before and after doping was performed using X-ray photoelectron spectroscopy (XPS). [*NB: All measurements and data interpretation were performed by Dr. J. P. Paraknowitsch*]. An overall elemental detection / quantification is possible with XPS (Figure C.1.10, Table C.1. 3), however, since XPS is a surface sensitive method and the morphology of CMPs are three dimensionally amorphous, exact values are not expected to be observed. Nevertheless, quantification of XPS survey spectra was performed even if it's only representative of the material's surface (Figure C.1.10, Table C.1. 3).

Table C.1. 3: Quantified XPS survey data of TTFCMP (black) and TTFCMP$^{\bullet+}$-I_n^- (red), all values are in at.%.

	C1s	S2p	I3d$_{5/2}$	Pd3d	P2p	O1s
TTFCMP	66.5	15.2	0.3	0.7	< 0.1	17.3
TTFCMP•$^+$-I_n^-	73.4	13.5	3.1	0.6	< 0.1	9.4

One of the most important outcome of the survey scans is the observation of residual unreacted end cap iodides over the outer shell of the pristine TTFCMP (Figure C.1.10, Table C.1. 3). This finding is not surprising, considering end cap halogens are usually observed for Sonogashira-Hagihara type

polycondensation reactions.[74, 272, 273] Additionally, it is important to note that the detection of oxygen-related BEs derives from oxygenated surface sites, which typically occur on samples stored under atmospheric conditions, although indium oxide species on the sample holder may also contribute. Furthermore, the found traces of Pd and P are assumed to be associated with synthesis catalyst residues.

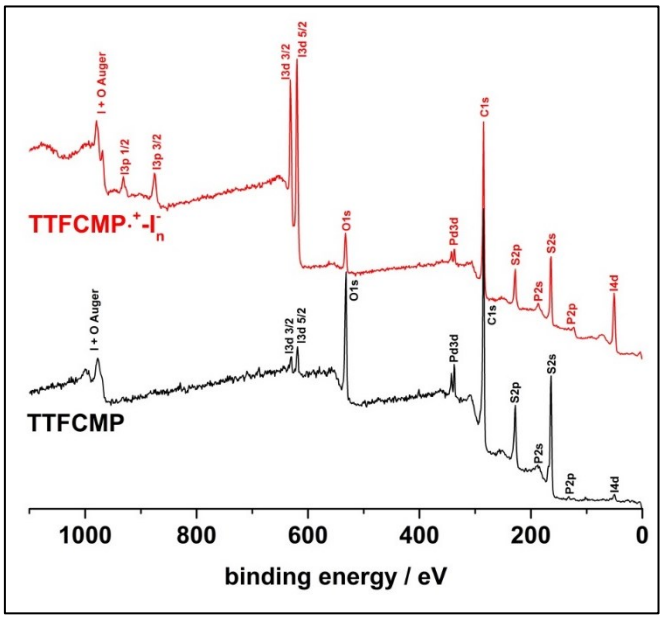

Figure C.1.10: Normalised XPS survey spectra of TTFCMP (black) and TTFCMP$^{\cdot+}$-I_n^- (red).

Besides other elemental species within the structure, investigation of the type of iodide(s) formed (i.e. I^-,I_3^-, I_5^-) was of special interest since, as discussed above, the gravimetrical detection had not given a solid information. Two different states of iodine, with BEs of 618.63 eV and 620.43 eV, can be detected by deconvolution of the I3d 5/2 core level spectrum of TTFCMP$^{\cdot+}$-I_n^-. According to the literature, I^- and I_3^- species typically present peaks with binding energies (BE) of 618.63 and 620.43 eV, respectively (Figure C.1.11).[258, 274, 275] Yet, other reports suggest that these BEs may correspond to triiodide (I_3^-, 618.83 eV) and pentaiodide (I_5^-, 620.43 eV) structures.[276-278] Because of these contradictory findings, it is not clear whether there are isolated I^- moieties or mixtures of different polyiodides (I_n^-). Consequently, the higher intensity peak at BE = 620.43 eV is typically associated with the formation of polyiodide structures, and most probably I_3^- since these type of polyiodides are frequently observed[250, 257-259] and their formation do not require any special conditions, unlike I_5^-.[279, 280] However, it should be considered that some XPS studies aiming at the assignment of iodide species indicated that pentaiodides essentially consist of molecular iodine and triiodide (I_2+I_3^-=I_5^-), and that they decompose under vacuum through I_2 sublimation yielding only I_3^- moieties within the structure.[277, 281] Since XPS measurements require high vacuum, probable decomposition of pentaiodides should be taken to account.[277, 278, 281] Thus, XPS results supported the probable presence of a mixture (poly)iodide within the polymeric networks as already established by the gravimetrical studies.

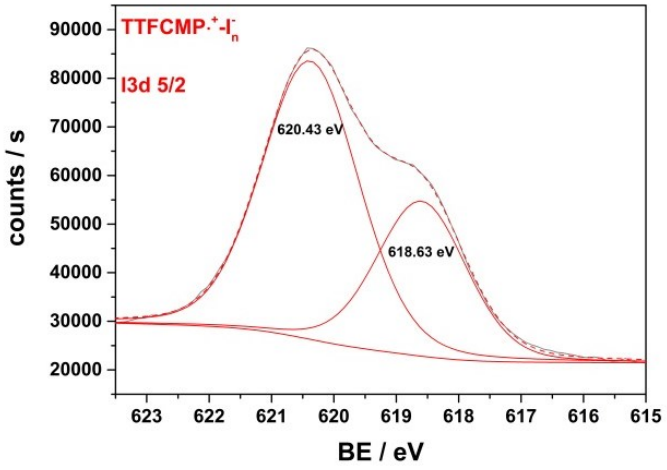

Figure C.1.11: XPS I3d$_{5/2}$ core level spectrum of TTFCMP$^{\cdot+}$-I$_n^-$.

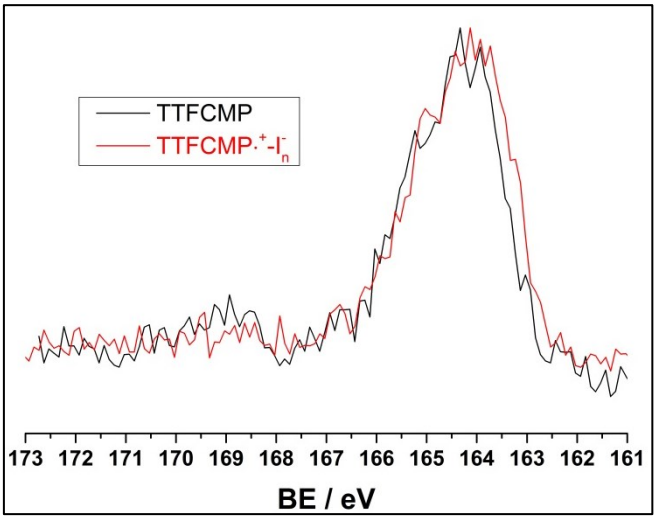

Figure C.1.12 Normalized overlay of XPS S2p core level spectra of TTFCMP and TTFCMP$^{\cdot+}$-I$_n^-$

After determination of the iodide structure(s), typical sulphur BE for TTF or thiophene like materials were revealed in S2p core level spectra of TTFCMP and didn't change dramatically in TTFCMP$^{\cdot+}$-I$_n^-$ (Figure C.1.12).[274, 275, 282] Nevertheless, after the iodide charge transfer salt was formed, the broadening of the S2p signal to lower BEs indicates altered chemical state for the sulphur of TTF moieties, in agreement with published results.[274]

In conclusion, co-polymerisation of TEB and diiodo-TTF by Sonogashira-Hagihara polycondensation reaction was successfully achieved and a TTF based CMP was obtained. Conventional synthetic procedures using a 1:1 TEA/DMF solvent mixture only yielded relatively low surface areas. Thus, optimisation of the reaction conditions has been undertaken and the critical parameters appeared to be the nature and amount of base used for the polymerisation. We found that optimal synthetic conditions for the present system were the use of a catalytic amount of DIA, which allowed reaching higher polymerisation degrees by avoiding early stage precipitation. The networks exhibited high surface areas of up to 434 m^2g^{-1}. Unlike for the conventional CMPs, the use of an excess molar ratio of

ethynyl to iodine functionalities did not result in a significant increase of surface area. In following, electron-donating properties of the networks were proven by successful chemical doping. The radical cationic form of TTFCMP obtained after iodine exposure, denoted as $TTFCMP^{\cdot+}$-I_n^- was fully characterised. Both the gravimetric iodide/TTF molar ratio and the evaluation of the iodides chemical state by X-ray photoelectron spectroscopy were used to determine the (poly)iodide structure formed within the porous network and could be assumed to be mostly triiodides (I_3^-). These findings prove that formation of local charges over a neural polymeric network *via* chemical doping is possible, and results presented here are a step towards the application of conjugated microporous polymers in organic electronics.

C.2. INVESTIGATION OF THE EFFECT OF MONOMER RATIOS ON THE SURFACE AREA OF CONJUGATED MICROPOROUS POLYMERS

Poly(arylene ethynylene)s (namely, PAEs) have been studied intensively since their conjugated rigid backbone might make them useful especially for sensing and organic electronics.[283-286] One of the most employed reactions in order to obtain such compounds is the Sonogashira-Hagihara cross-coupling reaction.[287, 288] This polycondensation reaction basically takes place between a dihalo (X-A-X) and diacetylene (H-C≡C-B-C≡C-H) monomer yielding a polymer backbone in which the repeating units are connected by triple bonds (-[A-C≡C-B]-).[247] However, obtaining defect-free structures from this polycondensation method is not possible.[288] For example, polymers obtained *via* Sonogashira-Hagihara cross-coupling reaction using a Pd(0) catalyst under inert atmosphere also carry butadiyne groups (X-C≡C-C≡C-Y) from 1 to 10% although such homocouplings is just expected in presence of Pd(II) catalyst or oxidizing species like ambient oxygen.[288]

Obtaining porous polymers built on poly(arylene ethynylene)s are one important topics in the field of porous materials[114] since conjugated microporous polymers (CMPs) with high permanent porosity were presented by Cooper et al.[49] In this paper, the coupling of 1,3,5-triethynylbenzene (TEB) and 1,4-dibromobenzene was employed *via* Sonogashira-Hagihara cross-coupling and the formed insoluble precipitate, namely CMP-1, presented permanent porosity.[49] One striking point for these first CMPs was the applied non-stoichiometric monomer ratio of ethynyl to halogen functionalities of 1.5:1.[49] Further studies by the same group indicated that the small excess of ethynyl groups with respect to halogens yielded higher surface area in various polymeric networks with respect to equimolar ratio of corresponding functionalities (halogen to acetylene).[239] However, that molar ratio was chosen empirically rather than on an understanding[49, 239, 249] and explained as the non-stoichiometric ratio of functional groups drives the reaction further in order to *prevent early stage phase separation*[249] which yields higher surface areas as a consequence of higher polymerisation degrees.[248] Although this assumption is contradictory to the general principle of such step-growth processes which require equimolar functional groups of co-monomers for higher polymerisation degrees,[289] in case of "infinite molecular weight" polymeric network formation, can be applicable to Sonogashira-Hagihara reaction since it is known that resulting polymers from this polycondensation reaction *usually* contain halogens in the end caps instead of terminal alkynes.[272, 273, 290] Thus, introducing an excess acetylene units may carry the polymerisation further.[248, 290] Nevertheless, one should be careful about possible butadienic (homocoupling of acetylenes) defects along the structure will be increased in parallel with the concentration of acetylenic moieties where was also pointed in the latest work of Cooper et. al (Figure C.2.1).[249]

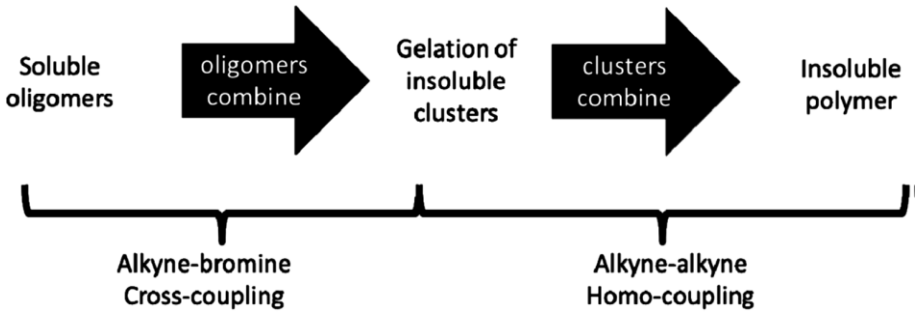

Figure C.2.1: Proposed reaction process of CMP-1 formation with an excess of ethynyl to halogen functionalities.[249]

During the studies on the improvement of the reaction conditions for TTFCMPs, the effect of monomer ratios to surface area has been studied and was found that using an equimolar ratio of functional groups yield materials with higher surface area compared to using a small excess of acetylene which is contradictory to the conditions reported in the literature. Therefore, it was decided to investigate this effect in more detail by applying various monomer concentrations in the synthesis of CMP-1 and studying the effect on the surface area. It should be noted that the reaction conditions were also varied compared to the earlier studies[239] such as use of DMF was preferred as solvent instead of toluene since it was indicated Sonogashira-Hagihara cross-coupling in DMF gave higher surface areas with respect to other frequently used solvents.[240]

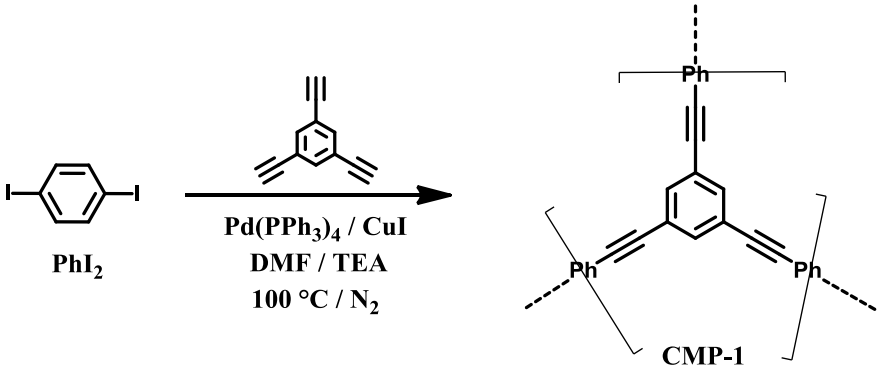

Figure C.2.2: Synthetic scheme of CMP-1 by Sonogashira-Hagihara cross-coupling reaction.

In order to investigate the influence of monomer ratio on the surface area of CMP-1, an exact molar ratio (denoted as **3:2**), a small excess (1.5 eq., denoted as **3:3**) and a large excess (5 eq., denoted as **3:10**) of the ethynyl- to halogen- functionalized monomers was chosen. Furthermore, solely TEB monomer was tested under the same reaction conditions to prove if TEB can undergo a self-reaction. This aspect is critical since acetylene-acetylene homocouplings are known to occur as side products of Sonogashira-Hagihara cross-coupling reaction even though Pd(0) is used under inert atmosphere as discussed above.[288]

After the reactions with different monomer ratios, significant effects on the macroscopic appearance and texture of the synthesised polymeric networks were observed (Figure C.2.3). Indeed, a fluffy pale

yellow powder was collected when the exact molar ratio was used (Figure C.2.3, vial A) while a small excess of TEB (1.5 eq. ethynyl) produced a grey/brown solid with small amounts of pale yellow residues (Figure C.2.3, Vial B). Using a large excess of TEB (i.e. 5 eq. ethynyl per iodo group), a predominantly maroon powder precipitated with both pale yellow and grey/brown particles inside (Figure C.2.3, Vial C).

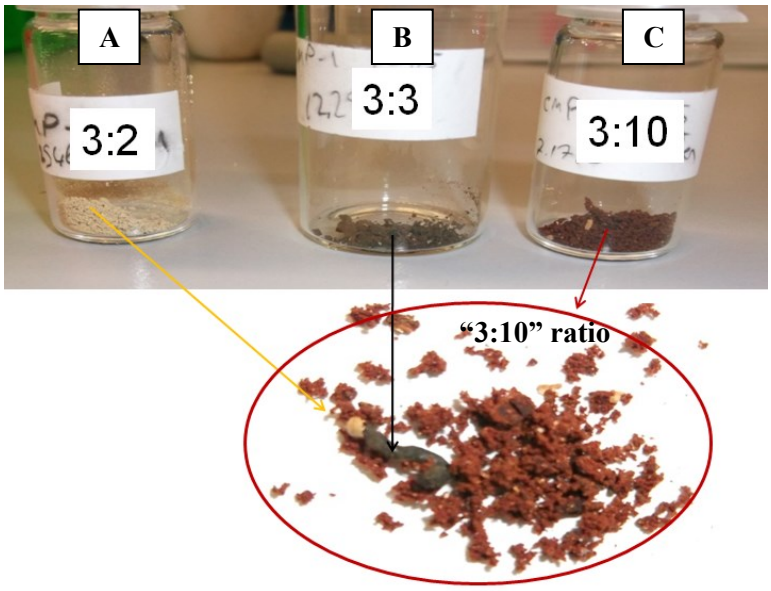

Figure C.2.3: Picture showing the changes in macroscopic appearance of polymers synthesised with varying monomer ratios. The powder shown in the bottom was collected after the reaction using a large excess of TEB (vial C, 3:10 PhI_2/TEB). It can be seen that the powder is inhomogeneous, predominantly maroon with residues of polymers formed from the exact (vial A, 3:2 PhI_2/TEB, yellow powder) and the small excess (vial B, 3:3 PhI_2/TEB) reaction conditions.

The examination of the polymerization yields indicated that homocoupling reactions must have occurred when an excess of TEB was used as the yield were systematically above a 100 % since the theoretical yields were calculated for formation of the ideal structure, i.e. without incorporation of the excess TEB. Although it is common to obtain yields above the theoretical full conversion (typically between 100 and 130 %) due to entrapped solvent molecules, catalyst or terminal groups within the porous structure,[74] the unusual yields of 160 % and 300 % obtained when an excess of TEB was used clearly indicate that the excess of monomer is incorporated within the polymeric structure.

In the following, the control reaction using exclusively the TEB monomer under identical reaction conditions was performed, and unlike CMP-1 networks which have the tendency to precipitate in fewer than 15 mins, no precipitation was observed before two hours. This is not surprising and can be explained comparing cross- and homo-couplings, in which cross-coupling reactions (i.e. the Sonogashira Hagihara coupling) is at least 9 times faster than acetylene-acetylene homo-couplings.[288] After a reaction time of > 2 h, small particles were observed to precipitate and the control reaction was left to run for an additional 72 h like the procedure employed for other CMP synthesis. A dark brown solid which occupied most of the solvent volume was isolated (denoted as H-AcAc), and soxhlet

purification applied with MeOH and THF. Unlike the other polymeric networks described in this section, H-AcAc shrinked rapidly during the drying process under vacuum at 90 °C and a yield of 124% (this time calculated for the idealized structure shown in Figure C.2.4) was recorded which is probably due to remaining DMF or catalyst residues within the pores.

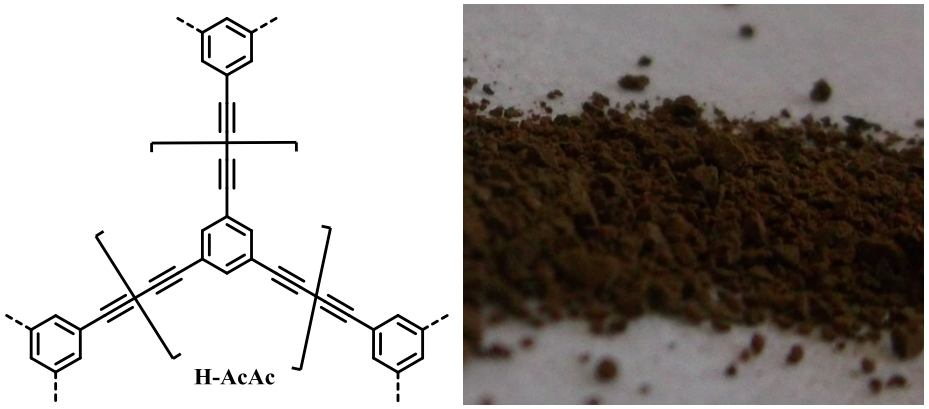

Figure C.2.4: Ideal structure of homopolymerised TEB and dark brown powder of the obtained polymer.

N_2 sorption measurements were carried out for all the polymers (Table C.2.1). The evaluation of surface area as a function of the monomer molar ratio yield a different tendency as the one reported in a similar study performed with toluene as a solvent.[239] Indeed, it was reported that the use of 1.5 equivalents of ethynyl to halogen functionalities yield polymers with the highest surface area and that the surface area was lower when either the equimolar ratio was used or the excess of ethynyl groups was further increased.[239] In our case, however, the surface area measured for the polymers synthesised with an exact molar ratio (3:2) and a small excess of TEB (3:3) were similar, i.e. around 750 m^2g^{-1}. When the ethynyl content was further increased to 5 eq. per iodo group (3:10) the surface area was measured to be even significantly higher (1150 m^2g^{-1}) which is the highest surface area among all the polymers studied. The surface area of the latter polymer was recorded in the same range with the TEB homopolymer, H-AcAc, indicating that a high degree of homocoupling/side-reactions occurred when ahigh excess of acetylene groups (3:10) were applied to obtain CMP-1 and that these homocouplings are responsible for the increased surface area.

Table C.2.1: Effect of different molar ratios on CMP formation. The yields for CMPs were calculated according to the theoretical ideal structure formation (without incorporation of excess TEB).

PhI_2/TEB Ratio	**Ethynyl/Halogen Ratio**	**Solvent**	**Yield, %**	**T, °C**	**Surface Area (m^2g^{-1})**	**$V_{0.1}$[a] (cm^3g^{-1})**	**V_{total}[b] (cm^3g^{-1})**
3:3 (ref[49])	1.5/1	Toluene	65	80	834	0.33[c]	0.47[d]
3:2	1/1	DMF	105	100	759	0.69	0.42
3:3	1.5/1	DMF	160	100	749	0.42	0.69
3:10	5/1	DMF	300	100	1150	0.69	0.64
H-AcAc	--	DMF	124	100	1010	0.94	0.39

[a]pore volume at P/P_0 = 0.1 [b]total pore volume at P/P_0 = 0.95 [c]micropore volume was calculated by using the t-plot method based on the Halsey thickness equation [d]total pore volume at P/P_0 = 0.99.

The overall shape of the isotherms changed along with the reaction conditions used and gave additional information on the resulting changes in porosity (Figure C.2.5-A). Generally, a high uptake at low relative pressures was observed indicating a pronounced level of microporosity, as typically observed for CMP-1 synthesised in toluene[49, 239] or in DMF.[240] The polymers synthesised from exact monomer ratios (3:2) and small excess acetylene (3:3) did not indicate a significant difference for the obtained SAs and QS-DFT pore size distributions (Figure C.2.5-B), however while polymer 3:3 showed a nearly perfect *Type I* isotherm, 3:2 polymer had an additional steep increase in the nitrogen volume adsorbed at high relative pressures of the isotherm, which is commonly explained as inter-particulate adsorption. Polymer 3:10 exhibited a small hysteresis and showed a similar isotherm shape and QS-DFT pore size distribution as H-AcAc. The hysteresis and the observed uptake in the mesoporous pressure range point to a more complex pore geometry with pores of different shapes and sizes (mainly microporous with some larger micropores and smaller mesopores) and/or to cavitation effects.

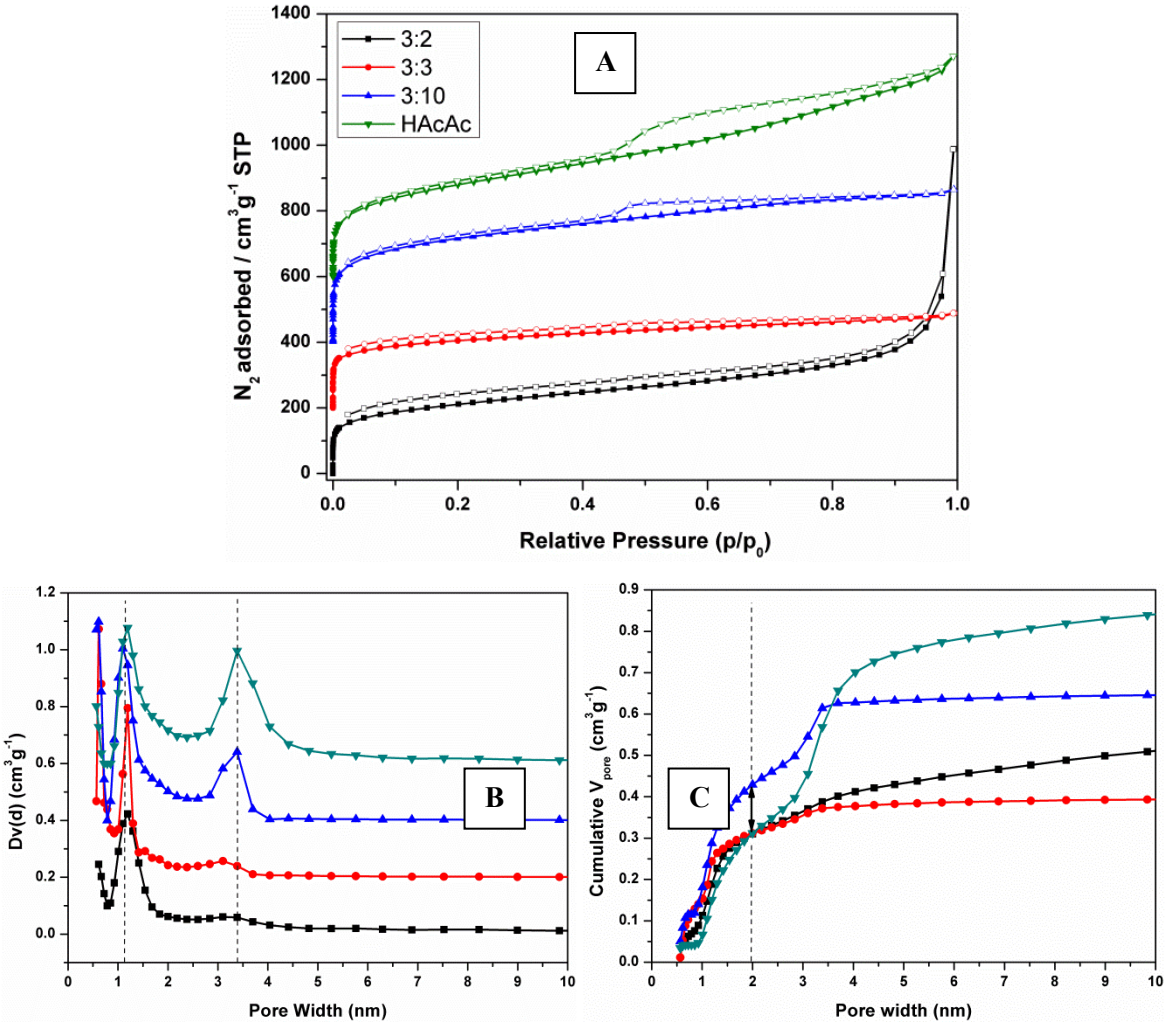

Figure C.2.5: Graph A represents N_2 sorption isotherms (the 3:3, 3:10 and H-AcAc isotherms were shifted up by 200, 400 and 600 cm^3g^{-1} respectively) Graph B shows the plots of QS-DFT pore size distributions (the 3:3, 3:10 and H-AcAc pore size distributions were shifted up by by 0.2, 0.4 and 0.6 cm^3g^{-1} respectively) Graph C demonstrates the plots of "cumulative pore volume" to the pore sizes for the CMPs with different PhI_2/TEB ratios.

This difference could point to an additional condensation mechanism in polymer 3:3. Using an exact molar ratio (polymer 3:2) yield precipitation of small, microporous polymer particles, showing a high external surface area whereas when the excess of TEB was used in polymer 3:3 can now yield an additional cross-linking of the first formed CMP-1 particles (i.e. *gelated insoluble cluster*[249], Figure C.2.1) with a following ethynylene homo-coupling. Thus, the crosslinking of the CMP-1 particles which will create a second microporous polymer phase can be seen in the large reduction of external surface area which is similar to the *post-synthetic modification*s of microporous polymers which have been studied intensively.[91, 291, 292]

The effects of further crosslinking can also be detected from the isotherm of polymer 3:10 which showed the highest N_2 uptake in the micropore range. QS-DFT calculations of cumulative pore volume (Figure C.2.5-C) can be helpful at this stage in order to visualize the porous behaviour of the polymers by indicating the contribution of the pore sizes to the adsorbed N_2 volume although these values are calculated for perfect porous carbon structures. The adsorbed N_2 volume below the micropore range (< 2 nm) was nearly identical for all polymers except polymer 3:10. The apparent highest amount of micropore contribution to total amount of condensed nitrogen is responsible for the obtained highest surface area of polymer 3:10 polymer. As indicated above, the combination of the microporosity of ideal CMP-1 structure and additional microporosity obtained by the further coupling may result the highest surface area. Note that the additional but fully separated formation of individual homocoupled polymer, namely H-AcAc, in the final mixture has to be considered since different fractions can be observed from the powder of polymer 3:10 (Figure C.2.3).

For further structural characterisation, ^{13}C cross-polarization magic-angle spinning (CP-MAS) NMR spectroscopy was performed for all polymers (Figure C.2.6). The peaks at δ = 128.9 and 121.1 ppm can be assigned to the tertiary and quaternary aromatic carbons, respectively, whereas the peak at δ = 87.9 ppm can be assigned to the internal acetylenes (-C≡C-) in the ideal CMP-1 structure and the peak at δ = 79.4 ppm to non-reacted terminal acetylenic moieties (≡C-H).

Furthermore, the appearance of the additional peaks with the further increase of TEB equivalent should be as a consequence of alkyne-alkyne homocouplings which can be notified by the peak at δ = 134.7 ppm with the multiple peaks in the acetylenic region (i.e. δ = 80 - 100 ppm range). Interestingly, for a perfect butadienic (homocoupled alkynes) contribution, expected impurities should be visible as one extra acetylene peak (-C≡***C***-***C***≡C-) with overlapped or indistinct shoulders since the other carbons along the homocoupled polymer is nearly chemically identical.

In this aspect, several reports in literature were referred to described the formation of the issued additional peaks where it is found that enynes are formed as side products in the synthesis of butadienic structures in presence of palladium catalyst.[293-295] Thus a fair assumption would be that the peak appearing at δ = 134.7 ppm can be assigned to enyne double bonds within the structure.[296]

Furthermore, the peaks in the δ = 80 - 100 ppm range should be due to formation of several non-identical acetylenic carbons. Following the same assumption and according to the literature reports, the peaks in the acetylenic region at 94.6 ppm could be assigned to the non-neighbouring acetylene carbon of enynes (=C-C≡***C***-Ph),[297] while the ones at 79.9 ppm can be assigned to terminal alkynes (≡***C***-H)[298] and the resonance at 72.0 ppm to the internal diyne carbons (Ph-C≡***C***-***C***≡C-Ph).[299] Two peaks might overlap in the broad region near 87.9 ppm, representing the external (Ph-***C***≡C-C≡***C***-Ph) carbons of diyns and acetylene carbons near the double bond of an enyne (=C-***C***≡C-Ph).[296, 299]

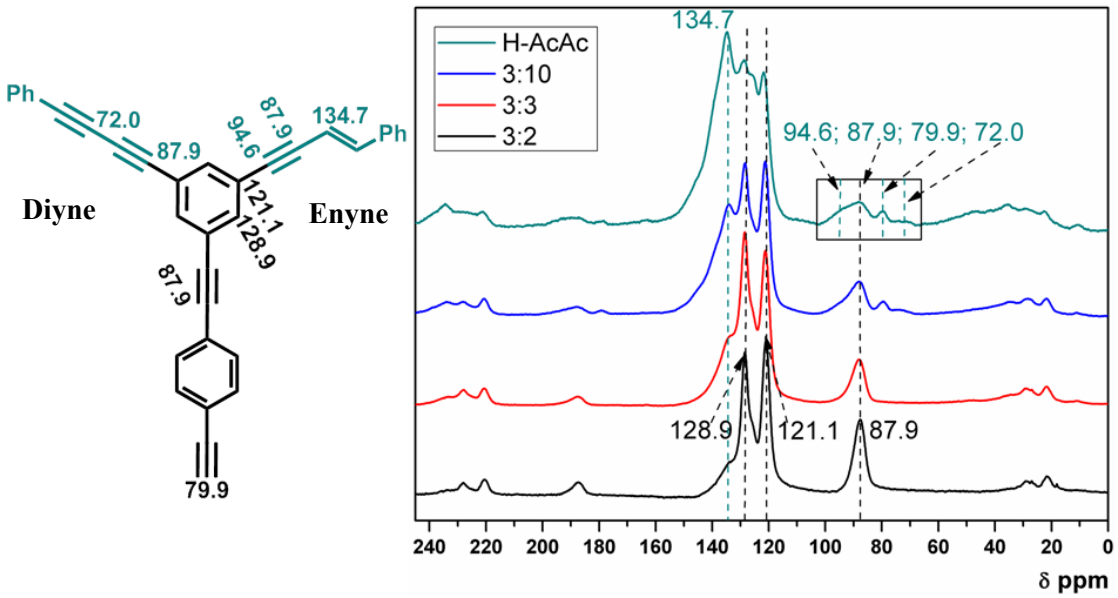

Figure C.2.6: Solid state ^{13}C CP-MAS NMR spectra for H-AcAc and TTFCMPs synthesised with different molar ratios.

This aspect is critical as it was reported that the homopolymer (HCMP-1) prepared from TEB with catalytic Pd(II) species (Figure C.2.7-A) is highly porous (842 m^2g^{-1}) and showed a N_2 sorption isotherm closer to *type I* (Figure C.2.7-C) with respect to H-AcAc (Figure C.2.5-Graph A).[298] A comparison with the published solid state NMR spectrum of this TEB homopolymer, HCMP-1, clearly indicates that higher content of the terminal alkynes can be found than H-AcAc judging by the sharp peak at δ = 82.7 ppm (Figure C.2.7-B). This could be due to lower polymerisation degrees of HCMP-1 in toluene with respect to H-AcAc in DMF where similar behaviour was also indicated in literature for CMP formations *via* Sonogashira-Hagihara cross coupling.[240] Additionally, comparison of the surface areas of the final polymeric networks can help at this point where HCMP-1 gave 842 m^2g^{-1} whereas H-AcAc has a surface area of 1050 m^2g^{-1} which is highly probably due to further polymerisation of oligomers in DMF.[240, 248]

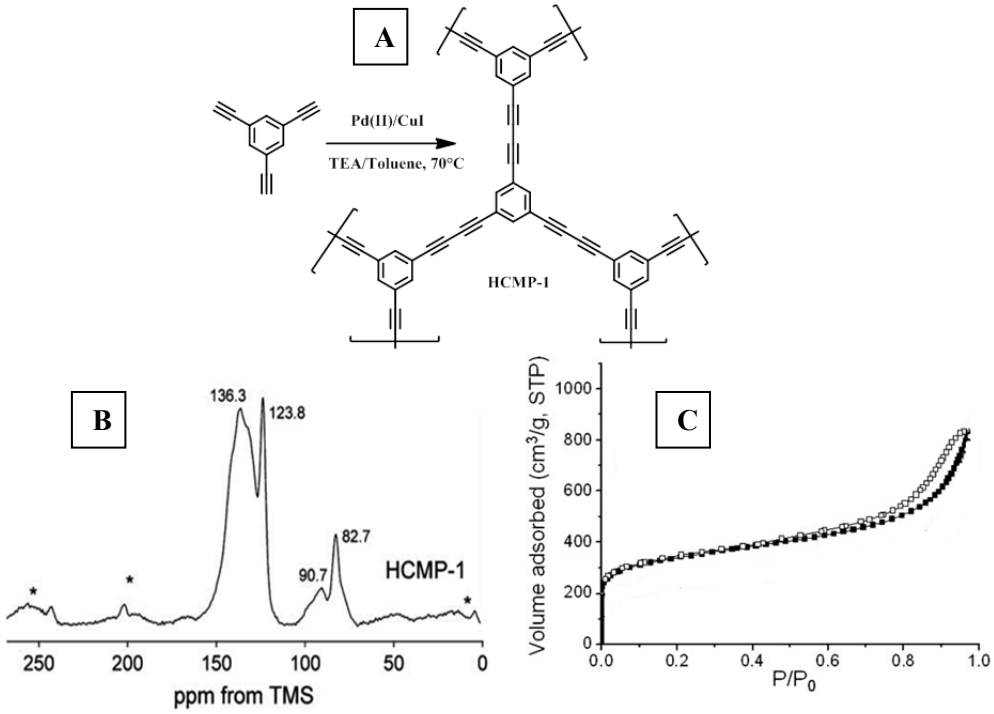

Figure C.2.7: Ideal structure of TEB homopolymer (HCMP-1) prepared with Pd(II)/CuI as catalytic system (A). ^{13}C solid state NMR spectra (B) and N_2 sorption isotherm (C) of HCMP-1 (figures retrieved from ref[298]).

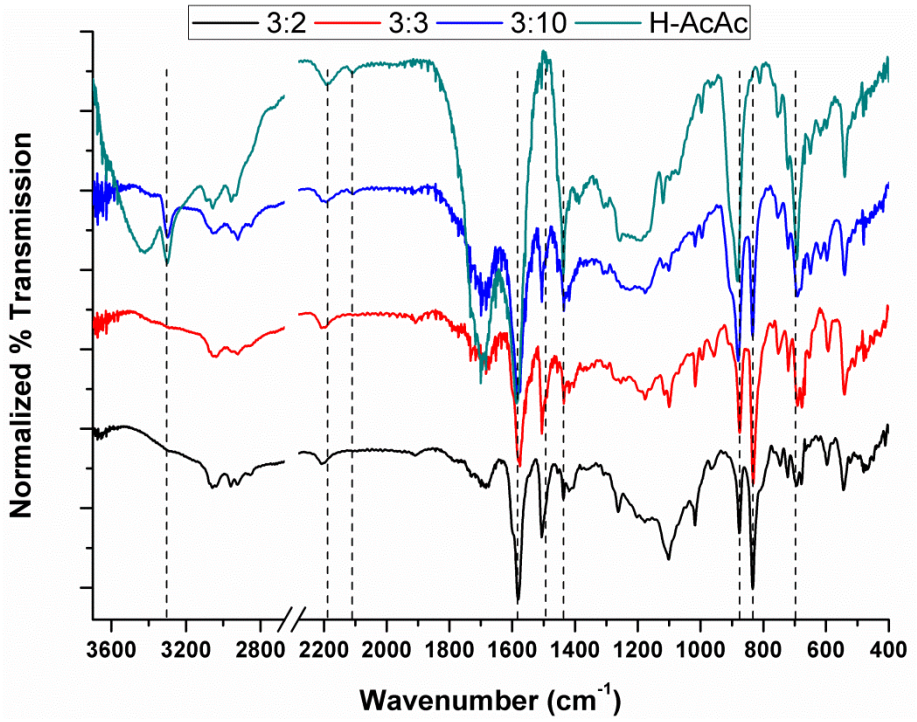

Figure C.2.8: FT-IR spectra of the CMPs with different molar ratios.

FT-IR spectra of the polymer networks confirmed the expected differences in the polymer structure (Figure C.2.8). The peak at 2188 cm^{-1}, characteristic of internal alkynes can be seen for each network. The terminal acetylene vibrations at 2109 cm^{-1} along with an intense band at 3297 cm^{-1} were attributed

to the stretching mode of terminal C-H acetylene bond are only visible for H-AcAc and for polymer 3:10 (Figure C.2.6) with the strong peak due to C-H deformation of terminal acetlyenes at 695 cm^{-1}.

Additionally, in the –C=C– stretching region of benzene moieties two peaks were observed for H-AcAc (1575, 1431 cm^{-1}) whereas the copolymerised networks showed three peaks (1575, 1506, 1431 cm^{-1}) with an additional peak probably arising from the 1,4-functionalised benzenes moieties. Moreover in case of H-AcAc, the only peak in the region of the –C-H *out of plane* bending of benzenes (600 – 900 cm^{-1}) was observed at 876 cm^{-1} and the absence of the peak at 832 cm^{-1} which was observed for CMP-1 based systems is probably due to the same reason.

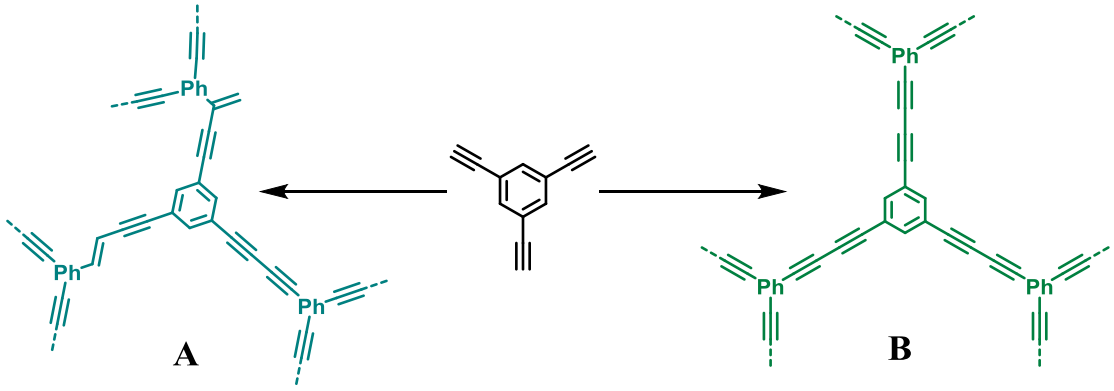

Figure C.2.9 Proposed structures for H-AcAc. Structure A is more probable considering the results discussed above compared to the idealised homocoupling of TEB (structure B).

In conclusion of this section, different monomer ratios in the synthesis of CMP-1 have been employed and the effect on chemical structure and porosity of the resulting networks has been investigated. This study was mainly motivated by the original report on CMP-1 and also later works on polymer networks prepared by Sonogashira-Hagihara coupling as described that an excess of the acetylene monomers are needed to yield high surface area in which contradicts with the common idea of equimolar functionalities for higher degrees of step-growth co-polymerisation. Depending on the applied conditions in this work, it was observed that using a small excess molar amount of TEB does not change the surface area from the equimolar ratio. On the other hand, using a large excess of TEB causes a significant increase of the surface area, and also the homopolymer made exclusively out of TEB has a much higher surface area then the one reported for CMP-1. There is therefore a certain risk that in the conventional CMP-1 synthesis using an excess of TEB results a second polymer phase is formed yielding further crosslinking of the first formed *gelated insoluble clusters* likewise the postulation by Cooper *et al.* in a recent publication[249] with following acetylene-acetylene homocoupling as second polymer phase can artificially increase the surface area of the assumed Sonogashira networks. Therefore the increased surface area found in Sonogashira derived networks using an excess amount of TEB can, as copolymerization theory predicts, not explained by higher polymerization degrees, but by the formation of a second, high surface area phase generated by homocoupling of the excess TEB monomers. Furthermore, it was shown that homocouplings of

acetylenic moieties form enynes and diynes within the structure under Sonogashira conditions, which result in structural variations to the idealized acetylene homocoupling network (e.g. HCMP-1)[298]

C.3. DITHIENOTHIOPHENE BASED CONJUGATED MICROPOROUS POLYMERS

Dithienothiophenes (DTTs) have been discussed in the previous chapter and their applications ranging from organic electronics to catalysis have already been mentioned.[177, 192, 216-218, 300, 301] Notably the extended conjugated system which is provided by the three fused thiophene rings proved to be beneficial and was consequently highly exploited for applications in OFETs and organic solar cells.[179, 184-186, 188-190] Furthermore, derivatives of DTT such as *S,S*-dioxides are frequently used in OLED applications due to their enhanced luminescence properties, and tunability of their spectral responses with various co-monomers.[192, 212, 213, 302] As it was stated in the chapter on TTFCMPs, the use of electron rich heteroatom based monomers as building blocks to obtain functional porous polymers is an emerging topic, especially, regarding potential organoelectronic applications.[105, 106, 229] In this aspect, thiophene derivatives are good candidates to be introduced into porous polymers due to their numerous applications in the field of (opto)electronics and sensing.[177, 180, 193, 230-232, 300-305] However, devices based on thiophenic porous materials have not been able to present outstanding properties so far.[106, 306, 307] Nevertheless, their high potential was predicted in recent perspective articles which strongly proposes 2D/3D compounds are promising materials to be applied in organic electronic devices.[103, 104]

In order to obtain a novel thiophene based CMP, we collaborated with Prof. Dr. Turan Ozturk and Dr. Ipek Osken from Istanbul Technical University who have recently investigated the electronic capacitance behaviour of a DTT monomer with peripheral thiophenes ($DTTPh_2$-Th_4, Figure C.3.1).[308]

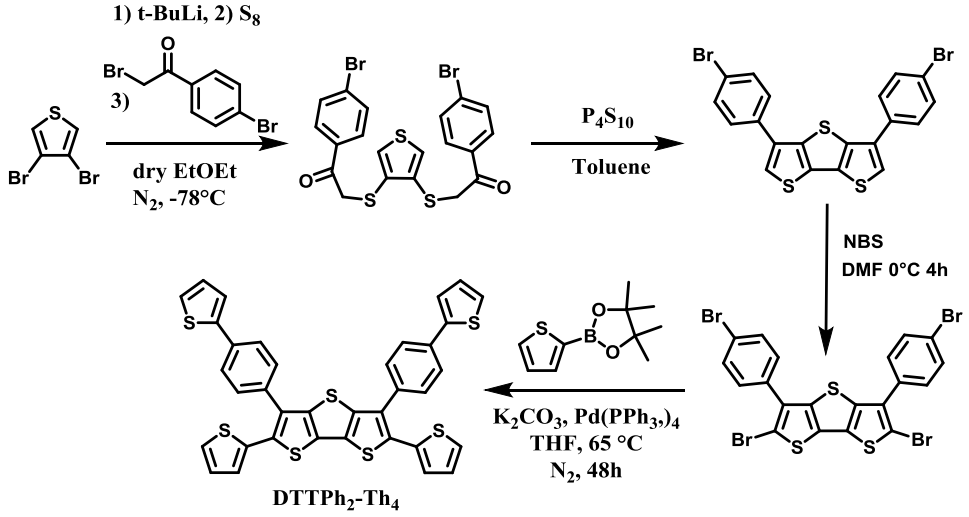

Figure C.3.1: Synthesis of $DTTPh_2$-Th_4.[308]

This monomer appeared interesting to us for two different reasons. First it would allow obtaining a novel CMP with a functional DTT core. More interestingly, since the peripheral thiophenes in this DTT derivative are not chemically identical, the morphology of the polymer could be possibly tuned

electrochemically from a linear to a cross-linked structure (Figure C.3.1). Thus, a porous CMP-film could theoretically be addressed and compared to its linear analogue.

For the preparation of a CMP based on the $DTTPh_2$-Th_4 *via* oxidative polymerisation, the corresponding monomer was dissolved in $CHCl_3$ and added to the slurry of $FeCl_3$ in $CHCl_3$ at room temperature under inert atmosphere (Figure C.3.2). After one day the formed precipitate was isolated by filtration and the polymer (denoted as DTT-CMP) was collected after extensive washing as an insoluble red powder in 82% yield. Nitrogen sorption analysis indicated the DTT-CMP exhibits a SA of 790 m^2g^{-1}, a value comparable to other microporous polymers synthesised *via* oxidative polymerisation.[50, 86, 309]

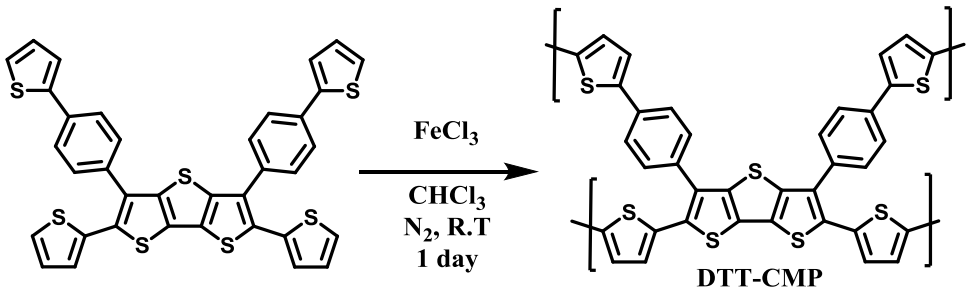

Figure C.3.2: Synthesis of DTT-CMP *via* Fe^{3+}-catalysed oxidative polymerisation.

In the next step, the chemical oxidation/reduction of the DTT-CMP was attempted in order to compare electronic and physical properties of pristine and doped material. For this purpose, the network was exposed to I_2 crystals in a closed vessel in order to locally form charge transfer salts between the thiophenic moieties and iodine resulting in an oxidised polymer (denoted as DTT-CMP^+-I_n^-; Figure C.3.3). Upon exposure to iodine vapour, the red colour of the DTT-CMP quickly turned darker and showed a dark maroon colouration after 30 mins (Figure C.3.3, picture B) which progressively turned to black, as expected for such oxidation process in thiophene based materials, by extending the exposure time to 24 h. To ensure complete (or maximal) oxidation of the network, the iodine exposure was conducted over 7 days in total.

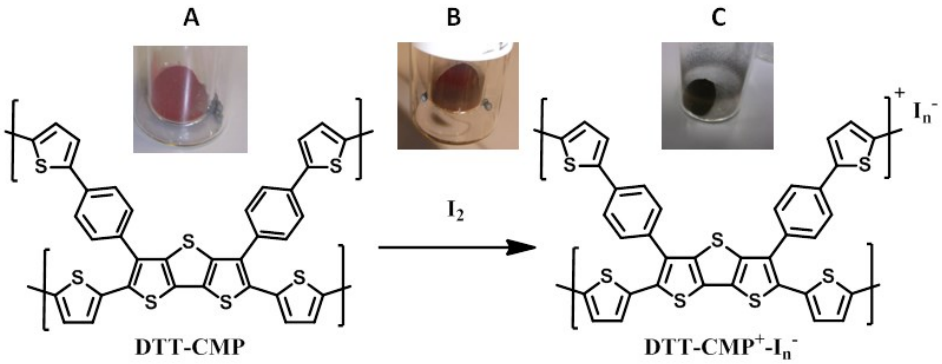

Figure C.3.3: Chemical oxidation of DTT-CMP to DTT-CMP^+-I_n^- *via* iodide charge transfer salt formation. Picture A represents the pristine DTT-CMP network over I_2 crystals. Pictures B and C were taken after 30 mins and 7 days of iodine exposure, respectively.

Before further characterisation, the excess of iodine in DTT-CMP$^+$-I_n^- was removed by treating the network at 40 °C under vacuum overnight as indicated by the significant weight loss observed after the evacuation step (the iodide/monomer ratio dropped from 6.14 to 1.06, Table C.3.1). Besides removal of unreacted iodine from the system, it is probable that the charge-transfer salts formed with peripheral (bi)thiophenes were also neutralized and removed. This observation is in agreement with the reported decomposition of thiophene-iodides charge transfer salts, as they are known to be unstable under vacuum.[310] DTTs, on the other hand, should form more stable charge transfer salts located on the central ring due to strong cross conjugation with the two neighbouring fused thiophene rings. Thus, the remaining iodide charge transfer may only be located on the central ring of the DTT moieties. Furthermore, since the equivalent of iodide is nearly equimolar like the examples in literature, it is assumed that only mono iodides are present in the network (DTT-CMP$^+$-I^-).

Table C.3.1: Iodine doping of DTT-CMP.

DTT-CMP		**DTT-CMP$^+$-I_n^-**	**DTT-CMP$^+$-I^-[a]**
Pristine DTT-CMP (mg)	Pristine DTT-CMP (mmol)[b]	I^- uptake (mg[c]-**mmol**[d]-I^-/DTT[e])	I^- uptake (mg[c]-**mmol**[d]-I^-/DTT[e])
33.6	0.05[b]	38.9[c]-**0.31**[d]-6.14[e]	6.7[c]-**0.05**[d]-1.06[e]

[a] after vacuum treatment at 40 °C, [b] theoretical value assuming formation of an ideal DTTPh$_2$-Th$_4$ network, [c] total uptake of I_2 in mg, [d] calculated mol of formed iodides from the gravimetrical uptake [e] molar ratio of iodide uptake to DTTPh$_2$-Th$_4$ moieties in the network.

The N_2 sorption analysis of the DTT-CMP$^+$-I^- revealed an expected reduction of the SA to 380 m^2g^{-1} (from initially 790 m^2g^{-1}), presumably mainly as a result of iodide pore-blocking within the network. This effect is reflected in the corresponding sorption isotherms as a decrease in the overall gas uptake, notably at low relative pressures (Figure C.3.4-A).

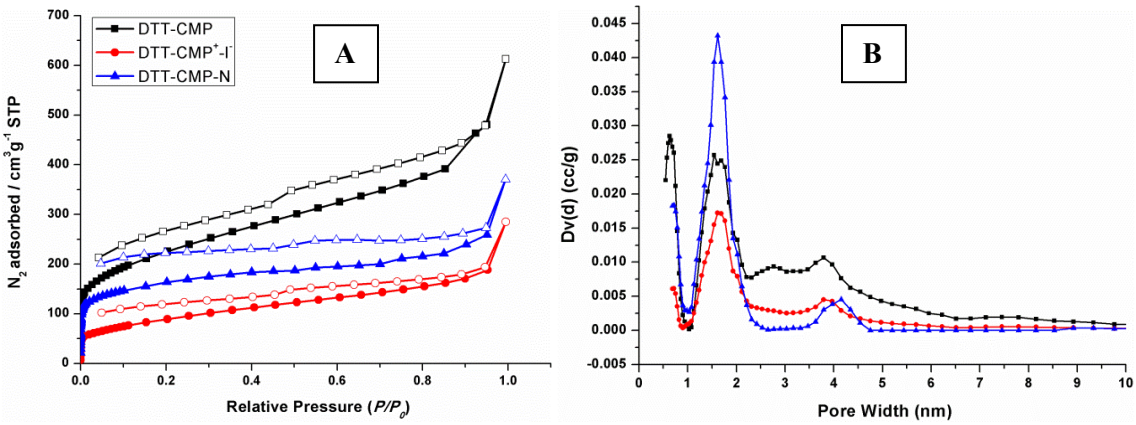

Figure C.3.4: N_2 sorption isotherms (A) and NL-DFT pore size distributions (B) of the DTT-CMPs.

The corresponding pore size distributions revealed a specific blockage of the smaller pore population occurred within the structure (Figure C.3.4-B). It should also be mentioned that the weight increase of

the building blocks due to iodine incorporation will also contribute distinctly to the observed reduction in the gravimetric SA.

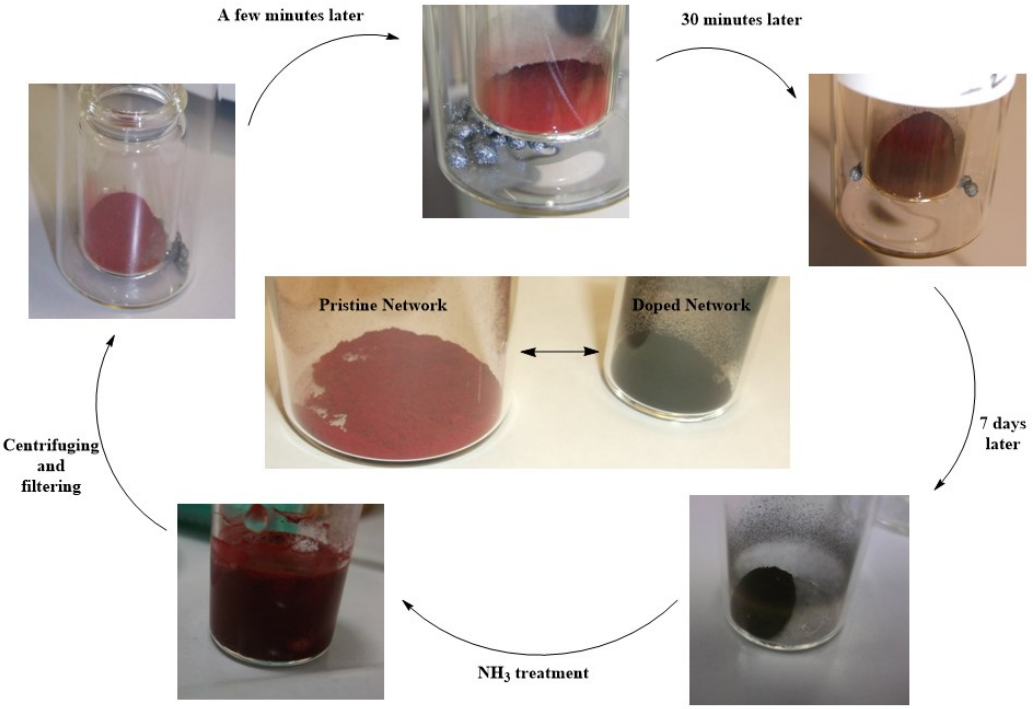

Figure C.3.5: Pictures of the different states of the DTT-based CMPs.

Unlike TTFCMPs, the chemical reduction of the network to its initial oxidation state is possible for thiophenic systems and was attempted by treating DTT-CMP$^+$-I$^-$ with NH_3,with the aim to decompose all charge transfer salts by removal of all iodides as ammonium salt ($NH_4^+I^-$), thus achieving a full chemical oxidation/reduction of the network.[311-314] Exposure of DTT-CMP$^+$-I$^-$ to ammonia gas ($NH_{3(g)}$) resulted in a macroscopic colour change of the material. Nevertheless, since a gas phase ammonia treatment will probably not remove the formed ammonium salts which will remain within the network, the DTT-CMP$^+$-I_n^- network was stirred in an aqueous 32% ammonia solution for a period of 2 h. Subsequent washing/centrifuging and drying at 90 °C (overnight) resulted in a network (denoted as DTT-CMP-N) with a satisfactorily increased SA of 568 m^2g^{-1}. Even though, after the treatment in ammonia solution, the SA of the pristine CMP material could not be fully recovered.

FT-IR spectroscopy analysis of the DTT-CMP polymers after the successive chemical treatments revealed the reversibility of the oxidation-reduction process. The expected changes in the *stretching* and *bending* vibrations for typical thiophenic materials have been observed (i.e. for DTT-CMP, DTT-CMP$^+$-I_n^-, DTT-CMP$^+$-I$^-$, DTT-CMP-N; Figure C.3.6). [261, 315, 316]

The spectra of the doped polymers (Figure C.3.6) revealed an overall enhancement of band intensities probably caused by the polarisation of the network especially observed for the *C=C* stretching bands and the ring deformation bands at 1178, 1261 and 1335 cm^{-1} that were reported for similar thiophene

based structures.[261, 315, 316] Moreover, reduction of the intensities of the *-C-H in plane* bending vibrations (i.e. 1020, 1042 and 1092 cm^{-1}) after the 40 °C heat treatment under vacuum can be attributed to the partial reduction of the polymer network occurring at the hydrogen rich (bi)thiophenic moieties. This observation can also be compared to similar examples reported in literature.[261, 262] Ammonia treatment of DTT-CMP^{+}-I^{-} produced a material showing an almost identical spectrum to that recorded for the pristine DTT-CMP.

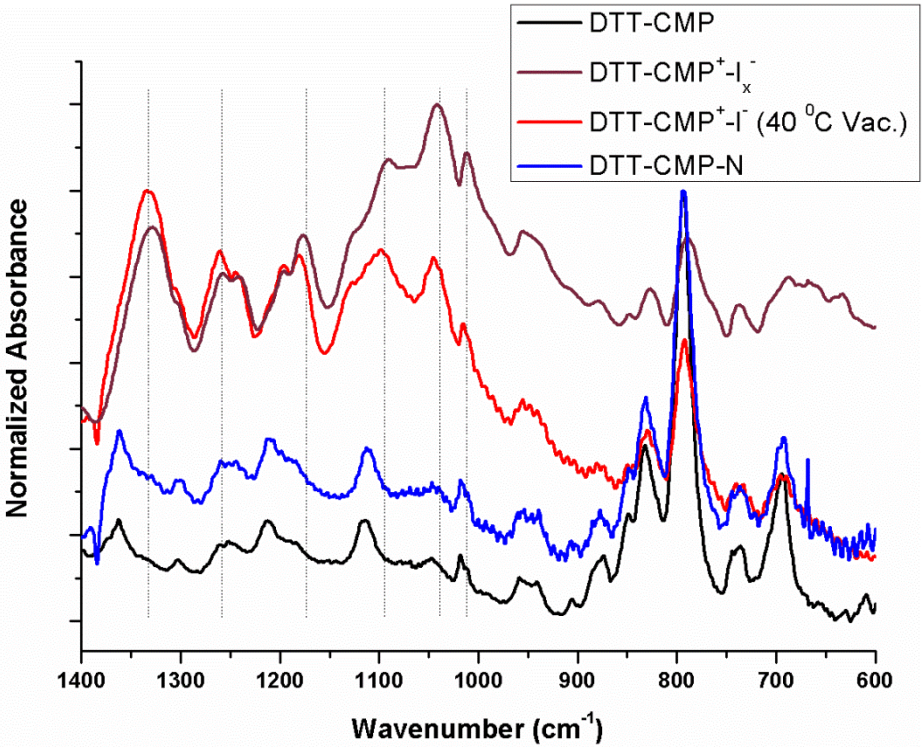

Figure C.3.6: FT-IR spectra of DTT-CMP, DTT-CMP^{+}-I_n^{-}, DTT-CMP^{+}-I^{-} and DTT-CMP-N.

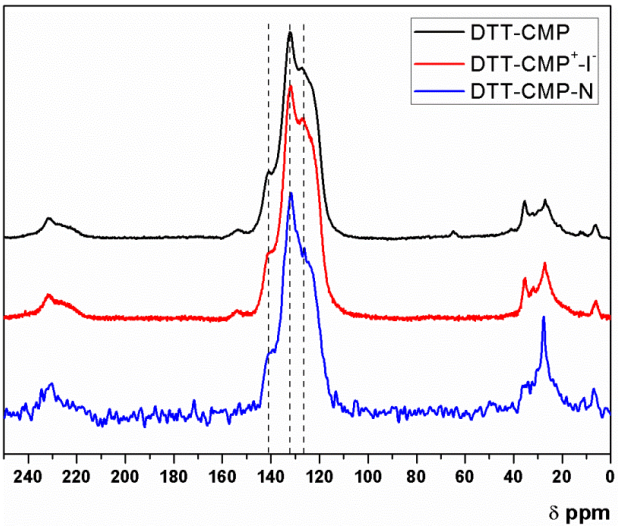

Figure C.3.7: ^{13}C CP-MAS NMR spectra of the synthesised DTT-CMP, DTT-CMP^{+}-I^{-}, and DTT-CMP-N polymers.

Since aromatic behaviour along sp^2 carbons are not altered significantly during the chemical redox process, the ^{13}C CP-MAS NMR spectra of the DTT-based CMP networks did not change dramatically

(Figure C.3.7). However, resonances at δ = 132 and 127 ppm should be representing the tertiary carbons of benzene and thiophenes, respectively, judging by their high intensities in the decoupling method. The shoulder at δ = 141 ppm can be assigned to carbons of DTT core and α-carbons of (bi)thiophenic units due to their highly conjugated quaternary form.

Electrochemical polymerization of $DTTPh_2$-Th_4 has also been investigated as another approach to obtain DTT-CMP network (Figure C.3.8).

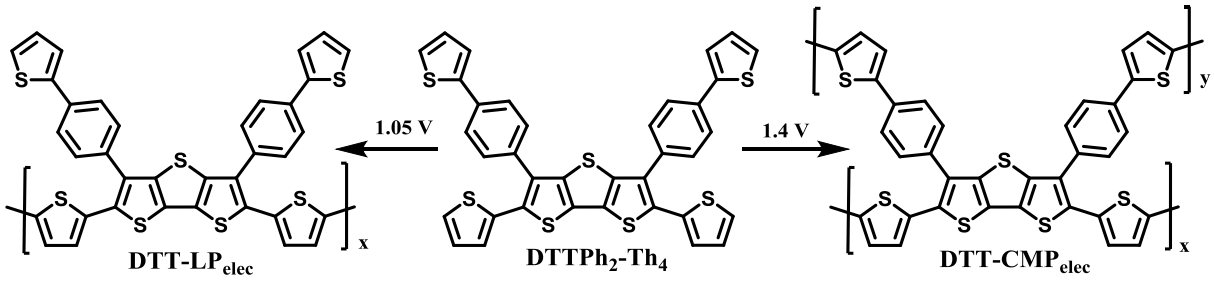

Figure C.3.8: Electropolymerisation of $DTTPh_2$-Th_4 in different potential range to obtain linear (DTT-LP_{elec}) and cross-linked (DTT-CMP_{elec}) analogues.

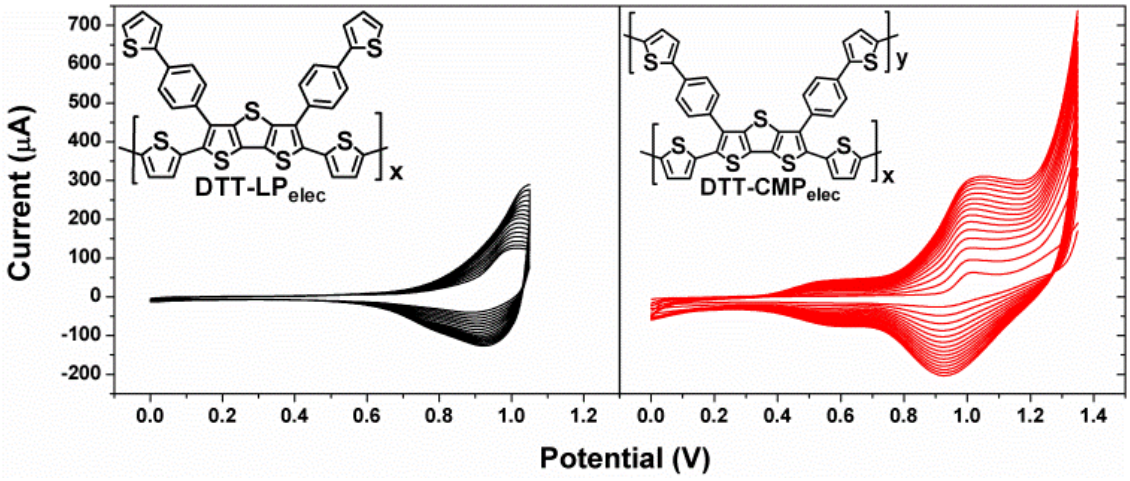

Figure C.3.9: Cyclic voltammograms of DTT-LP_{elec} and DTT-CMP_{elec} reactions were performed in an electrolyte solution of $NaClO_4$/$LiClO_4$ mixture (0.1 M / 0.1 M) in ACN/DCM (9:1 v/v) where the reference electrode was Ag/AgCl, and Pt wires were employed as both counter and working electrodes.

By considering the non-identical environment of the peripheral thiophenic units, the $DTTPh_2$-Th_4 monomer can be polymerized in a linear (DTT-LP_{elec}) or a cross-linked fashion (DTT-CMP_{elec}). Indeed, the regiospecific linear polymerisation at lower potentials selectively occur at the thiophenes directly attached to the DTT core since they have a lower first oxidation potentials due to an increased conjugation with the adjacent thiophenic moieties, (i.e. bithiophene have a lower first potential with respect to thiophene).[317]

The anodic scan of the monomer in two different potential ranges exhibited different cyclic voltammograms (Figure C.3.9). The scan between 0 – 1.05 V yielded a linear polymer deposition through the polymerization of the thiophenes directly connected to DTT moieties (designated as DTT-LP_{elec}). When the upper limit of the scan range was set to 1.4 V (in a fresh electrolyte solution, in

the same conditions, i.e. electrolyte, concentration of monomer), an additional peak at *ca*. 0.5 V was observed after the polymer growth over the working electrode. This peak is attributed to the enhanced electron density as a consequence of additional conjugation obtained in phenylic thiophenes after cross-linking of monomer (DTT-CMP_{elec}). However, it is not possible to obtain a perfect equimolar cross-linking of the thiophenes in the two different environments although the DTT-CMP_{elec} structure should contain defects (i.e. x should be slightly higher than y, Figure C.3.8). Similar electrochemical response have been observed during the potential-controlled electro-deposition of related compounds *via* altering the scan range.[318, 319]

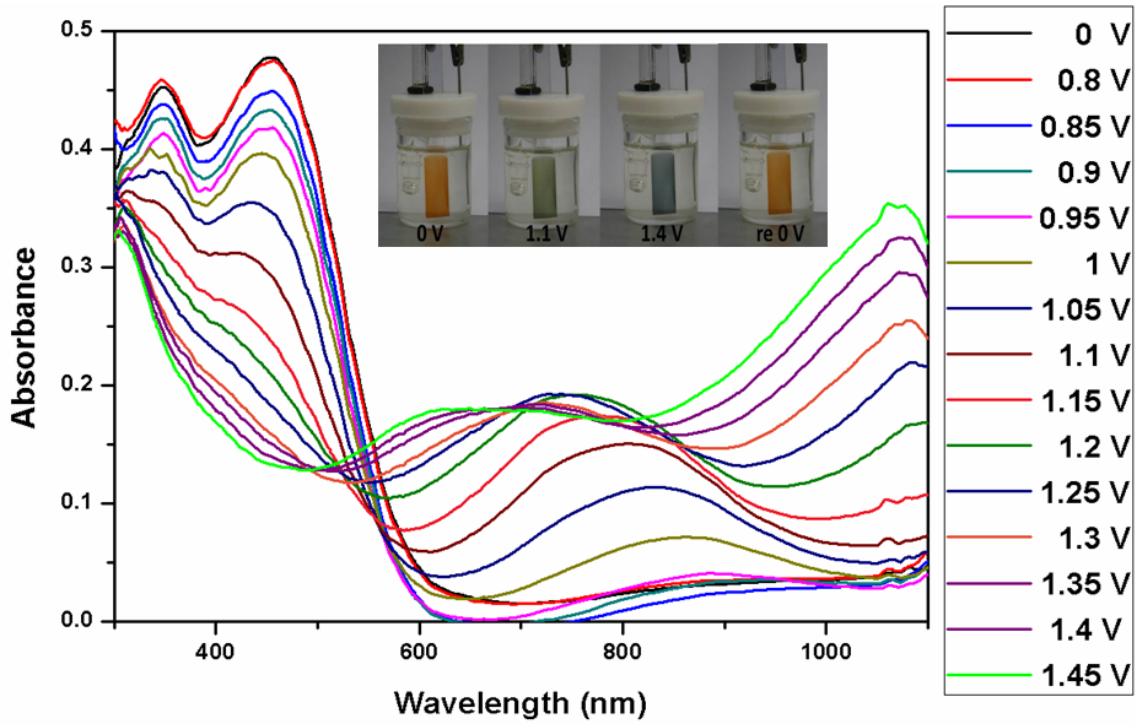

Figure C.3.10: Spectroelectrochemical investigation of DTT-CMP_{elec}.

Spectroelectrochemical measurements for DTT-CMP_{elec} were performed to investigate optical redox response (Figure C.3.10). For this purpose, $DTTPh_2$-Th_4 was coated on an indium tin oxide (ITO) electrode under the same conditions as described above. The DTT-CMP_{elec} modified ITO working electrode was then placed in a monomer-free electrolyte solution ($NaClO_4$/$LiClO_4$ mixture (0.1 M / 0.1 M) in ACN/DCM (9:1 v/v)) in a UV cell with a reference (Ag wire) and a counter electrode (Pt wire). Absorbance spectra in different potentials were identical until 1.0 V where a new peak appeared at *ca*. 855 nm (formation of polarons over DTT-CMP_{elec}). Further increasing the potential resulted in this peak shifting to shorter wavelengths where a new peak at *ca*. 1080 nm appeared at 1.2 V (formation of bipolarons over DTT-CMP_{elec}), which reached a maximum intensity at a potential of 1.4 V. Finally, the initial absorption spectrum was observed again when the potential was set back to 0.0 V that proves the reversibility of the process. Furthermore, macroscopic photochromism of the DTT-CMP_{elec}

film was visible as the initial orange red film (0 V) turned light green (1.2 V) and finally light blue (1.4 V) before showing its initial orange red colour when 0 V was reapplied (inset of Figure C.3.10).

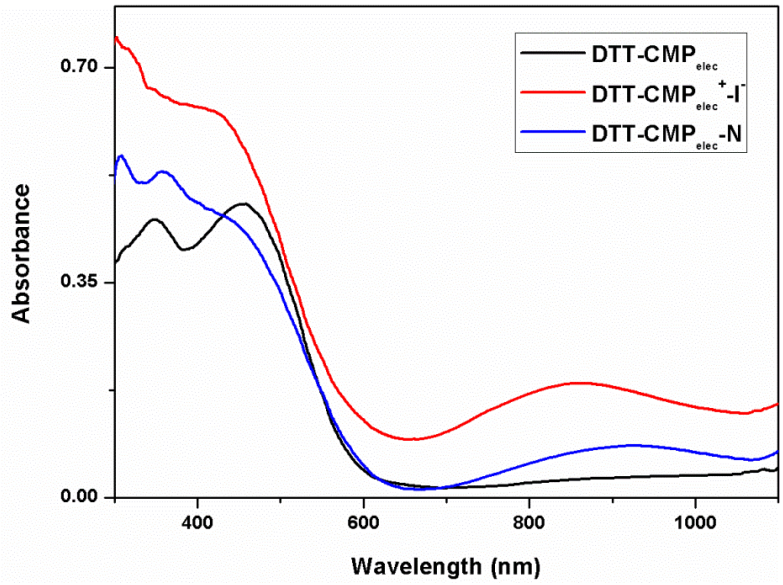

Figure C.3.11 UV-Vis measurement of DTT-CMP$_{elec}$ and its doped-dedoped forms on ITO substrate.

Investigations on the chemical doping of DTT-CMP$_{elec}$ were also performed by introducing the coated ITO substrate into a vessel filled with iodine crystals. After sealing the reaction vessel, the orange pristine films started to get darker and after 1 day exposure a dark maroon DTT-CMP$_{elec}^{+}$-I^{-} was obtained. Interestingly, the colour of the film became dark red in ambient atmosphere probably due to partial reduction of doped states. Nevertheless, UV-Vis measurements revealed the formation of radical cationic states with appearance of peak at ca. 855 nm and along with the reduction of the peak at ca. 480 nm. Identical changes were observed for the formed polaronic state during spectroelectrochemical measurements. Further gas phase ammonia treatment of the DTT-CMP$_{elec}^{+}$-I^{-} film unfortunately did not indicate a full reduction of the network as relatively low increase of the peak around 480 nm and decrease of the band at 855 nm indicated that only partial reduction of the DTT-CMP$_{elec}^{+}$-I^{-} film occurred. The coated ITO substrate was not introduced to aqueous ammonia solution in order to preserve the homogeneity of the film.

Conductivity properties of the all the synthesized DTT-based polymers were evaluated by the four-probe method which was frequently applied for such porous materials (Table C.3.2).[234-237] Among the three pristine DTT polymers, DTT-LP$_{elec}$ showed the highest conductivity probably as a result of the higher amount of material per surface unit due to its linear nature. Furthermore, DTT-CMP$_{elec}$ showed a higher conductivity than DTT-CMP probably as its electrochemical deposition yielded partially linear polymers, thus, lower amount of cross-linking were obtained compared to the bulk DTT-CMP as discussed above.

Table C.3.2: Conductivity measurements of the DTT-based polymers.

	DTT-CMP	**DTT-LP$_{elec}$**	**DTT-CMP$_{elec}$**
Pristine	$8.0x10^{-5}$ Scm^{-1}	$3.1x10^{-4}$ Scm^{-1}	$1.4x10^{-4}$ Scm^{-1}
Iodine-doped	$3.0x10^{-2}$ Scm^{-1}	$1.2x10^{-3}$ Scm^{-1}	$9.0x10^{-3}$ Scm^{-1}

Iodine exposure of all three polymers resulted in an enhanced conductivity and the highest conductivity was measured for the bulk DTT network obtained by oxidative polymerization for which the conductivity increased by three orders of magnitude. This can probably be attributed to an effect of the high porosity of the polymer obtained by bulk polymerisation whose structure resemble the most to the predicted cross-linking. Thus, iodine can enter the open network structure more easily to yield higher amount of oxidized DTT species. Furthermore, higher conductivity of DTT-CMP$_{elec}$ compared to DTT-LP$_{elec}$ was presumably also a result of the corresponding cross-linking. Additionally, the reduction of the doped materials by NH_3 vapour treatment did not result in reliable conductivity measurements, especially for the electrochemically formed films. Thus, the values gained from the four-probe instrument were systematically fluctuating. Unfortunately, the use of aqueous ammonia for the reduction of the films was not also possible since the vigorous stirring damaged the films.

As conclusion, DTT based CMPs were synthesised *via* chemical oxidative polymerisation (DTT-CMP) and by electrochemical depositions on an ITO electrode (DTT-CMP$_{elec}$). The chemical doping of DTT-CMP with iodine was successfully achieved according to the expected changes monitored in the spectroscopic properties and gas sorption measurements. Reversible dedoping *via* ammonia treatment was also demonstrated proving the full chemical redox properties of the network. Moreover, regioselective electrochemical polymerisation of DTTPh2Th4 monomer was employed in order to form linear (DTT-LP$_{elec}$) and crosslinked (DTT-CMP$_{elec}$) backbones since the peripheral thiophenes of the monomer are not identical chemically. *In-situ* spectroelectrochemical measurements of DTT-CMP$_{elec}$ films showed the fully reversible formation of polaron and bipolaron moieties with the increased potential. During the spectroelectrochemical investigations, the electrochromic behaviour of DTT-CMP$_{elec}$ film was observed as a reversible colour change in neutral, polaron and bipolaron state as well as chemical oxidation (I_2)/reduction (NH_3) process of the bulk material. Finally, conductivity measurements of the three different polymers were recorded and an enhanced conductivity was measured upon iodine doping. The positive effect of porosity was demonstrated by the significantly larger increase of conductivity of bulk DTT-CMP which has the highest number of crosslinking in ideal. These findings prove that the introduction of porosity and dimensionality might be beneficial in organic electronic applications, especially for devices such as bulk heterojunction solar cells where introduction of additives like fullerenes are generally necessary for higher

efficiencies. Additionally, this work also demonstrates that DTT based microporous polymers are promising materials for sensing applications e.g. for detection of ammonia based explosives.

C.4. THIOXANTHONE BASED MICROPOROUS POLYMERS

In the Methods and Materials Chapter, it is mentioned that thioxanthone (TX) and its derivatives are often used as efficient *type II* photoinitiators. One of the challenges in this research field is the preparation of TX derivatives featuring suitable hydrogen donor functionalities, so that these monomers can potentially be employed in polymer initiation without the need for additional co-initiator. Moreover, there has been thus far no attempt to immobilise TX to obtain heterogeneous photoinitiators since TX derivatives are used homogenously in photopolymerization reactions. Heterogenisation of TX and its derivatives would thus be of interest as, with respect to sustainable/green chemistry, the reusability of such initiator systems would be an additional benefit for photopolymerization besides using light instead of traditional methods (i.e. heating). Thus, in the following section, the synthesis of three different microporous polymers having non-, partially, and relatively high acidic hydrogen containing backbones will be discussed with the aim to observe if it is possible to have one component suitable for heterogeneous macrophotoinitiation (Figure C.4.1).

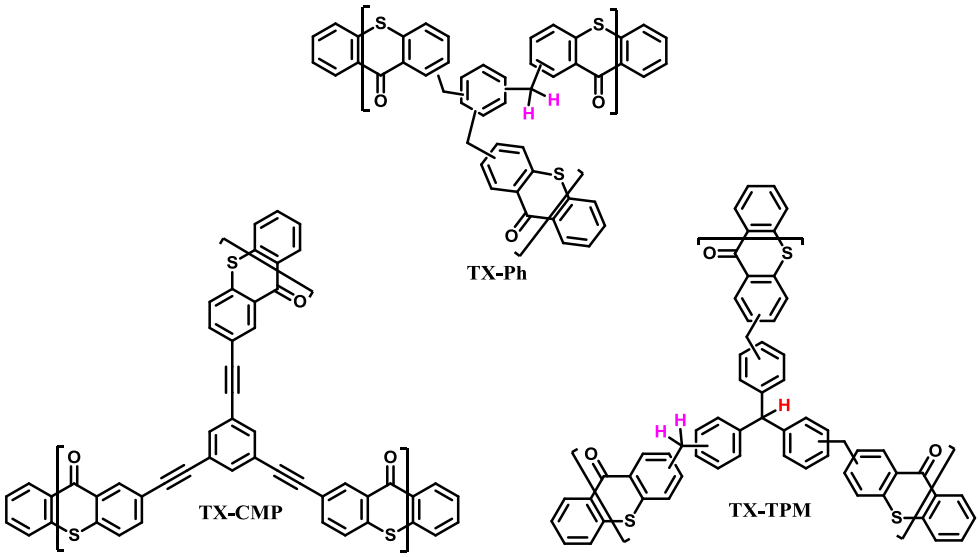

Figure C.4.1: Microporous polymers for macrophotoinitiation synthesized in this.

As it can be seen from the structures of the microporous polymers (Figure C.4.1), TX-CMP is the most rigid network and has no acidic hydrogens, TX-Ph presents a network with methylene linkages where partially acidic hydrogens are located, and for TX-TPM, besides having methylene linkages, additional acidity were introduced *via* incorporation triphenylmethane groups. The followed synthetic procedure for TX-CMP was the conventional method for such CMPs as previously published by the Cooper Group[49] after obtaining 2,7-dibromo-TX (TX-Br_2) which was also employed from a published procedure (Figure C.4.2).[320]

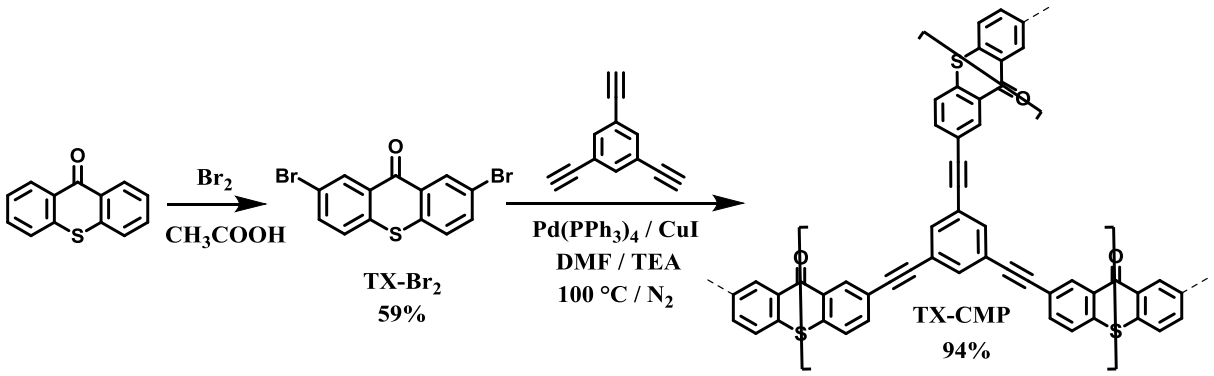

Figure C.4.2: Synthetic scheme of TX-CMP.

The synthesis of TX-Ph and TX-TPM was based on a Friedel-Crafts alkylation process which is commonly used to obtain "hypercrosslinked microporous polymers" (Figure C.4.3).[56, 60] In that case the TX monomers were copolymerized with benzene and triphenylmethane to yield the functional TX microporous polymers.

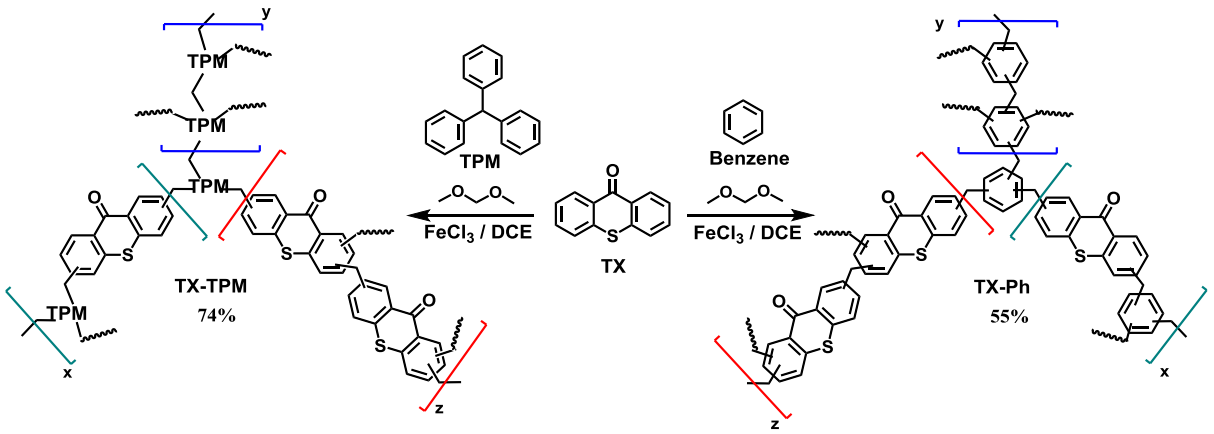

Figure C.4.3: Synthetic scheme for TX-Ph and TX-TPM based on Friedel-Crafts akylation chemistry.

Table C.4.1: N_2 sorption analysis results for the synthesised TX-based networks.

TX type	Surface area ($m^2 g^{-1}$)	Pore size (nm)
TX-CMP	497	1.4
TX-Ph	537	1.4
TX-TPM	749	1.4

After obtaining all the polymers (synthetic details are described in more detail in the Experimental section) N_2 sorption analysis indicated the formation of porous materials with SAs in the range of 497 - 749 m^2g^{-1} which is acceptable for this class of polymers (Table C.4.1, and see Figure C.4.4

isotherms). NL-DFT pore size distributions indicated a dominant pore size of 1.4 nm for all polymers (i.e. predominantly microporous materials) (Figure C.4.5).

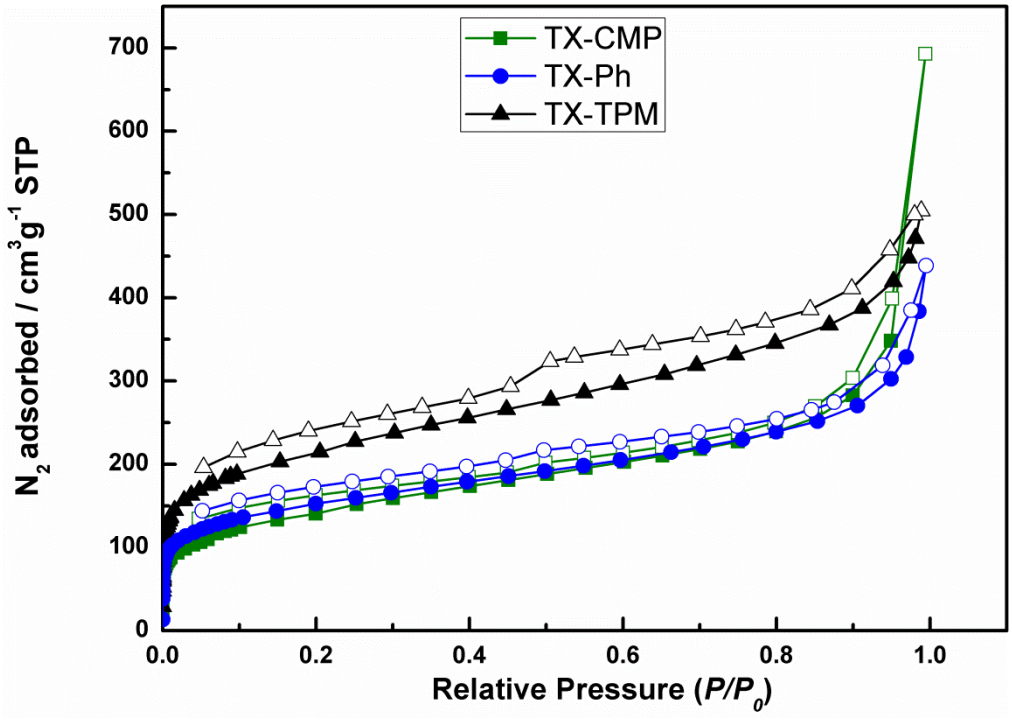

Figure C.4.4: N_2 sorption isotherms of the synthesised TX-based networks.

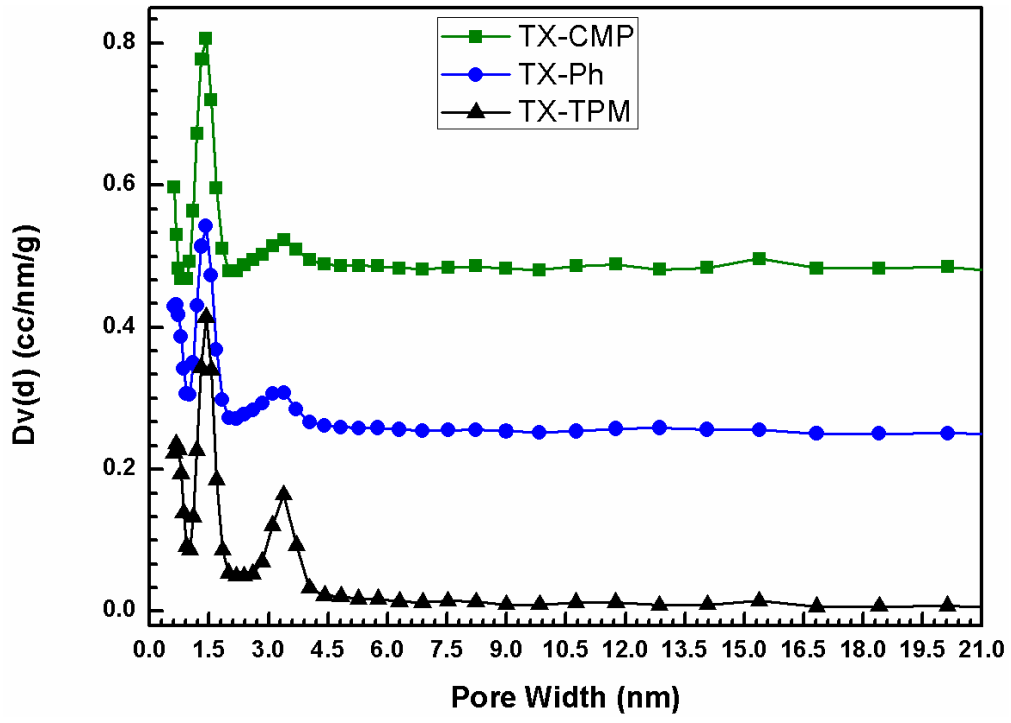

Figure C.4.5: NL-DFT pore size distribution graphs of TX networks derived from N_2 sorption analysis (graphs were shifted up by addition of 0.22 cm^3 for clarity).

Solid state ^{13}C NMR characterisation of TX-CMP presented the expected resonances for this type of network (Figure C.4.6).[74] A comparison of the solid state ^{13}C NMR of network with its corresponding co-monomers (in $CDCl_3$), demonstrated the perfect incorporation of the two monomers into the networks as evidenced by the resonance at δ = 89 ppm corresponding to acetylene carbons and δ = 176 ppm representing the carbonyl group of TX. Furthermore, aromatic carbon resonances at δ = 122, 128, and 135 ppm fit the characteristics of both monomers.

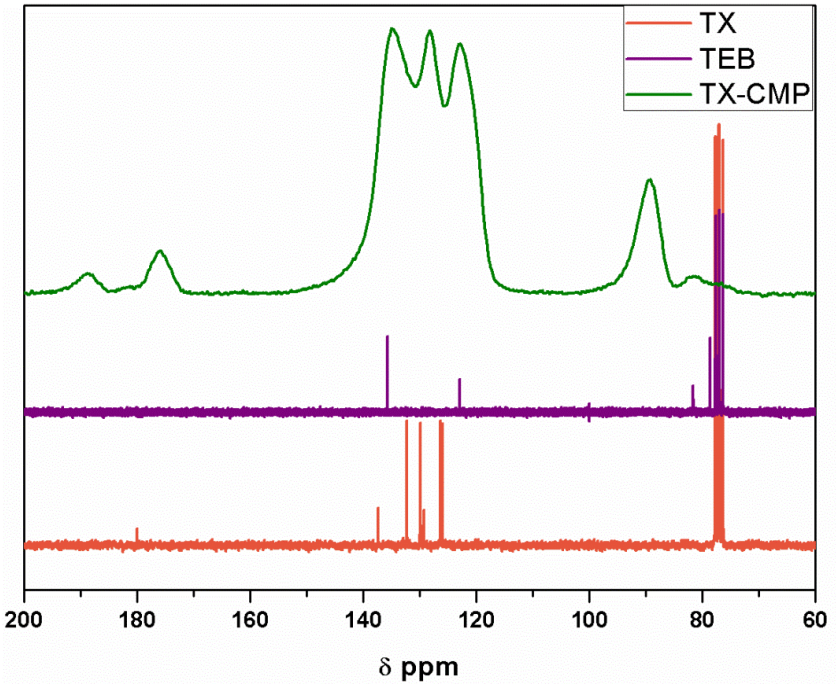

Figure C.4.6: Solid state ^{13}C NMR spectra of TX-CMP and ^{13}C NMRs of related monomers in $CDCl_3$ solution.

The solid state ^{13}C NMR spectra of TX-Ph and TX-TPM also presented spectral resonances corresponding to the respective random co-polymers containing both the respective building blocks (Figure C.4.7 and Figure C.4.8, respectively). To have a clear comparison, homopolymers of benzene (0-Ph) and triphenylmethane (0-TPM) were prepared with the same procedure and solid state ^{13}C NMR spectra of these polymers were also recorded. Between the spectra of TX-Ph and 0-Ph, the enhancement of the resonance at δ = 129 ppm with a slight shift to 127 ppm, and the carbonyl resonance of TX moieties at δ = 176 ppm can be easily observed when TX were introduced to the structure. Moreover, the slight shift from δ = 134 to 133 ppm revealed a change in the aromatic environment of the backbone. A similar slight shift from δ = 136 to 134 ppm is also observed for TPM polymers after TX was incorporated to backbone. Additionally, an identical increase in the intensity of the resonance at δ = 126 ppm was observed, with the peak at δ = 176 ppm which was attributed to carbonyl groups within the TX polymer.

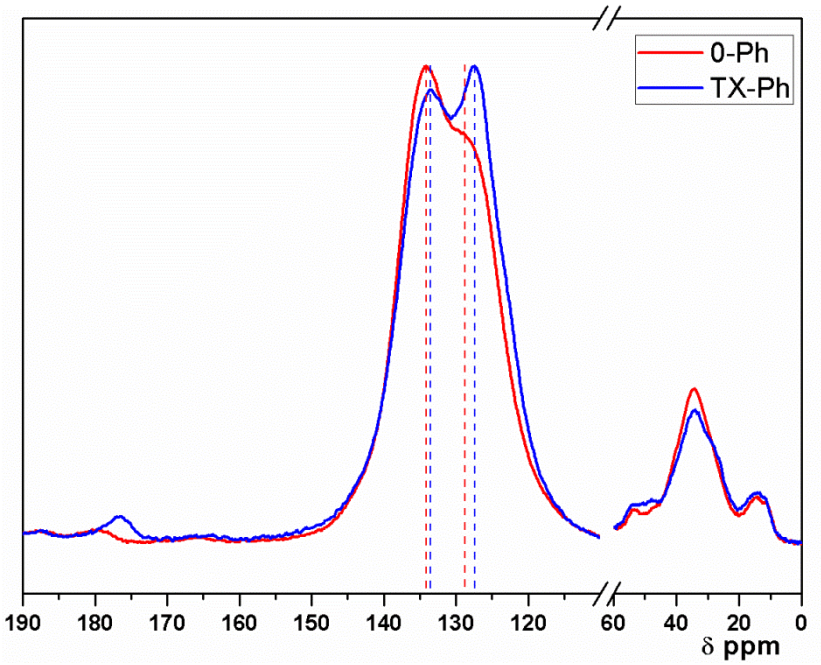

Figure C.4.7: Solid state ^{13}C NMR spectra of TX-Ph and 0-Ph.

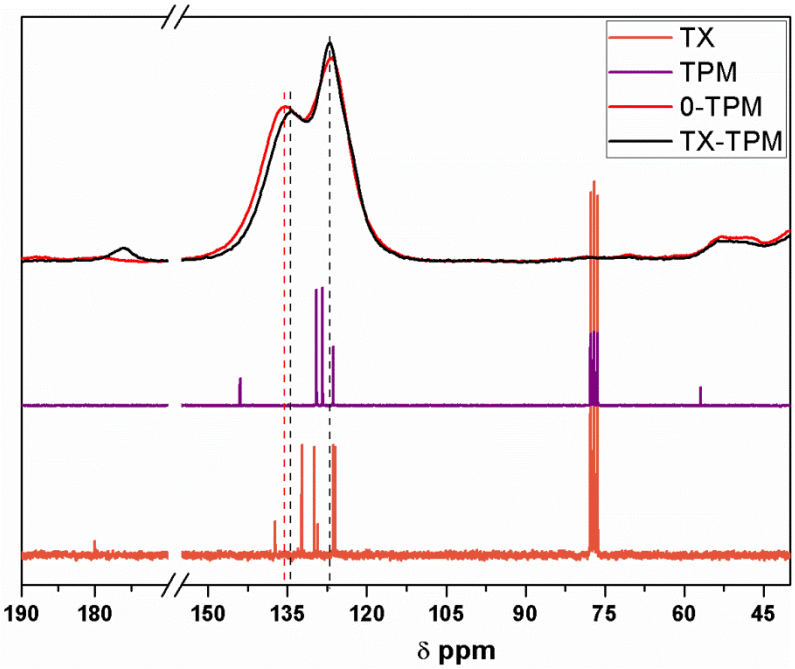

Figure C.4.8: Solid state ^{13}C NMR spectra of TX-TPM and 0-TPM, with a comparison with the spectra obtained for the corresponding monomers (recorded in $CDCl_3$).

Elemental analysis was performed to determine the polymer composition, i.e. the relative incorporation of both monomers (Table C.4. 2). Measurements indicated the sulphur content within the structure was much lower than expected. However, it is known that elemental analysis cannot give exact ratios for 3D amorphous structures due to lack of a full decomposition of material core, trapped solvent and gases, unreacted end groups or presence of catalyst residues. For example, the formation of TX-CMP *via* Sonogashira-Hagihara cross-coupling reaction should be a controlled A-B type co-polymerisation with full incorporation of both co-monomers, but elemental analysis gave in that case

36% less sulphur in the structure than expected (Table C.4. 2). Thus, elemental analysis cannot be used as a quantitative method in order to discuss degree of functionalisation for such 3D-amorphous co-polymers whereas it can be used as qualitative analysis in order to justify co-polymerisation of two monomers.

Table C.4. 2: Elemental analysis of TX polymers.

	Calculated			Found		
	%C	**%H**	**%S**	**%C**	**%H**	**%S**
TX-CMP	81.80	2.62	10.40	67.92	3.44	6.66
TX-Ph	83.42	3.74	8.56	77.57	4.47	2.12
TX-TPM	87.50	4.17	5.56	80.06	4.58	2.25

Since the aim of synthesising these TX-based polymers is their application as initiators in light driven processes, it is necessary to investigate the absorption characteristics. Therefore, diffuse reflectance UV spectroscopy of the as-synthesised polymers was performed (Figure C.4.9). The corresponding spectra showed characteristic TX absorption maxima[220] for each network in the near UV range (i.e. λ_{max} = 380 nm for knitted polymers; λ_{max} = 405 nm for TX-CMP where the red shift is probably due to enhanced conjugation in CMPs). Furthermore, the wide absorption over the entire UV/Vis spectrum is an advantage with respect to molecular TX derivatives since the application of corresponding materials is a light driven process.[321] These altered optical properties of such porous-2D/3D structures in comparison to their molecular and/or linear polymer analogues are not unexpected and have been discussed in previous chapter.[73, 104, 322]

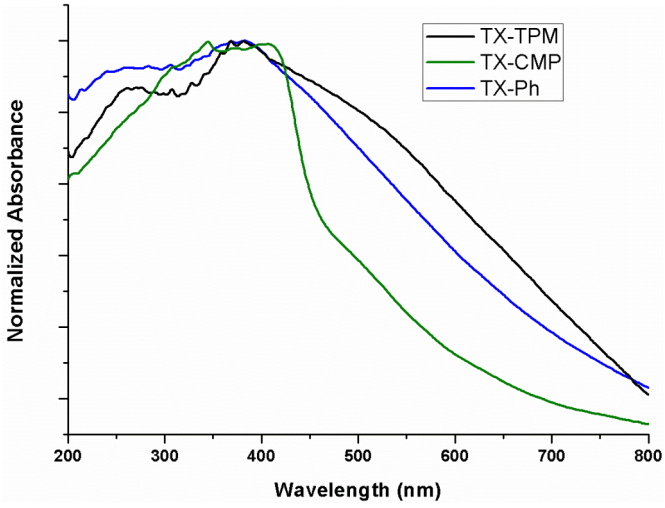

Figure C.4.9: Solid state (diffuse reflectance) UV spectroscopy analysis of TX-based polymer networks.

After characterisation of TX-based networks, macrophotoinitiation experiments were studied for free radical and cationic polymerisations, known to be the common application of TX derivatives. For this purpose, a collaboration was established with Sajjad Dadashi-Silab and Prof. Dr. Yusuf Yagci from Istanbul Technical University.

As mentioned in the Methods and Materials Chapter, co-initiators are usually required along with TX derivatives to initiate photopolymerisation (see the suggested mechanism of photo induced free radical polymerisation from Figure C.4.10).[219] To overcome this issue, acidic protons have been incorporated as functional side-groups within the molecular photoiniators. As discussed in the introduction, one of the aims of this work is the synthesis of *one component macrophotoinitiator* presenting acidic hydrogens across the polymer backbone which is expected to initiate polymerisation without the use of any additional co-initiator. Unfortunately, the polymerisation of methyl methacrylate (MMA) without additional co-initiator was unsuccessful, probably due to limitations of intramolecular H transfer within the rigid skeleton (i.e. lack of H transfer from sp^3 carbon of triphenylmethane to TX moieties) or due to a too weak acidity of these protons. Nevertheless, experiments were carried out using conventional co-initiators (i.e. TEA and $Ph_2I^+PF_6^-$).

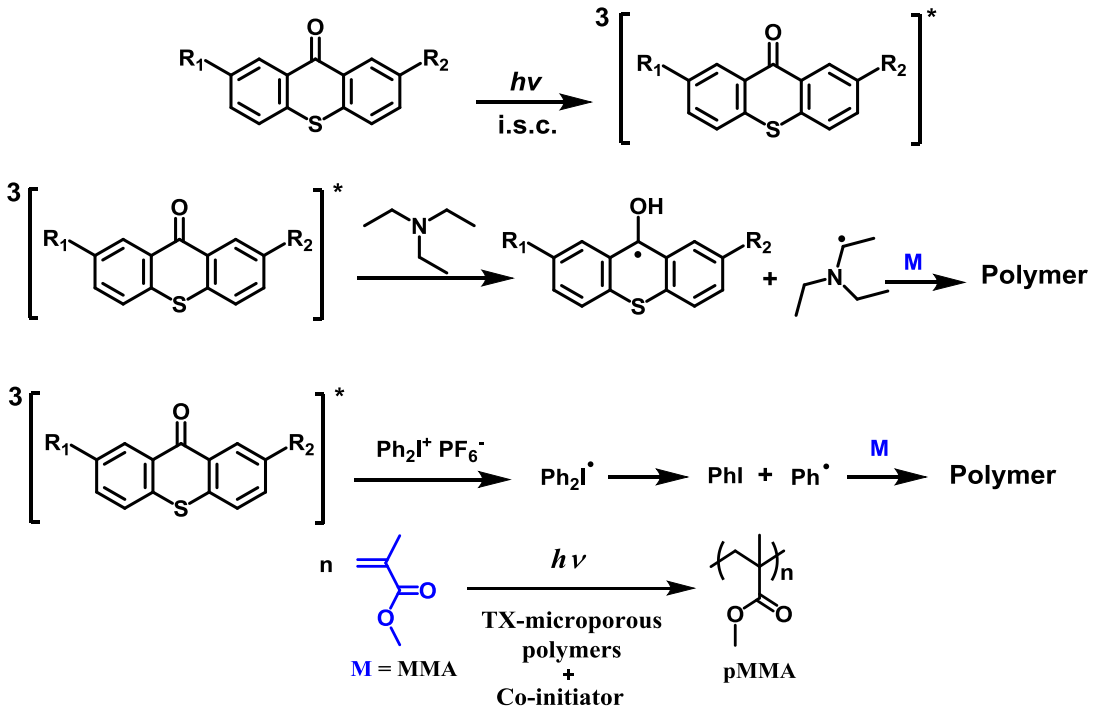

Figure C.4.10: Proposed initiation mechanism of free radical polymerization using thioxanthone macrophotoinitiators in the presence of amine or iodonium salt co-initiators under visible light or sunlight irradiation

Polymerisation of MMA was first attempted under visible light source and showed that all new macrophotoinitiators could initiate the polymerization. In addition, no polymer was resulted during a control experiment made in dark conditions signifying a light-driven process. The highest conversions were obtained by the TX-TPM (26%) systems (Table C.4.3) probably owing to its higher SA (Table C.4.1) and wider absorption in UV/Vis light (Figure C.4.9). Whilst TX-Ph and TX-CMP have nearly

the same SA, higher conversions were observed when TX-Ph was used and is possibly the result of its wider absorption and/or relatively more flexible backbone (methylene linkages) that provides a possible swelling[59] in solution which may result in improved pore accessibility. Additionally, it was observed that acidic H donor TEA as co-initiator yielded better conversions than the iodonium salt ($Ph_2I^+PF_6^-$).

Table C.4.3: Conditions and results of visible light induced free radical polymerisation of MMA.

Run	TX type	Co-initiator					
		TEA			$Ph_2I^+ PF_6^-$		
		Conv. (%)[b]	M_n (g mol^{-1}) [c]	M_w/M_n [c]	Conv. (%)	M_n (g mol^{-1})	M_w/M_n
1	TX-TPM	26	151000	1.85	22	163550	2.35
2	TX-CMP	15	202000	1.70	10	95200	1.80
3	TX-Ph	21	141500	2.10	16	154360	2.15

[a]Irradiation time = 4 h, [MMA] = 3.13 M, [TEA] = 0.023 M, [$Ph_2I^+ PF_6^-$] = 0.023 M, toluene = 2 mL, TX-polymer = 25 mg. [b] Measured gravimetrically. [c]Number average molecular weight (M_n) and molecular weight distribution (M_w/M_n) determined by GPC.

Table C.4.4: Conditions and results of sunlight induced free radical polymerization of MMA.

Run	TX type	Co-initiator					
		TEA			$Ph_2I^+ PF_6^-$		
		Conv. (%)[b]	M_n (g mol^{-1}) [c]	M_w/M_n [c]	Conv. (%)	M_n (g mol^{-1})	M_w/M_n
1	TX-TPM	31	114700	2.62	23	86400	1.95
2	TX-CMP	19	126700	2.25	14	114700	1.75
3	TX-Ph	25	112850	2.45	18	109650	2.05

[a]Irradiation time = 4 h, [MMA] = 3.13 M, [TEA] = 0.023 M, [$Ph_2I^+ PF_6^-$] = 0.023 M, toluene = 2 mL, TX-polymer = 25 mg. [b]Measured gravimetrically. [c]Number average molecular weight (M_n) and molecular weight distribution (M_w/M_n) determined by GPC.

Sunlight induced free radical free radical polymerization of MMA was also performed to observe if natural sunlight could be used for macrophotoinitiation since it is the ultimate expectation for all light driven systems (photocatalytic water splitting, solar cells etc.). For this purpose, the reaction flask was placed in the window of our collaborators laboratory at the Istanbul Technical University-Maslak

Campus in March 2014. A sunlight intensity of 15 mW/cm^2 was recorded at this location (for comparison, artificial visible light provides 40 mW/cm^2). Sunlight induced polymerisation results were comparable to the visible light induced polymerisation. Again, highest conversions were obtained with the use of TX-TPM (31%), followed by TX-Ph and TX-CMP, respectively. Since the intensity of light is relatively low, molecular weights were not as high as visible light induced system although still acceptable (Table C.4.4). Also here, TEA gave slightly higher monomer conversions compared to Ph_2I^+ PF_6^-.

To evaluate the photopolymerisation kinetics, triethylene glycol diacrylate (TEGDA) was used as a conventional bifunctional monomer that is frequently applied for the kinetic measurements in Photo-Differential Scanning Calorimetry (photoDSC).[323] This method determines any liberating heat during the photopolymerization process. This is directly proportional to the number of acrylate double bonds reacted in the photocuring process.

Consequently, the rate of polymerization (the number of monomers being consumed over total number of monomers per time), R_P (1/s), can be determined according to Equation C.4.1 where Q_t (J mol^{-1} s^{-1}) is the amount of released heat at time t, n the number of acrylate double bonds, and E_{db} (kJ mol^{-1}) is the energy of acrylate double bond (~86 kJ mol^{-1}).[324] By integrating the area under R_P-t graph, the conversion of the acrylate monomer is obtained.

Equation C.4.1: Rate of polymerisation equation.

$$R_P = \frac{Q_t}{n \times (E_{db}) \times 1000}$$

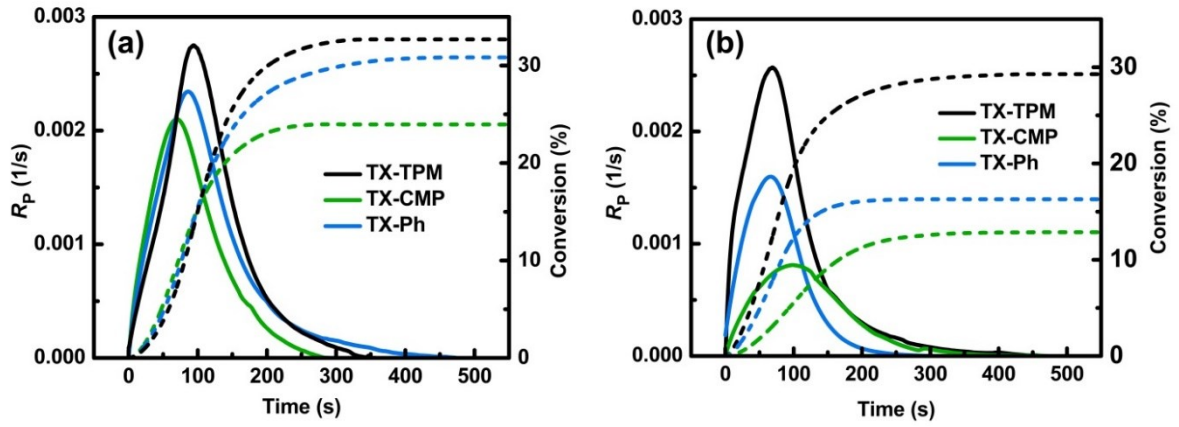

Figure C.4.11: Kinetic studies of the photopolymerisation of TEGDA with TX macrophotoinitiators using (a) TEA and (b) Ph_2I+PF6- as co-initiator measured by photoDSC. Solid lines: rate of polymerization (R_P (1/s)); dashed lines: conversion (%).

PhotoDSC results for TEA co-initiated polymerisation showed rapid rate of polymerisation that are nearly identical over 60 seconds for each network (solid lines, Figure C.4.11). The lowest pohotcatalytic activity was measured for TX-CMP for which the rate of polymerisation started to drop

after 60 seconds and no more monomer conversions (dashed lines, Figure C.4.11) was observed after 290 seconds. The photocatalytic activity of TX-TPM revealed to be the highest among all TX polymers. The kinetic studies in the presence of diiodonium salt also revealed the same order of efficiency with lower numbers of conversion in comparison to TEA co-initiated reactions. These results indicated parallel findings to the reactions of MMA monomer.

Reusability tests for each TX-based polymer network were also performed to prove sustainable use of the heterogeneous initiators (Figure C.4.12). Three different runs were performed, with the polymer collected by centrifugation after each run. Promisingly, and significantly in contrast to other similar heterogeneous macrophotoinitiation systems,[325, 326] the TX-based networks reported here could be recovered and reused over multiple catalytic runs.

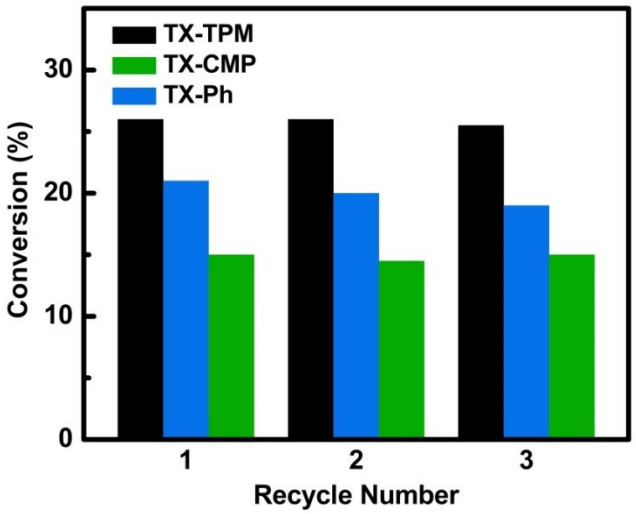

Figure C.4.12: Reusability tests of free radical polymerizations of TX based microporous polymers under visible light induced free radical polymerization (irradiation time = 4 h, [MMA] = 3.13 M, [TEA] = 0.023 M, toluene = 2 mL).

To expand the applicability of TX macrophotoinitiators even further, cationic polymerization of cyclohexene oxide (CHO) was also examined using all of three TXs under visible light irradiation. Cyclohexene oxide was chosen as a monomer as it is commonly used for this type of reaction as a reactive cyclic ether.[226, 228, 327] For cationic polymerisation reactions, two different H-donor co-initiators, namely *N,N*-dimethyl aniline (DMA) and THF were used, with $Ph_2I^+PF_6^-$ employed as an additional oxidant to obtain cations from THF or DMA radicals (Figure C.4.13). DMA was deliberately chosen as the amine co-initiator in the cationic system so as to prevent possible termination reactions. Because of the higher basicity, aliphatic amines are known to terminate cationic polymerization.[328]

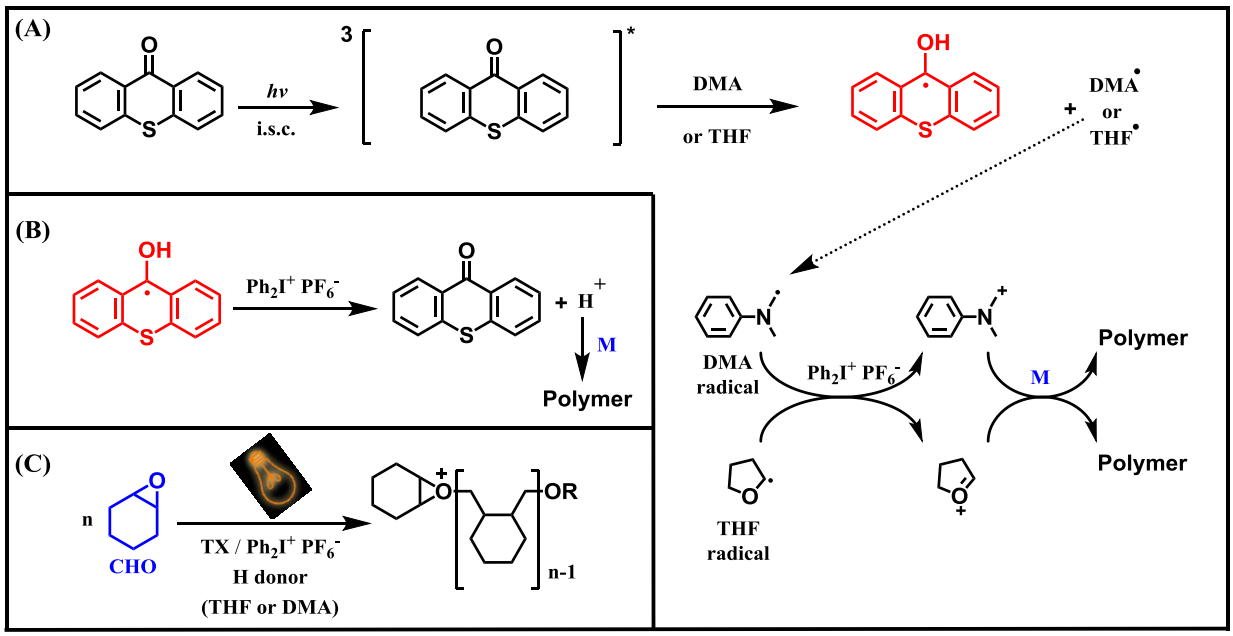

Figure C.4.13: Proposed free radical promoted cationic polymerization of CHO by using TX polymers and $Ph_2I^+PF_6^-$ in the presence of a hydrogen donor compound (DMA or THF) under visible light irradiation. (A) Cationic polymerisation initiated by DMA or THF co-initiators, (B) cationic polymerisation initiated by protonium cation, (C) cationic polymerisation of cyclohexene oxide (CHO) where R group is corresponding initiator.

Cationic polymerisation has a slightly more complicated (proposed) mechanism compared to the free radical polymerisation and this method requires an additional oxidation step after the photochemically electron donor radical species have been generated on the TX moieties. The radicals formed on the co-initiators (i.e. DMA, THF) are further oxidized by reacting with the iodonium salt, $Ph_2I^+PF_6^-$, to their corresponding carbocations that can initiate the polymerisation (Figure C.4.13-A). TX ketyl radical also undergoes electron transfer reactions with iodonium salt to yield protonic acids capable of initiating cationic polymerization (Figure C.4.13-B).

Table C.4.5: Conditions and results of visible light induced cationic polymerization of CHO.

Run	TX type	H-donor					
		DMA			THF		
		Conv. (%)[b]	M_n (g mol^{-1}) [c]	M_w/M_n [c]	Conv. (%)	M_n (g mol^{-1})	M_w/M_n
1	TX-TPM	37	4960	3.25	31	5120	2.80
2	TX-CMP	18	2140	2.70	15	2610	2.15
3	TX-Ph	29	3250	2.90	28	3100	3.10

[a] Irradiation time = 4 h, [CHO] = 3.30 M, [$Ph_2I^+PF_6^-$] = 0.023 M, [DMA] = 0.023 M, [THF] = 0.023 M, toluene = 2 mL, TX-polymer = 25 mg, [b] Measured gravimetrically. [c] Number average molecular weight (M_n) and molecular weight distribution (M_w/M_n) determined by GPC.

The photo induced cationic polymerisation of CHO (Figure C.4.13-C) without additional co-initiator was unsuccessful, as observed for the free radical polymerization of MMA. All three investigated macrophotoinitiators successfully lead to polymerisation of the CHO monomer in presence of both DMA and THF (Table C.4.5). Conversions were in the same range as for the free radical polymerisation results; although in this case the molecular weights of the polymers were lower. Nevertheless the observed monomer conversions and molecular weights of the latter polymers (pCHO) were comparable with homogenously catalysed systems, proving the efficiency of the issued heterogeneous macrophotoinitiation process.[228, 327]

As for the investigated free radical polymerisation, reusability tests were performed for all macrophotoinitiators. Three different runs were performed, with the polymer collected by centrifugation after each run and no significant loss of activity has been recorded in the cationic pathway (Figure C.4.14).

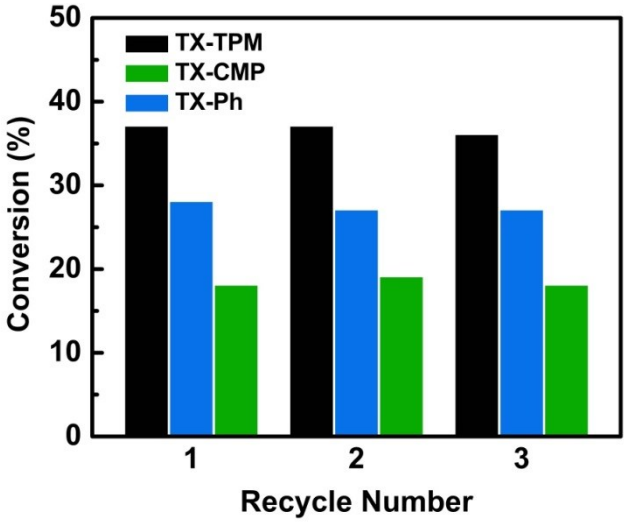

Figure C.4.14: Reusability tests of free radical polymerizations of TX based microporous polymers under visible light induced cationic polymerization in co-initiation of DMA (irradiation time = 4 h, [CHO] = 3.30 M, [Ph_2I^+ PF_6^-] = 0.023 M, [DMA] = 0.023 M, toluene = 2 mL).

In conclusion, three different microporous TX-based polymer networks with high porosity (500-750 m^2 g^{-1}) were synthesised. The TX monomers were copolymerized with three different comonomers via two different cross-coupling reactions. The employed comonomers allowed to prepare microporous polymers having non-, partially, and relatively high acidic hydrogen containing backbones, whereas the cross-coupling reaction employed, i.e. sonogashira-hagihara cross-coupling and Friedel-Craft alkylation, allowed to prepare microporous polymers with different degrees of flexibility, i.e. rigid and swellable. The TX-based networks were fully characterized and notably showed excellent optical characteristics allowing their use as macrophotoinitiators for photopolymerisation reactions. The three TX-based macrophotoinitiators readily initiated the free radical polymerisations of MMA under visible and natural sunlight with comparable activities to molecular homogeneous analogues. Additionally, photo induced cationic polymerisation of

cyclohexene oxide were also successfully carried out to obtain poly(cyclohexene oxide) again with comparable activities with homogeneous molecular initiators where this work was the first attempt for the use of microporous polymers as heterogeneous macrophotoinitiators in photo induced cationic polymerisation. Among all the polymers studied, the random co-polymer prepared from TX and triphenylmethane precursors showed the highest activity, owing to its higher surface area. Facile separation of these heterogeneous photoinitiators from the polymer mixture proved their successful recyclability as several catalytic runs could be achieved while maintaining the original photocatalytic activity. The polymers synthesised in this work constitute therefore, owing their activity, stability and versatility, a new series of high potential photoinitiators for widespread applications.

D. SUMMARY

Incorporation of electron rich heteroatom containing struts within the skeleton of porous organic polymers was employed during this PhD study in order to widen the application fields of porous polymers to organic electronics and light driven sustainable catalytic processes.

In this aspect, strong electron donors were introduced into the backbone of conjugated microporous polymers (CMPs) and the structure, porosity and optical and chemical properties of the networks were investigated. At first tetrathiafulvalene (TTF) moieties were used as monomers in a CMP synthesis yielding TTF-CMPs. The TTF-CMPs were synthesized *via* Sonogashira-Hagihara cross-couplings. Optimization of the reaction conditions yield enhancement of the specific surface areas for TTF-CMPs from 50 to 434 m^2g^{-1}. Furthermore, it was demonstrated that after exposure of iodine to pristine TTF-CMPs, charge transfer complexes formed within the porous network in order to obtain a charged polymeric network.

In the following, the observed strong influence of reaction conditions on the structure and porosity of the obtained TTF-CMP networks, lead us to investigate the effect of different parameters, especially the co-monomer ratios to the development of CMPs. Consequently, the synthesis of the first described CMP network (CMP-1), was re-investigated especially considering the reported but counterintuitive observation, that not the equimolar ration of the two comonomers in this polycondensation, but a relatively large excess of one of the monomers (the acetylenic compound) yield the highest surface area networks. The here presented experiments show that the conventionally used excess of acetylenic monomer did not changed the surface area significantly compared to an equimolar ratio of the co-monomers. However, to explain the commonly reported conflicting observations, the amount of the acetylenic co-comonomer was arbitrarily increase to a large excess with respect to the halogen functionalised monomer and indeeda positive effects regarding the surface area (759 → 1150 m^2g^{-1}) was observed. However, it is shown by this experiment that a side reaction, namely a hompolyomerization of the acetylenic compounds is responsible for the formation of high surface area networks resulting in great deviations from the ideal CMP-1 structure. This was further proven by polymerising exclusively the the acetylenic monomer under the same reaction conditions which indeed also yield a network with similar surface area (1010 m^2g^{-1}). Therefore, the often reported excess of acetylenic moieties may indeed result in higher surface area networks however this is not due to the attempted Sonogashira-Hagihara couplings, but to acetylene-acetylene homocouplings and therefore deviations from the ideally assumed CMP structures have to be considered.

The next investigations were focused on incorporation of another electron donor, namely dithienothiophene (DTT), into CMPs. DTT as relatively weaker donor than the previous used TTF system was chosen to obtain a reversible chemical doping. The obtained DTT-CMP, synthesized by

oxidative polymerisation of a thiophene functionalized DTT with $FeCl_3$ yielded a surface area of 790 m^2g^{-1}. The accessible surface decreased to 380 m^2g^{-1} after iodine doping. However, the subsequent removal of iodide moieties from the pores after aqueous ammonia treatment, accompanied with the reduction of the oxidized DTT moieties, yielded again an increase of the surface area to 568 m^2g^{-1}. Furthermore, regioselective electrochemical film formation was employed to yield linear and crosslinked polymers deposited on ITO electrodes. Spectroelectrochemical studies of the DTT-CMP films also showed the reversible electrochemical oxidation and reduction of the DTT moities depending on the applied potential. Furthermore conductivity measurements revealed the benefit of a porous backbone for organic electronic applications, seen in a sequential increase of conductivity from non-porous (linear electrochemical polymer film) to highly porous polymers (crosslinked electrochemical polymer and bulk DTT-CMP, respectively) after iodine doping.

Finally, novel microporous polymer networks are presented which can act as macrophotoinitiators for photopolymerisation reactions, i.e. heterogenous photocatalysts. The synthesis of different thioxanthone (TX)-based polymer networks is presented, synthesized by either Sonogashira-Hagihara cross-couplings or Friedel-Crafts alkylations. The TX networks exhibit specific surface areas between 500-750 m^2g^{-1}. These microporous polymers were found to be suitable and reusable heterogeneous macrophotoinitiators in free radical and cationic photopolymerisation in which their efficiencies were comparable to their molecular TX equivalents. Additionally, the free radical polymerisation of methylmetacrylate under sunlight in the presence of the TX-based porous networks was demonstrated and therefore successfully fulfilled the aim of using direct solar energy in polymer production.

In conclusion, in this PhD work a variety of novel, functional microporous polymers is presented. Strong electron donating moieties are introduced into the conjugated backbones of microporous polymers and the reversible formation of charge transfer salts with electron acceptors entering the porous system is proven, an important prerequisite for their furutre application in organic electronic devices. Furthermore the introduction of photoinitiators is presented, showing the potential of microporous polymer networks in the field of photocatalysis.

E. EXPERIMENTAL DETAILS

The experiments that were performed during this PhD research were explained below in detail and most of these result were published elsewhere.[61, 78] N_2 gas sorption and pXRD measurements were performed by our technicians, Christina Eichenauer and Maria Unterweger, respectively. Solid state ^{13}C CP-MAS NMR measurements were performed by Dr. Kamalakannan Kailasam. X-ray photoelectron spectroscopy was recorded by Dr. Jens. P. Paraknowitsch. Electron paramagnetic resonance (EPR) spectrums were recorded by Prof. Dr. Peter Strauch from University of Potsdam. SEM images were taken by Maria Colmenares from TU Berlin.

Other collaborations were stated in the corresponding titles.

Materials

Tetrathiafulvalene (TTF; 97.0%, Alfa Aeasar), 1,3,5-triethynylbenzene (TEB; 98%, Alfa Aesar), perfluoro-1-iodohexane - stab. with copper (98+%, Alfa Aeasar), iodine (≥99.8%, Carl Roth), 1,4-diiodobenzene (99% Aldrich), iron (III) chloride ($FeCl_3$; 97%, Aldrich), chloroform - anhydrous - contains amylenes as stabilizer (≥99%, Aldrich), aquaous ammonia solution (32% (v/v), Carl Roth), thioxanthone (TX; 97.0%, Aldrich), formaldehyde dimethyl acetal (98%, Alfa Aesar), dimethylformamide (DMF; anhydrous, 99.8%, Aldrich), tetrakis(triphenylphosphine)palladium(0) ($Pd(PPh_3)_4$; 99%, Aldrich), copper (I) iodide (CuI; 99.5%, Aldrich), benzene (99.8%, Aldrich), triphenylmethane (TPM; 99%, Aldrich), 1,2-dichloroethane (DCE; 99.8%, Aldrich), Triethylene glycol dimethacrylate (TEGDA; M_n = 286.32 g mol^{-1}, Aldrich), triethylamine (TEA; 99%, Aldrich), *N*,*N*-dimethylaniline (DMA, Fluka), tetrahydrofuran (THF; 99.9%; Aldrich), diphenyliodonium hexafluorophosphate (Ph_2I^+ PF_6^-; 98%, Alfa Aesar), toluene (Merck), and methanol (MeOH; 99.9%, Merck) were used as received. Methyl methacrylate (MMA, 99%; Aldrich) was purified by passing through a basic alumina column to remove inhibitor. Cyclohexene oxide (CHO; 98%, Aldrich) was vacuum distilled over calcium hydride.

Instruments

Nuclear magnetic resonance (NMR) spectra were obtained from a Bruker Avance II 200 MHz (50.3 MHz for ^{13}C), and solid state (cross-polarization magic-angle spinning (CP/MAS)) spectra were recorded on a Bruker Avance 400MHz (100.6 MHz for ^{13}C measurements). Varian 640-IR was used for infra-red spectroscopy measurements using either KBr pellets or ATR. UV and luminescence spectra were recorded on a Varian Cary 300 and LS 50 B from PERKIN ELMER, respectively. Powder X-Ray diffraction (pXRD) measurements were recorded on a Bruker D8 Advance. N_2 gas sorption measurements were performed using a QUADRASORB SI and Autosorb 1-MP, and thermal gravimetric analysis was recorded on a Perkin-Elmer STA 6000. APCI mass spectrum was recorded

using a LTQ Orbitrap XL. EI mass was recorded in Finnigan MAT95S. BrukerBiospin CW ELEXSYS E 500 (equipped with ER 49X Microwave Bridge, variable temperature unit ER 4131 VT, and ER 4122SHQE-LC High Sensitivity Cavity) is used for electron paramagnetic resonance (EPR) measurements for powders at 150 K. Thermo FlashEA 1112 Organic Elemental Analyzer was used for elemental analysis studies. Scanning electron microscope (SEM) images were taken in Phillips XL 20 SEM.

Cyclic voltammetry (CV) studies were performed using CH-Instruments Model 400A as a potentiostat. UV−vis measurements were studied on HITACHI U-0080D. Solid state electrical conductivity measurements were conducted at 25 °C in air on DTT-CMPelec and DTT-CMP by a Keithley 2400 source meter connected to a four-probe head with gold tips.

Gel permeation chromatography (GPC) measurements were performed on a Viscotek GPC max auto sampler system consisting of a pump, a Viscotek UV detector, and Viscotek a differential refractive index (RI) detector with three ViscoGEL GPC columns (G2000H HR, G3000H HR, and G4000H HR, 7.8 mm internal diameter, 300 mm length) in series. The effective molecular weight ranges were 456 − 42800, 1050 − 107000, and 10200 − 2890000, respectively. THF was used as an eluent at flow rate of 1.0 mL min^{-1} at 30 °C. Both detectors were calibrated with PS standards having narrow-molecular-weight distribution. Data were analyzed using ViscotekOmniSEC Omni-01 software.Photo-differential scanning calorimetry (photo-DSC) measurements were carried out by means of a modified Perkin-Elmer Diamond DSC equipped with a Polilight PL400 Forensic Plus light source between 320 and 500 nm. Light intensities were measured via Delta Ohm model HD-9021 radiometer.

E.1 SYNTHETIC DETAILS FOR TTFCMP

Synthesis of TTF-I_2 - (E,Z)-4,4'-diiodo-2,2'-bi(1,3-dithiolylidene)

0.2 g (0.97 mmol) of TTF was dissolved in dry diethyl ether under inert conditions and cooled down to -78°C using a dry ice/acetone bath. Then, 1.75 mL (3.5 eq.) of 2 M lithium diisopropylamide solution in THF/heptane/ethylbenzene (as received from Aldrich) was added dropwise and the mixture was stirred for 3 hours. Afterwards 0.85 mL (4 eq.) of perfluorohexyl iodide was added dropwise. The reaction mixture was then allowed to reach room temperature and stirred further overnight.

Subsequently, all solvents were removed by distillation and the organic phase was extracted by dichloromethane (DCM)/water mixture, dried over $MgSO_4$, filtered and purified via flush chromatography as described in the literature.[72] TTF-I_2 was collected as an orange-red solid with 60% yield. ^{1}H NMR (200 MHz, $CDCl_3$) 6.40 (s, 2H).^{13}C NMR (50 MHz, $CDCl_3$) 121.19, 113.71, 63.57. APCI *m/z* for C6H2S4I2 $[M]^+$calc: 456.7201 found: 456.7201.

Synthesis of Conjugated Microporous Polymers from TTF-I_2 (TTFCMP):

To find optimized conditions for the synthesis of CMPs with TTF moieties, the amount of reactants and type of base have been varied as shown in Table E.1.

Table E.1. Conditions for synthesis of TTFCMP

TTF-I_2eq.	(TEB)	Solvent	Temp^{0}C	Time	Yield	Surface Area m^2/g
1	1	DMF/TEA (15/15 mL)	100	3 days	110%	180
1	1	DMF/DIA (15/15 mL)	100	3 days	90%	264
1	1	DMF/DIA (25/0.6mL)	100	3 days	105%	413
3	2	DMF/DIA (25/0.6 mL)	100	3 days	85%	434*
1	1	DMF/TEA (25/0.75 mL)	100	3 days	107%	130
3	2	DMF/TEA (25/0.5 mL)	100	3 days	99.5%	99
3	2	DMF/TEA (5/5 mL)	100	3 days	97 %	54

**Isotherms were derived from Autosorb-1-MP whilst other measurements were performed using a Quadrasorb SI instrument.*

Here just the conditions for the polymer with highest surface area is described in detail: 0.165 g of TTF-I_2 and an equivalent molar amount of TEB (0.036 g) were dissolved in dry DMF and dry diisopropylamine (DIA) and heated to 100 °C under inert atmosphere in a sealed schlenk flask. 0.024 g of $Pd(PPh_3)_4$ and 0.005 g CuI were dissolved/dispersed in a vial under inert atmosphere in 1 mL of dry DMF and added after 15 min to the reaction mixture. The reaction mixture was further stirred for 3 days at 100 °C.

The precipitated brown powder was filtered and washed with THF, $CHCl_3$, water and methanol. The powder was further purified by soxhlet extraction for one day using THF and methanol, respectively. The powder was dried at 90°C in vacuum, giving TTFCMP in high yields

Iodination of TTFCMP to form TTFCMP$^{\cdot+}$-I_n^-:

50 mg TTFCMP was transferred into a 10 mL flask with 138 mg of I_2 and 5 mL EtOH and the mixture stirred overnight. The resulting black solid was separated from EtOH/I_2 solution by centrifugation. The powder was washed 3 times with EtOH until the solution remained colorless. After drying in vacuum at 40°C overnight, 66 mg of a black powder remained. For loading iodine *via* the gas phase, a certain amount of TTFCMP (Table 2) was added in a small vial which was placed into a larger vial containing an excess amount of iodine. The brown TTFCMP powder started to turn darker in less than 15 minutes. After 7 days, the smaller vial is removed and the resulting black powder of TTFCMP$^{\cdot+}$-I_n^- dried in vacuum at 40°C overnight to remove elemental iodine.

E.2. DETAILS FOR THE EFFECT OF DIFFERENT MONOMER RATIOS ON THE PROPERTIES OF CMP-1

Synthesis of Conjugated Microporous Polymers (CMP-1) and H-AcAc:

Corresponding molar amount of 1,4-diiodobenzene (Ph-I_2) and of TEB (see Table E.2) were dissolved in 5 mL dry DMF and 5 mL dry TEA mixture and heated to 100 °C under inert atmosphere in a sealed schlenk flask. 0.023 g of $Pd(PPh_3)_4$ and 0.004 g CuI were dissolved/dispersed in a vial under inert atmosphere in 1 mL of dry DMF and added after 15 min to the reaction mixture (0.066 g of $Pd(PPh_3)_4$ and 0.011 g CuI for H-AcAc - 3% molar ratio of 0.100 g TEB). The reaction mixture was further stirred for 3 days at 100 °C.

The precipitated powders were filtered and washed with THF, $CHCl_3$, water and methanol. The powder was further purified by soxhlet extraction for one day using THF and methanol, respectively. The powder was dried at 90°C in vacuum, giving CMP-1s and H-AcAc in high yields.

Table E.2. Synthetic details of CMP-1s and H-AcAc

Network	Ph-I_2	TEB	Yield*	Surface Area m^2/g
CMP-1 (3:2)	100 mg (0.3 mmol)	30 mg (0.2 mmol)	105%	759
CMP-1 (3:3)	100 mg (0.3 mmol)	45 mg (0.3 mmol)	160%	749
CMP-1 (3:10)	100 mg (0.3 mmol)	150 mg (1 mmol)	300%	1150
H-AcAc	———	100 mg (0.7 mmol)	124%	1010

**Yields were calculated for the reaction between 3 eq. of Ph-I_2 to 2 eq. TEB.*

E.3. SYNTHETIC DETAILS FOR DTT-CMP

Synthesis of DTT-CMP

To the suspension of $FeCl_3$ (0.18 g, 1.1 mmol) in dry $CHCl_3$ (20 ml), which was stirred for 10 min under nitrogen atmosphere prior to any process, was added a solution of $DTTPh_2$-Th_4 (0.138 g, 0.2 mmol) in dry $CHCl_3$ (10 ml) and the mixture was stirred for one day.[59] The precipitate was filtered and washed with THF, $CHCl_3$, H_2O, and MeOH, subsequently. Then, the crude product was subjected to a soxhlet extraction for 3 days, using MeOH and THF as solvents. The remaining red solid was dried overnight under vacuum at 90 °C to yield the title compound (0.113 g, 82%).

Iodine Doping of DTT-CMP

A certain amount of DTT-CMP (red powder, see Table 3 for the amounts) was filled in a small vial to plant inside a bigger one that was filled excess amount of I_2 crystals (~1 g). 15 minutes later of sealing system, almost all polymer inside turned to black. 7 days after, small vial was weighted directly after reaction (DTT-CMP^+-I_n^-), and vacuuming overnight in 40 °C (DTT-CMP^+-I^-).

Ammonia Dedoping of DTT-CMP^+-I^-

A 10 mL round bottom flask was filled with 50 mg iodine doped polymer and 5 mL of 32% aqueous ammonia, and stirred for 2 hours (colour change was observed even from the vapour of NH_4OH). 5 mL water added to system and mixture was centrifuged. Red precipitate was washed 2 times with water and 1 time with methanol, and each time liquid phase was separated via centrifuge. Powder dried in vacuum at 90 °C, and yielded 42 mg (particles were lost during decantation processes).

Electrochemical Investigations of DTT based CMPs (collaboration with *Prof. Dr. Turan Ozturk* from Istanbul Technical University)

Synthesis of DTT-LP and DTT-CMP_{elec} $DTTPh_2$-Th_4 was electropolymerized via potentiodynamic method in a three electrode cell where the electrolyte was a mixture of $NaClO_4$/$LiClO_4$ (0.1 M, 0.1 M) dissolved in ACN/DCM (9:1 v/v), Ag/AgCl was the reference and Pt wires were both counter and working electrodes. Electropolymerization was carried out in two different potential range which leaded to obtain two different types of polymers. The first polymerization was between the potential range of 0 to 1.05 V and the crosslinked polymer was obtained by stepping the potential up to 1.4 V. Electrochemical behaviors of the polymers films were studied in monomer free solutions via changing scan rates (Figure F. 10) Regression coefficients of I_p^- scan rate graphs for each polymer found to be higher than the regression coefficients of I_p^- (scan rate)$^{1/2}$ graph, which supported a thin layer behavior of the polymers DTT-LP and DTT-CMP_{elec} (Figure F. 11).

Conductivity Measurements Solid state electrical conductivity measurements were conducted at 25 °C in air on DTT-LP_{elec}, DTT-CMP_{elec} and DTT-CMP by a Keithley 2400 source meter connected to a four-probe head with gold tips. DTT-LP_{elec} and DTT-CMP_{elec} were electrodeposited on ITO potentiodynamically and removed from the electrode surface, where DTT-CMP powder was pressed into thin tape with a 12 mm diameter and 0.28 mm thickness. For iodine doping, the film or the tape was put in a chamber for 48 hours than removed and measured instantly.

E.4. SYNTHETIC DETAILS FOR TX BASED MICROPOROUS POLYMERS

Synthesis of 2,7-dibromo-9H-thioxanthene-9-one (TX-Br_2)

TX (2.5 g, 0.012 mol) is dissolved in 20 mL acetic acid, and 5 mL Br_2 was added dropwise in room temperature and heated to 130 °C. After 20 h of reflux, cooled mixture was poured over ice and filtered. Precipitation was washed with saturated solution of $NaHCO_3$, 20% aqueous solution of $NaHSO_3$, and water, subsequently. Solid part was dried in vacuum and recrystallized in toluene. Resulting bright yellow solid was yielded as 2.57 g (59%). ^{1}H NMR (400 MHz, $CDCl_3$) δ 8.75 (d, ^4J= 2.34 Hz, 2H), 7.75 (dd, ^3J= 8.60, ^4J= 2.32 Hz, 2H), 7.48 (d, ^3J= 8.60Hz, 2H) (Figure S1); EI *m/z* for $[M]^+$ calculated: 367.85006 found: 367.85089

Synthesis of TX-CMP

TX-Br_2 (0.200 g, 0.54 mmol), TEB (0.081 g, 0.54 mmol), CuI (0.015 g, 0.08 mmol), $Pd(PPh_3)_4$ (0.030 g, 0.026 mmol) were dissolved in 20 mL dry DMF and 15 mL dry TEA in glovebox. Sealed flask was stirred for 3 days at 100 °C. Precipitation were filtered and washed with THF, $CHCl_3$, deionized water, and MeOH. Pale yellow material was purified *via* soxhlete wash in THF and MeOH for 1 day, each. Dried in vacuum at 100 °C and yielded 0.181 g (94%). ^{13}C CP/MAS NMR (Cross-polarization *magic angle* spinning nuclear magnetic resonance) δ 176, 135, 128, 122, 89. Elemental analysis; Calculated: C 81.80 %, H 2.62 %, S 10.40 % and O 5.19 %. Found: C 67.92 %, H 3.44 %, S 6.66 %.

Synthesis of TX-Ph and TX-TPM networks (collaboration with *Dr. Robert Dawson* – TU Berlin)

Using a 100 mL two-necked flask TX (5 mmol, 1 eq) and one of either benzene or TPM (5 mmol, 1 eq) were dissolved in DCE (20 mL) under nitrogen. Formaldehyde dimethyl acetal (35 mmol or 50 mmol) was added followed by $FeCl_3$ (35 mmol or 50 mmol). The reaction was then heated to 80 °C after which the solution precipitated. Heating was continued for 18 hours after which the precipitate was removed by filtration and extensively washed with methanol until the filtrate became clear. The product was then soxhlet extracted with methanol and chloroform for 18 hours each after which the polymer was removed by filtration and dried in vacuo at 70 °C.

TX-Ph. Yield 0.9326 g (55 %). ^{13}C CP/MAS NMR δ 176, 134, 127, 34* (*overlaps with spinning side band). Elemental analysis; Calculated: C 83.42 %, H 3.74 %, S 8.56 % and O 4.28 %. Found: C 77.57 %, H 4.47 %, S 2.12 %.

TX-TPM. Yield 2.1404 g (74 %). ^{13}C CP/MAS NMR δ 176, 134, 127, 51*, 35* (*overlap spinning sideband). Elemental analysis; Calculated: C 87.50 %, H 4.17 %, S 5.56 % and O 2.78 %. Found: C 80.06 %, H 4.58 %, S 2.25 %.

Photopolymerizations with Thioxanthone Networks (collaboration with *Prof Dr. Yusuf Yagci* from Istanbul Technical University)

Visible light induced free radical polymerization In 2 mL toluene, 1 mL MMA (9.39 mmol) and co-initiators TEA or Ph_2I^+ PF_6^- (10 µL-0.07 mmol for TEA, 30 mg-0.07 mmol for Ph_2I^+ PF_6^-) were dissolved. Subsequently, TX macrophotoinitiator network (25 mg) was added to the mixture and the Pyrex tube was degassed with N_2 gas for 20 minutes. Afterwards, reaction flask was put in a photoreactor which was equipped with six light sources that illuminates between 400-500 nm (measured light intensity = 45 mW/cm2). After 4 hours, illumination of the flask was stopped and the crude mixture was solved in THF. TX macrophotoinitiator networks were removed via centrifugation and the resulted polymers (poly(methymetacrylate), pMMA) in THF phase were precipitated in MeOH. As following, the precipitation was filtered and dried under vacuo for 24 hours for futher analysis.

Sunlight induced free radical polymerization The same conditions above were applied but the illumination of the flask carried out under sunlight with a light intensity 15 mW/cm2 (in the campus of Istanbul Technical University in March 2014).

Free radical promoted cationic polymerization In 2 mL toluene, 1 mL CHO (9.88 mmol) and co-initiators Ph_2I^+ PF_6^- or DMA (30 mg, 0.07 mmol for Ph_2I^+ PF_6^- or 10 µL, 0.07 mmol for DMA) were dissolved in a Pyrex tube. Subsequently, TX macrophotoinitiator network (25 mg) was added to the mixture and the mixture was degassed with N_2 gas for 20 minutes. Afterwards, reaction flask was put in a photoreactor which was equipped with six light sources (light provided was between 400-500 nm with an intensity of 45 mW/cm^2). After 4 hours, illumination of the flask was stopped and the crude mixture was solved in THF. TX macrophotoinitiator networks were removed via centrifugation and the resulted polymer (poly(cyclohexeneoxide), pCHO) in THF phase were precipitated in MeOH. As following, the precipitation was filtered and dried under vacuo for 24 hours for futher analysis.

Preparation of photocurable formulations for photo-DSC A typical photopolymerization in photo-DSC is as follows: for 1 mL of TEGDA was added 10 µL of TEA or 30 mg of iodonium salt with corresponding TX polymer (5 mg) before irradiation of the reaction vessel. As following, 6-10 mg of the reaction solution was transferred to a photo-DSC pan and irradiated in an isothermal mood at 25 °C with a nitrogen flow of 20 mL min^{-1}.

F. APPENDIX

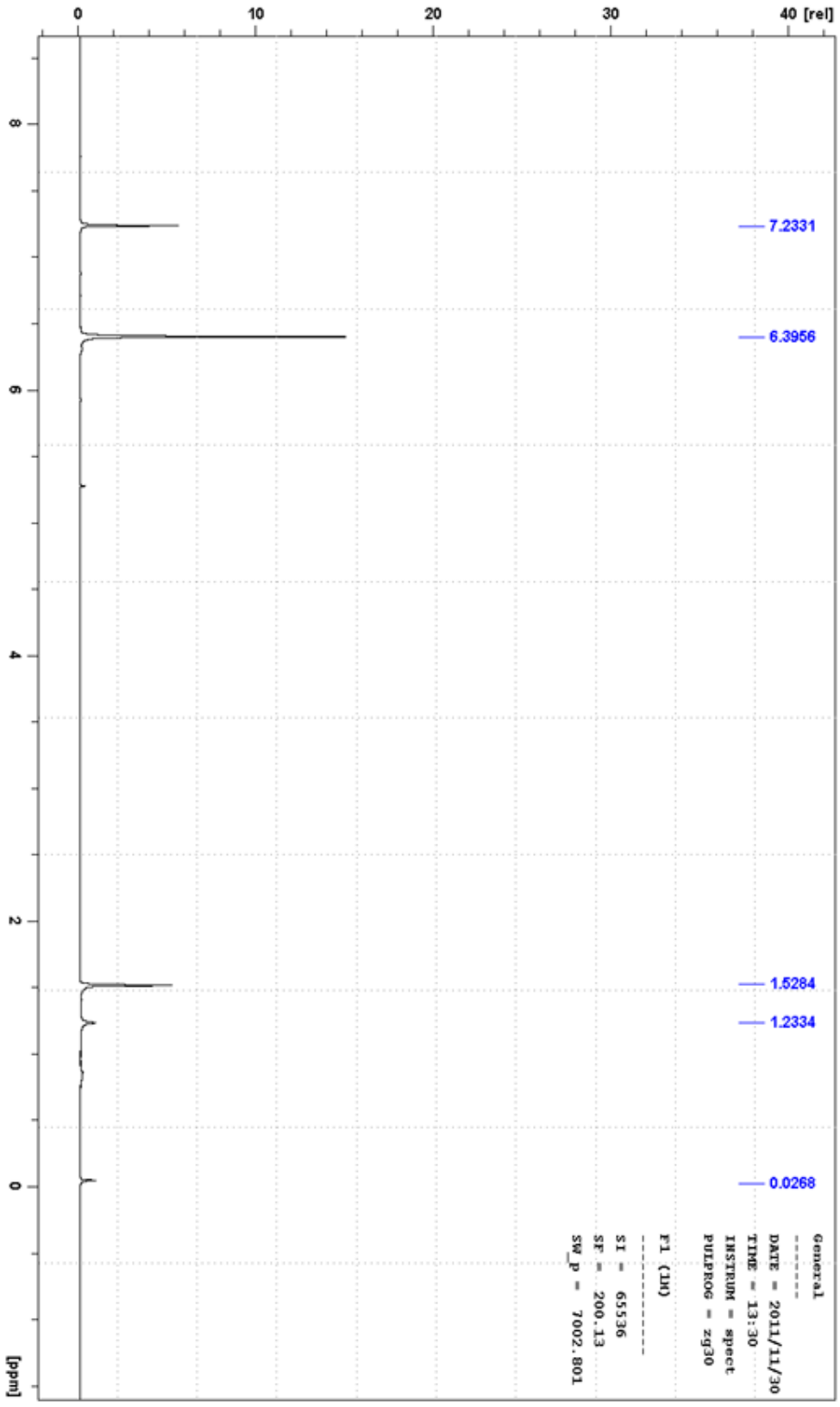

Figure F. 1 ^{1}H NMR spectrum of TTF-I_2 in $CDCl_3$

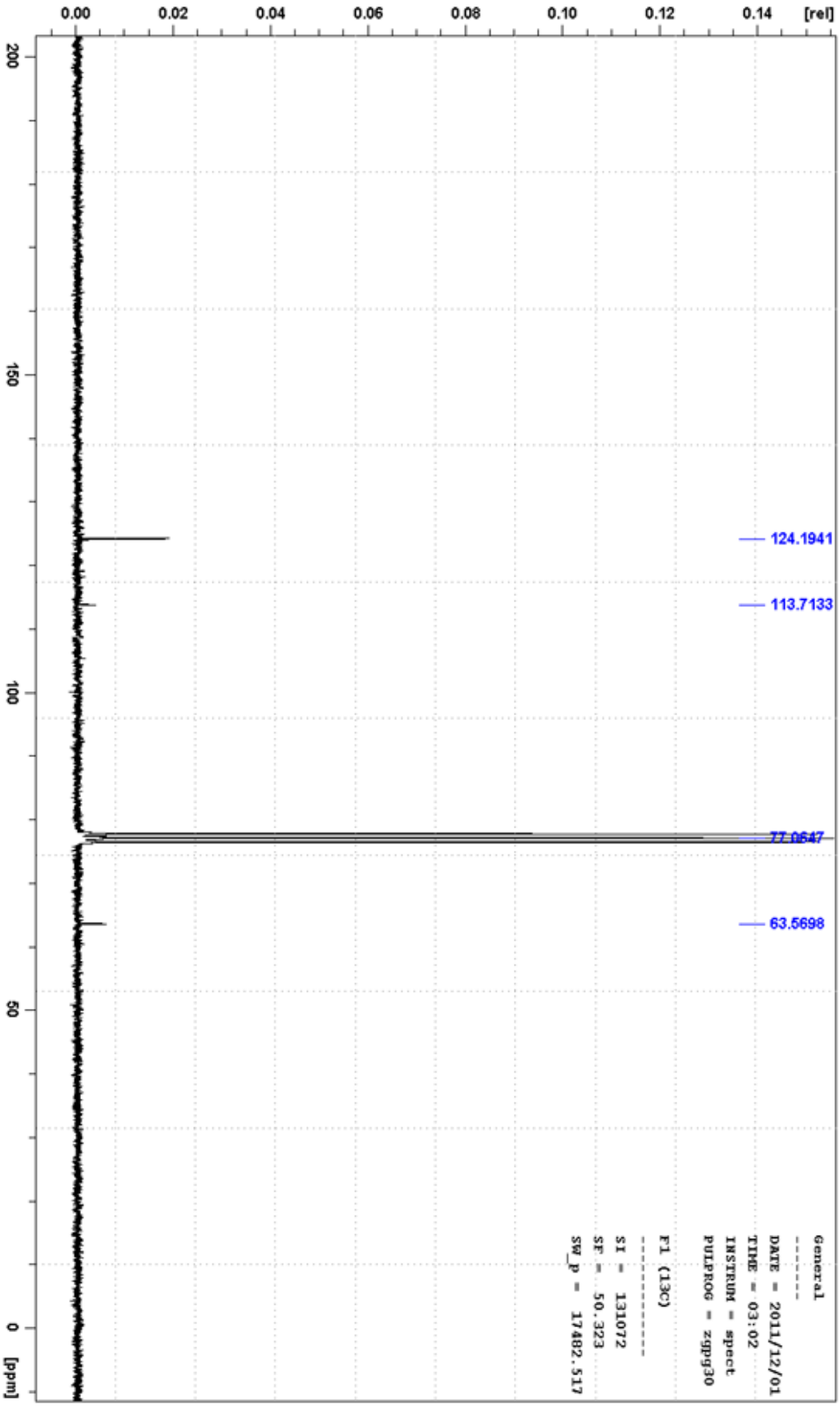

Figure F. 2 ^{13}C NMR spectrum of TTF-I_2 in $CDCl_3$

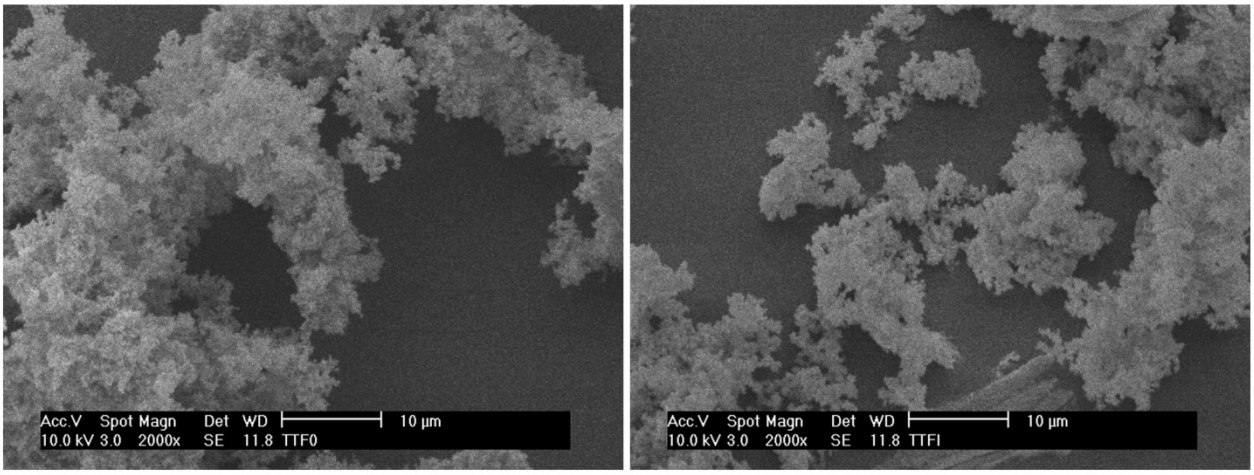

Figure F. 3 Scanning Electron Microscopy (SEM) images of TTFCMP (left) and TTFCMP$^{\cdot+}$-I$_n^-$ (right).

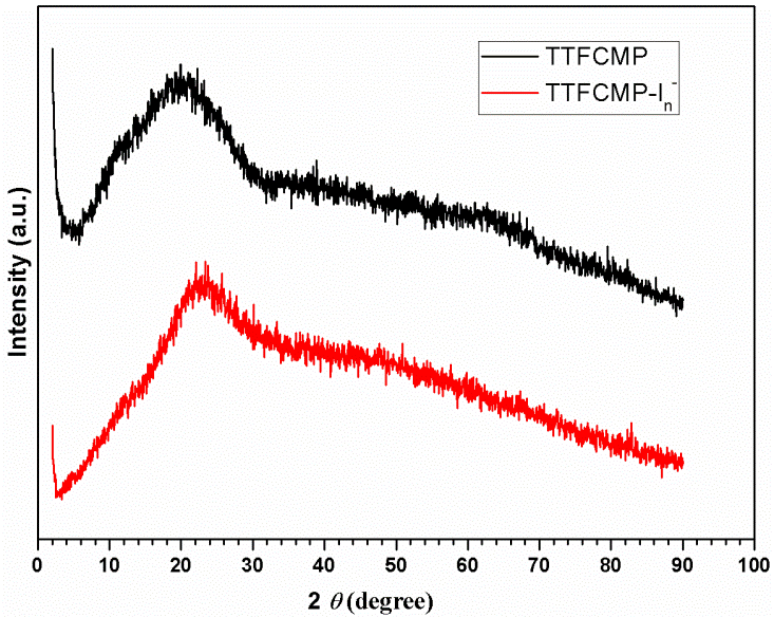

Figure F. 4 pXRD patterns of amorphous TTFCMP and TTFCMP$^{\cdot+}$-I$_n^-$

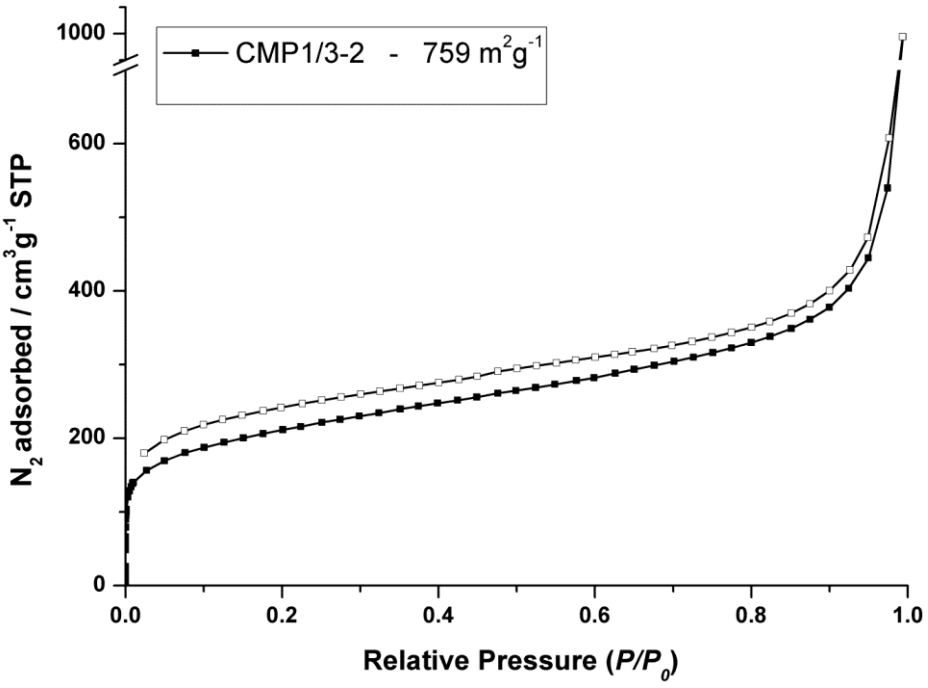

Figure F. 5 N_2 sorption isotherm of CMP-1 built from 3 eq. PhI_2 - 2 eq. TEB monomer ratio.

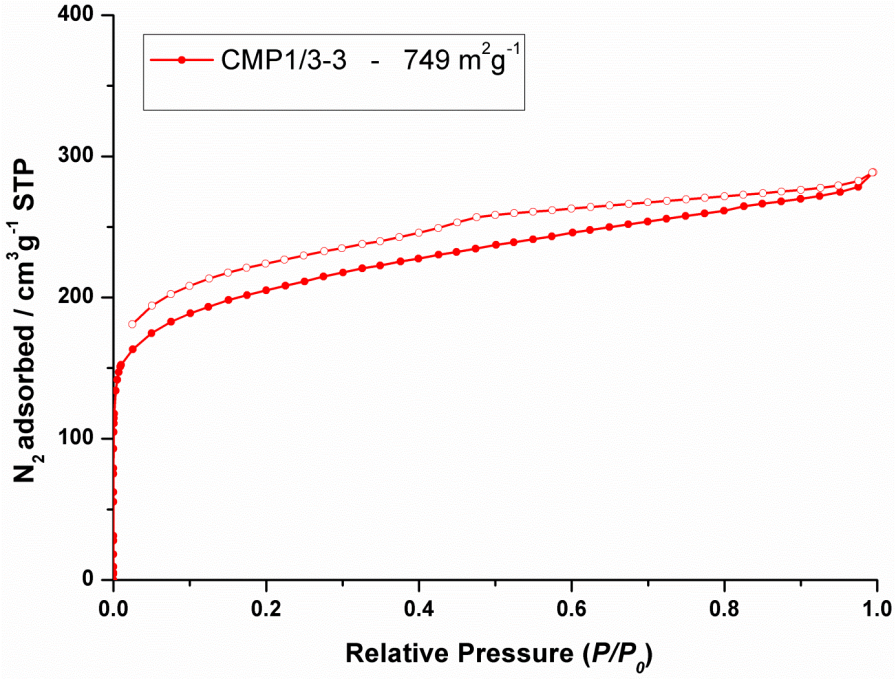

Figure F. 6 N_2 sorption isotherm of CMP-1 built from 3 eq. PhI_2 - 3 eq. TEB monomer ratio.

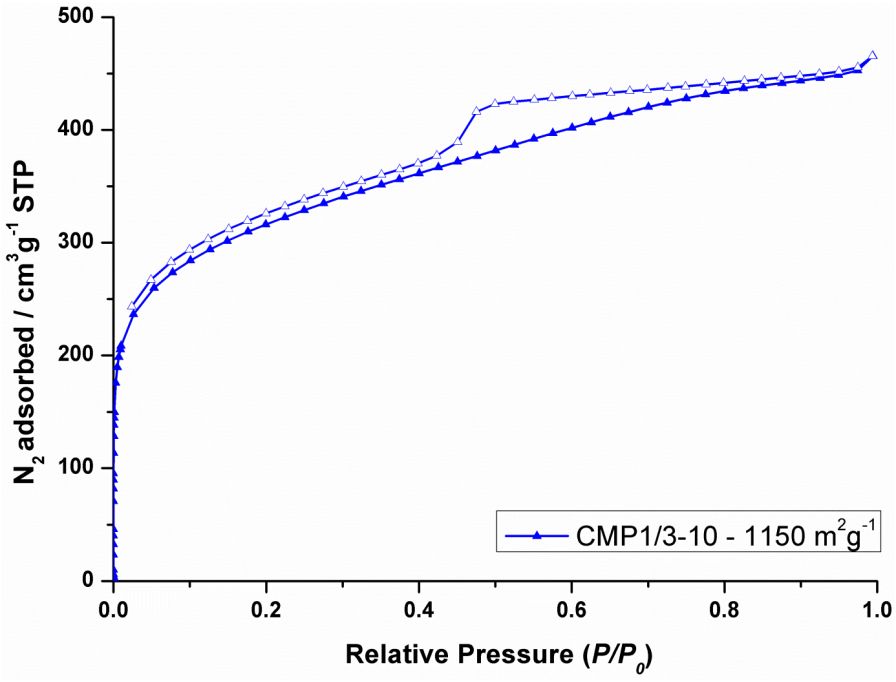

Figure F. 7 N_2 sorption isotherm of CMP-1 built from 3 eq. PhI_2 - 10 eq. TEB monomer ratio

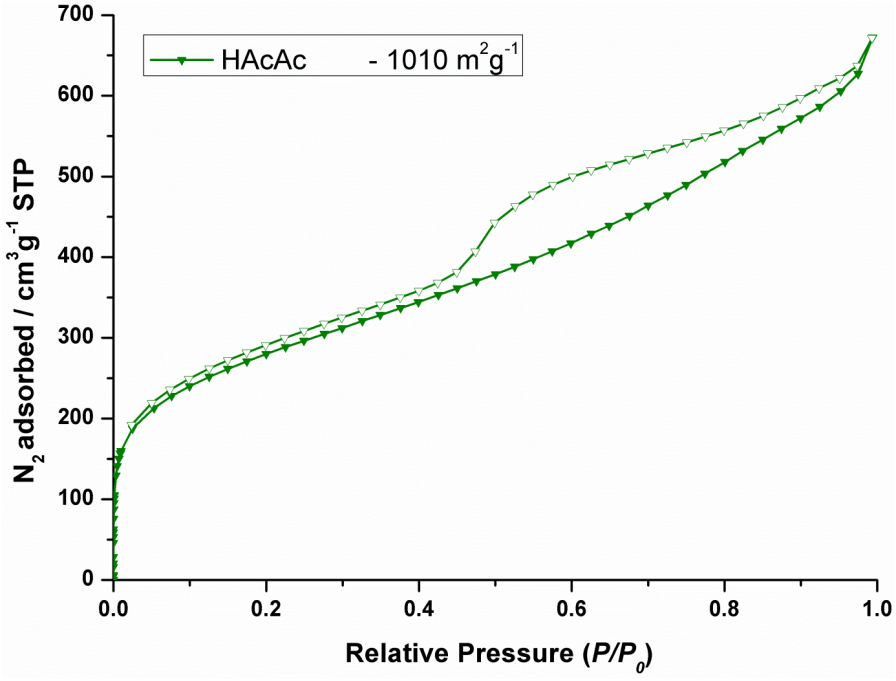

Figure F. 8 N_2 sorption isotherm of H-AcAc built from homocoupling of TEB monomer.

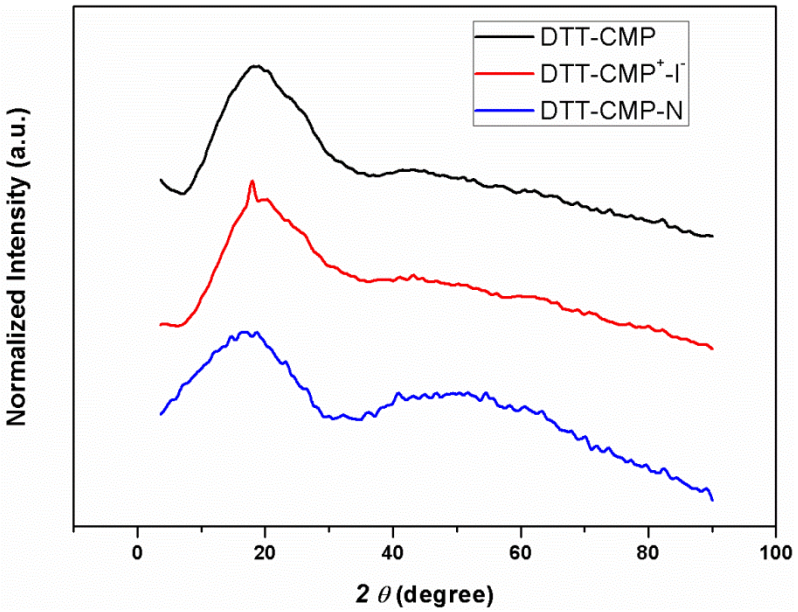

Figure F. 9 pXRD patterns of DTT based networks

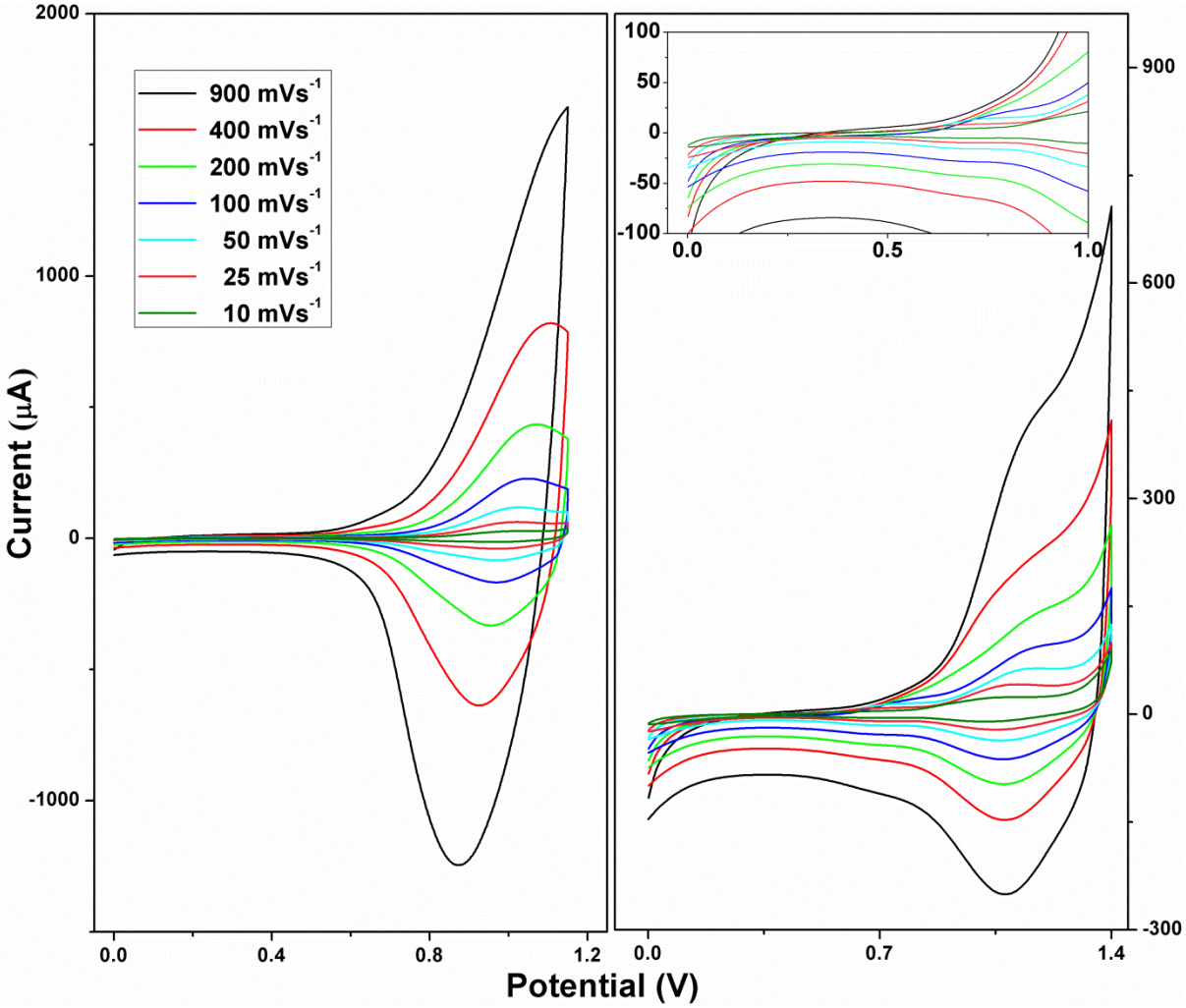

Figure F. 10 Cyclic voltammograms of DTT-LP$_{(elec)}$ (on left) and DTT-CMP$_{(elec)}$ (on right) films over ITO electrode in monomer-free electrolyte solution on various scan rates.

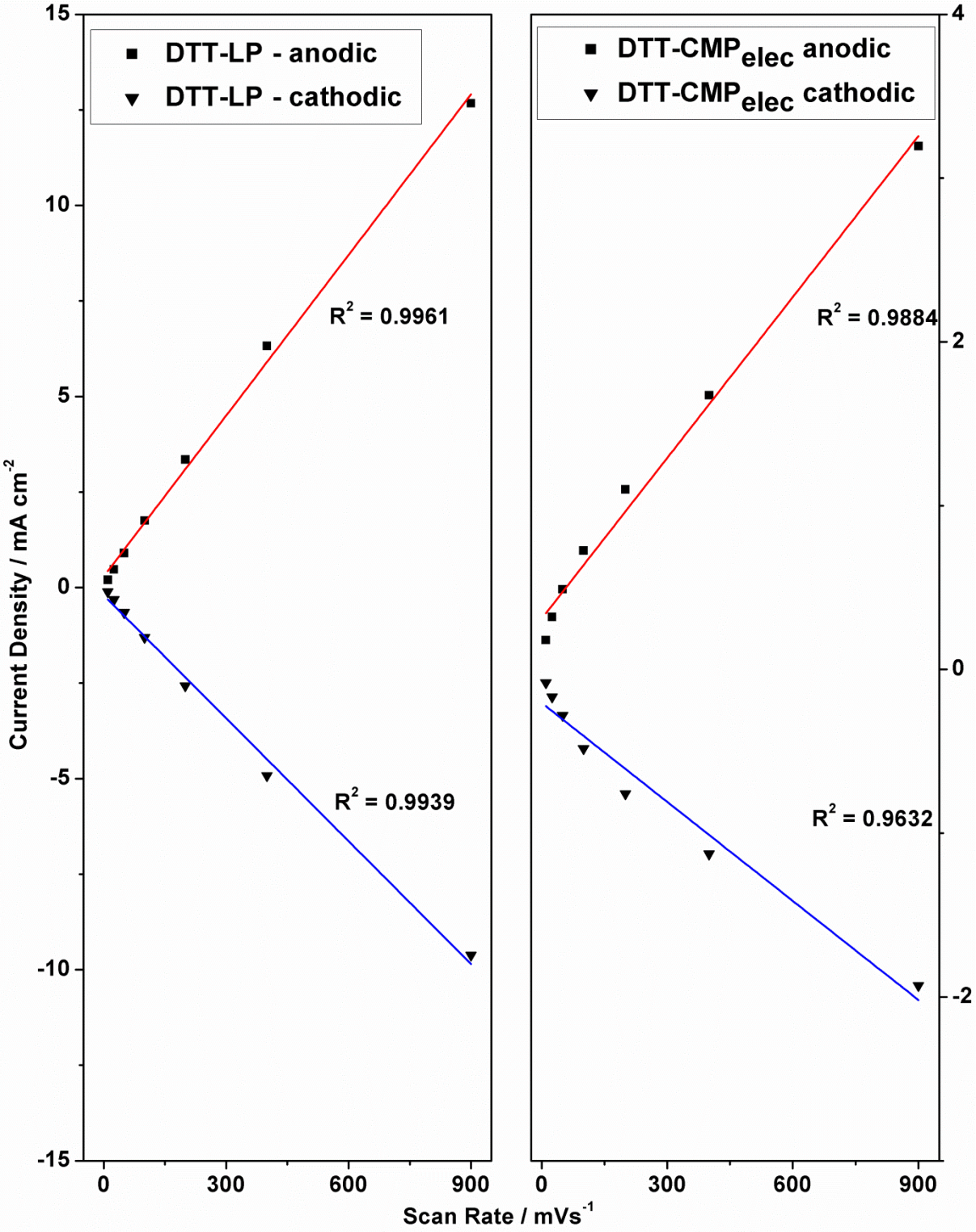

Figure F. 11 Cathodic and anodic behaviours of DTT-LP$_{(elec)}$ (on left) and DTT-CMP$_{(elec)}$ (on right) polymer thin films in monomer-free electrolyte solution on various scan rates.

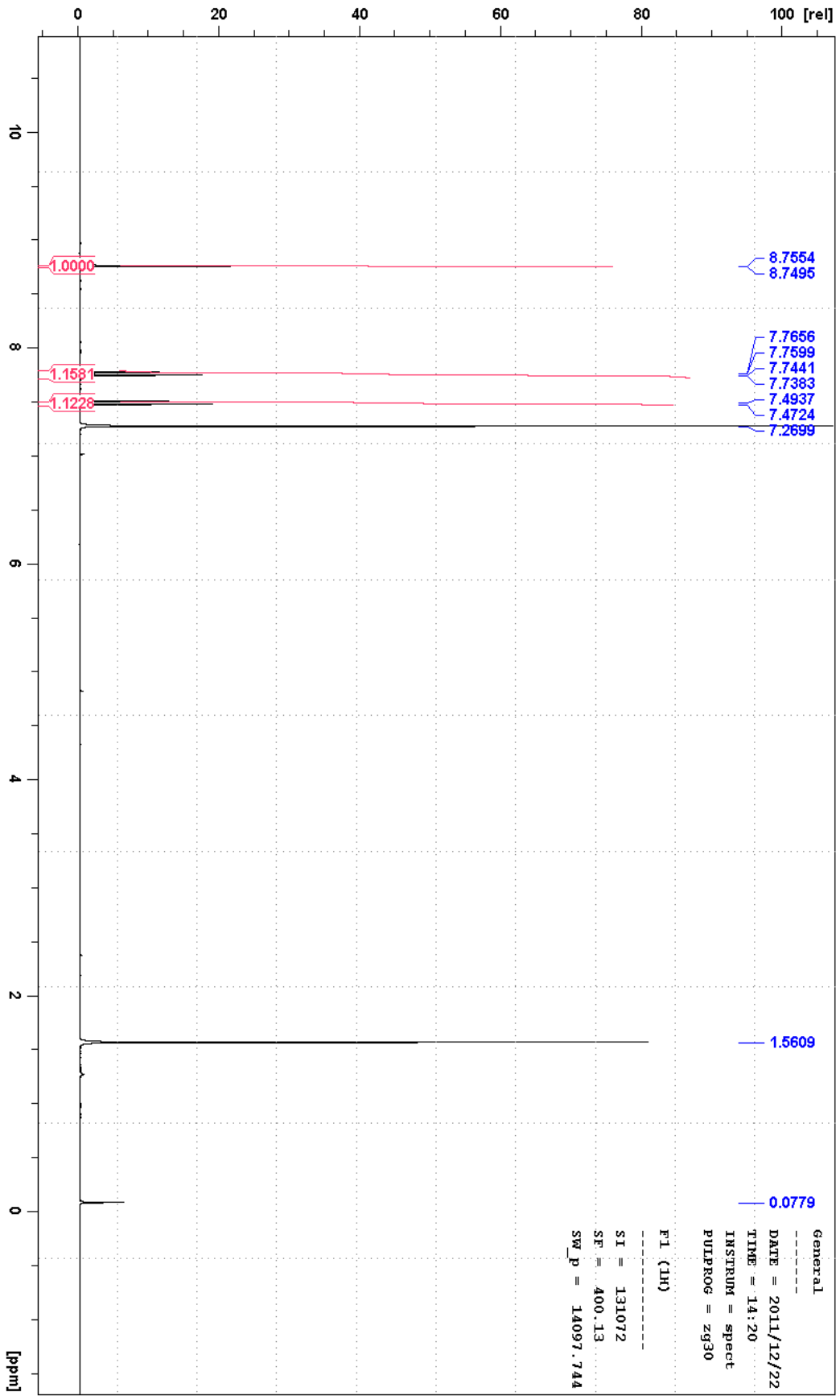

Figure F. 12 ^{1}H NMR of TX-Br_2 in $CDCl_3$.

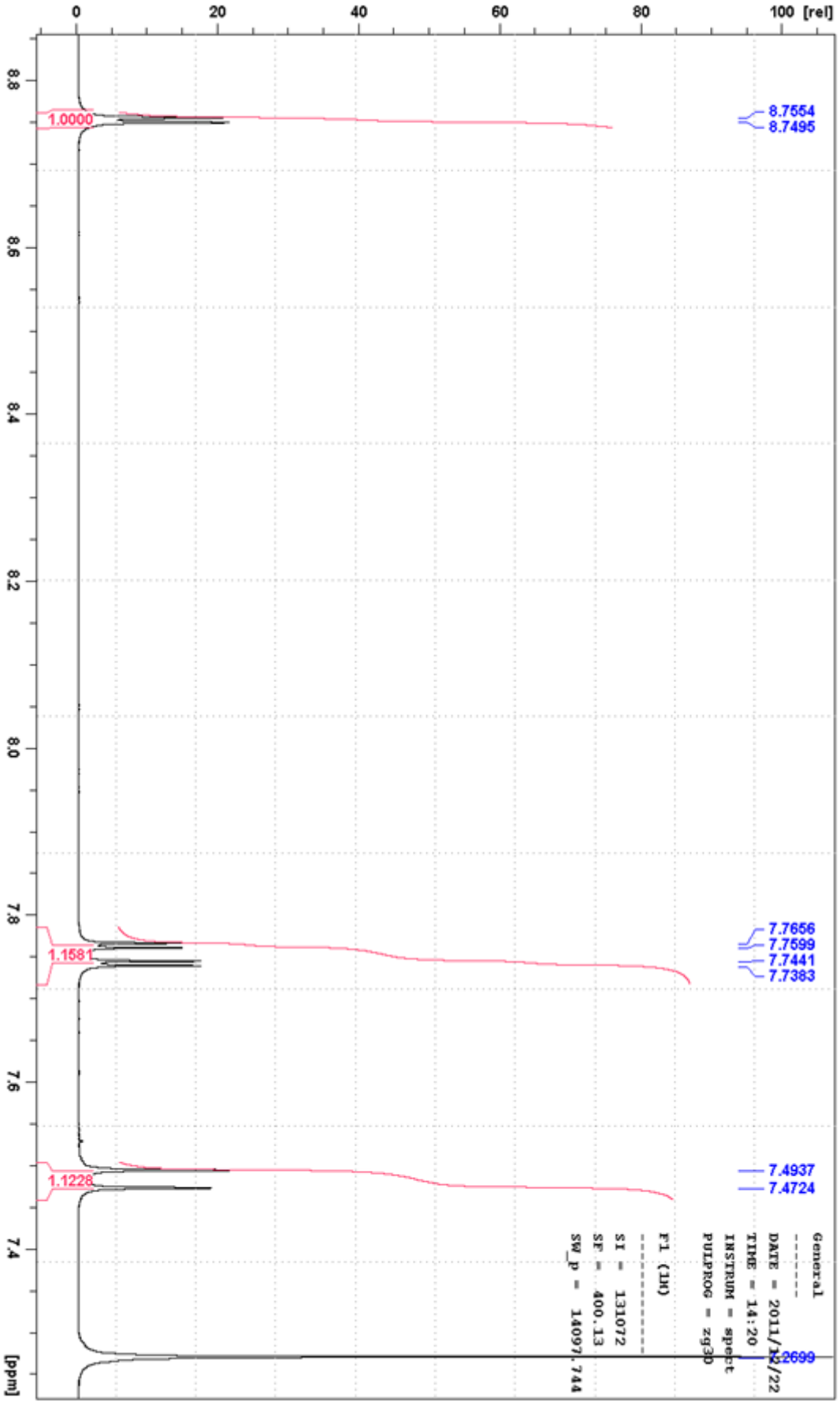

Figure F. 13 Expanded aromatic region for ^{1}H NMR of TX-Br2 in $CDCl_3$.

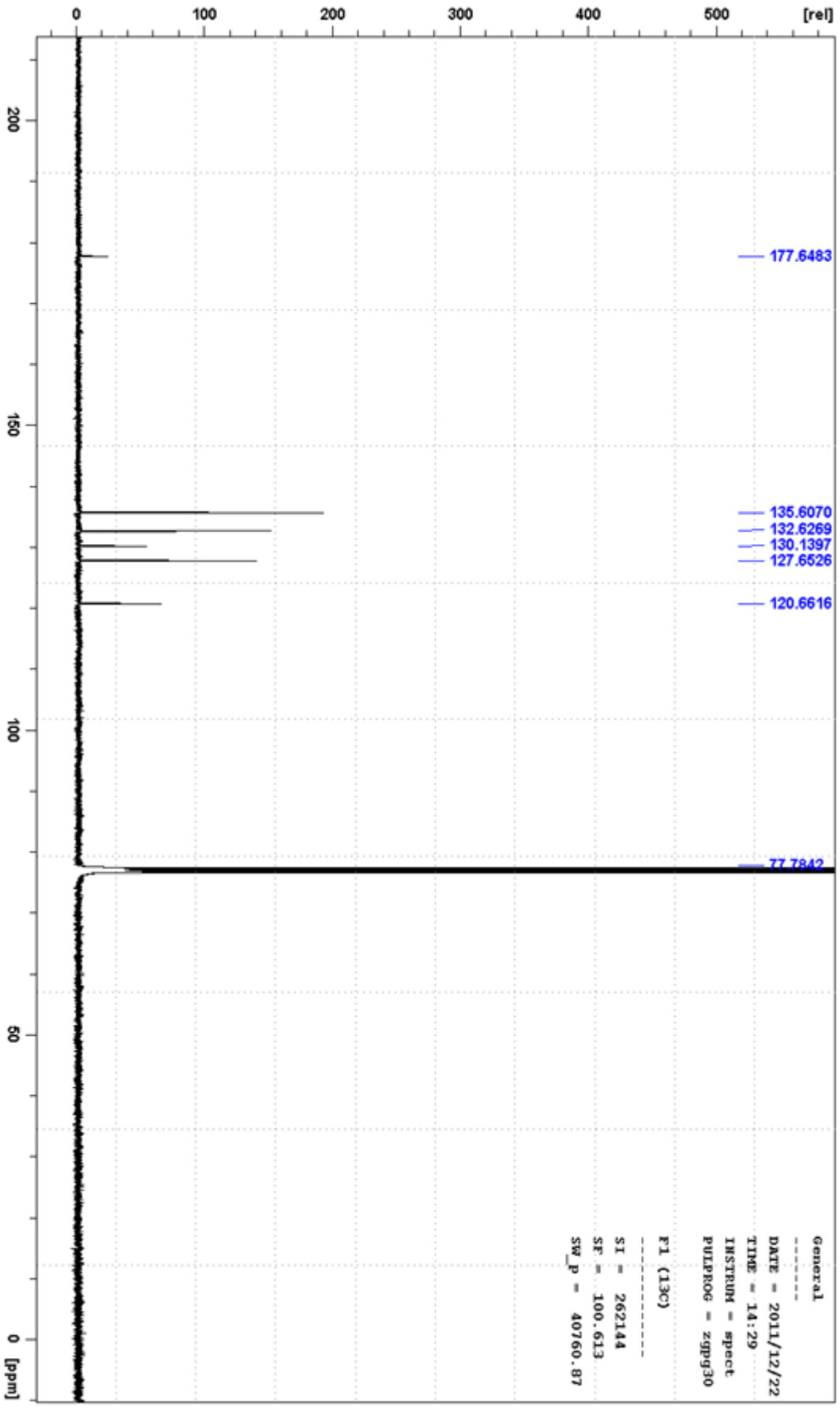

Figure F. 14 ^{13}C NMR of TX-Br_2 in $CDCl_3$

G. REFERENCES

[1] A. F. Masters, T. Maschmeyer, *Microporous Mesoporous Mat.* **2011**, *142*, 423.

[2] M. Rose, *Chemcatchem* **2014**, *6*, 1166.

[3] N. J. Turro, *Accounts of Chemical Research* **2000**, *33*, 637.

[4] Y. Zhang, S. A, Y. Zou, X. Luo, Z. Li, H. Xia, X. Liu, Y. Mu, *Journal of Materials Chemistry A* **2014**, *2*, 13422.

[5] E. Barea, C. Montoro, J. A. R. Navarro, *Chem. Soc. Rev.* **2014**, *43*, 5419.

[6] R. Dawson, A. I. Cooper, D. J. Adams, *Polym. Int.* **2013**, *62*, 345.

[7] J. P. Paraknowitsch, A. Thomas, *Energy Environ. Sci.* **2013**, *6*, 2839.

[8] T.-P. Fellinger, A. Thomas, J. Yuan, M. Antonietti, *Adv. Mater.* **2013**, *25*, 5838.

[9] A. Thomas, P. Kuhn, J. Weber, M.-M. Titirici, M. Antonietti, *Macromol. Rapid Commun.* **2009**, *30*, 221.

[10] J. Guo, Y. Xu, S. Jin, L. Chen, T. Kaji, Y. Honsho, M. A. Addicoat, J. Kim, A. Saeki, H. Ihee, S. Seki, S. Irle, M. Hiramoto, J. Gao, D. Jiang, *Nature communications* **2013**, *4*, 2736.

[11] M. Vallet-Regi, F. Balas, D. Arcos, *Angew. Chem.-Int. Edit.* **2007**, *46*, 7548.

[12] A. Thomas, *Angew. Chem.-Int. Edit.* **2010**, *49*, 8328.

[13] A. K. Cheetham, G. Ferey, T. Loiseau, *Angew. Chem.-Int. Edit.* **1999**, *38*, 3268.

[14] M. J. Rosseinsky, *Microporous Mesoporous Mat.* **2004**, *73*, 15.

[15] M.-C. Silaghi, C. Chizallet, P. Raybaud, *Microporous Mesoporous Mat.* **2014**, *191*, 82.

[16] E. Baktash, I. Zaharieva, M. Schroder, C. Goebel, H. Dau, A. Thomas, *Dalton Trans.* **2013**, *42*, 16920.

[17] K. Klingan, F. Ringleb, I. Zaharieva, J. Heidkamp, P. Chernev, D. Gonzalez-Flores, M. Risch, A. Fischer, H. Dau, *ChemSusChem* **2014**, *7*, 1301.

[18] R. J. Argauer, G. R. Landolt, Google Patents, **1972**.

[19] R. M. Dessau, Google Patents, **1984**.

[20] J. S. Beck, J. C. Vartuli, W. J. Roth, M. E. Leonowicz, C. T. Kresge, K. D. Schmitt, C. T. W. Chu, D. H. Olson, E. W. Sheppard, *J. Am. Chem. Soc.* **1992**, *114*, 10834.

[21] D. Zhao, Q. Huo, J. Feng, B. F. Chmelka, G. D. Stucky, *J. Am. Chem. Soc.* **1998**, *120*, 6024.

[22] P. Selvam, S. K. Bhatia, C. G. Sonwane, *Ind. Eng. Chem. Res.* **2001**, *40*, 3237.

[23] J. Lee, J. Kim, T. Hyeon, *Adv. Mater.* **2006**, *18*, 2073.

[24] P. Xiao, R. C. Davis, X. Ouyang, J. Li, A. Thomas, S. L. Scott, J. Zhu, *Catalysis Communications* **2014**, *50*, 69.

[25] P. Van Der Voort, D. Esquivel, E. De Canck, F. Goethals, I. Van Driessche, F. J. Romero-Salguero, *Chem. Soc. Rev.* **2012**, *42*, 3913.

[26] S. S. Park, M. Santha Moorthy, C.-S. Ha, *NPG Asia Mater* **2014**, *6*, e96.

[27] H. M. Lin, G. S. Zhu, J. J. Xing, B. Gao, S. L. Qiu, *Langmuir* **2009**, *25*, 10159.

[28] F. Auras, Y. Li, F. Löbermann, M. Döblinger, J. Schuster, L. M. Peter, D. Trauner, T. Bein, *Chem.-Eur. J.* **2014**, *20*, 14971.

[29] O. K. Farha, I. Eryazici, N. C. Jeong, B. G. Hauser, C. E. Wilmer, A. A. Sarjeant, R. Q. Snurr, S. T. Nguyen, A. O. Yazaydin, J. T. Hupp, *J. Am. Chem. Soc.* **2012**, *134*, 15016.

[30] S. M. Cohen, *Chem. Sci.* **2010**, *1*, 32.

[31] C. Janiak, J. K. Vieth, *New J. Chem.* **2010**, *34*, 2366.

[32] O. M. Yaghi, G. M. Li, H. L. Li, *Nature* **1995**, *378*, 703.

[33] S. S. Y. Chui, S. M. F. Lo, J. P. H. Charmant, A. G. Orpen, I. D. Williams, *Science* **1999**, *283*, 1148.

[34] S. Bordiga, L. Regli, F. Bonino, E. Groppo, C. Lamberti, B. Xiao, P. S. Wheatley, R. E. Morris, A. Zecchina, *Phys. Chem. Chem. Phys.* **2007**, *9*, 2676.

[35] H. Li, M. Eddaoudi, M. O'Keeffe, O. M. Yaghi, *Nature* **1999**, *402*, 276.

[36] A. Corma, H. Garcia, F. Xamena, *Chem. Rev.* **2010**, *110*, 4606.

[37] J.-R. Li, R. J. Kuppler, H.-C. Zhou, *Chem. Soc. Rev.* **2009**, *38*, 1477.

[38] P. Falcaro, R. Ricco, C. M. Doherty, K. Liang, A. J. Hill, M. J. Styles, *Chem. Soc. Rev.* **2014**, *43*, 5513.

[39] C. H. Hendon, D. Tiana, A. Walsh, *Phys. Chem. Chem. Phys.* **2012**, *14*, 13120.

[40] Y. H. Xu, S. B. Jin, H. Xu, A. Nagai, D. L. Jiang, *Chem. Soc. Rev.* **2013**, *42*, 8012.

[41] S. J. Xu, Y. L. Luo, B. E. Tan, *Macromol. Rapid Commun.* **2013**, *34*, 471.

[42] J. Y. Lee, C. D. Wood, D. Bradshaw, M. J. Rosseinsky, A. I. Cooper, *Chem. Commun.* **2006**, 2670.

[43] N. B. McKeown, P. M. Budd, *Chem. Soc. Rev.* **2006**, *35*, 675.

[44] N. B. McKeown, P. M. Budd, K. J. Msayib, B. S. Ghanem, H. J. Kingston, C. E. Tattershall, S. Makhseed, K. J. Reynolds, D. Fritsch, *Chem.-Eur. J.* **2005**, *11*, 2610.

[45] A. P. Cote, A. I. Benin, N. W. Ockwig, M. O'Keeffe, A. J. Matzger, O. M. Yaghi, *Science* **2005**, *310*, 1166.

[46] H. M. El-Kaderi, J. R. Hunt, J. L. Mendoza-Cortes, A. P. Cote, R. E. Taylor, M. O'Keeffe, O. M. Yaghi, *Science* **2007**, *316*, 268.

[47] P. Kuhn, M. Antonietti, A. Thomas, *Angew. Chem.-Int. Edit.* **2008**, *47*, 3450.

[48] M. J. Bojdys, J. Jeromenok, A. Thomas, M. Antonietti, *Adv. Mater.* **2008**, *22*, 2202.

[49] J. X. Jiang, F. Su, A. Trewin, C. D. Wood, N. L. Campbell, H. Niu, C. Dickinson, A. Y. Ganin, M. J. Rosseinsky, Y. Z. Khimyak, A. I. Cooper, *Angew. Chem.-Int. Edit.* **2007**, *46*, 8574.

[50] J. Schmidt, J. Weber, J. D. Epping, M. Antonietti, A. Thomas, *Adv. Mater.* **2009**, *21*, 702.

[51] E. Preis, C. Widling, G. Brunklaus, J. Schmidt, A. Thomas, U. Scherf, *Acs Macro Letters* **2013**, *2*, 380.

[52] E. Preis, C. Widling, U. Scherf, S. Patil, G. Brunklaus, J. Schmidt, A. Thomas, *Polym. Chem.* **2011**, *2*, 2186.

[53] M. P. Tsyurupa, V. A. Davankov, *Reactive and Functional Polymers* **2002**, *53*, 193.

[54] V. A. Davankov, M. P. Tsyurupa, *Reactive Polymers* **1990**, *13*, 27.

[55] M. P. Tsyurupa, V. A. Davankov, *Reactive and Functional Polymers* **2006**, *66*, 768.

[56] B. Y. Li, R. N. Gong, W. Wang, X. Huang, W. Zhang, H. M. Li, C. X. Hu, B. E. Tan, *Macromolecules* **2011**, *44*, 2410.

[57] M. P. Tsyuryupa, M. A. Papkov, V. A. Davankov, *Polymer Science Series C* **2009**, *51*, 81.

[58] R. Dawson, T. Ratvijitvech, M. Corker, A. Laybourn, Y. Z. Khimyak, A. I. Cooper, D. J. Adams, *Polym. Chem.* **2012**, *3*, 2034.

[59] R. T. Woodward, L. A. Stevens, R. Dawson, M. Vijayaraghavan, T. Hasell, I. P. Silverwood, A. V. Ewing, T. Ratvijitvech, J. D. Exley, S. Y. Chong, F. Blanc, D. J. Adams, S. G. Kazarian, C. E. Snape, T. C. Drage, A. I. Cooper, *J. Am. Chem. Soc.* **2014**, *136*, 9028.

[60] R. Dawson, L. A. Stevens, T. C. Drage, C. E. Snape, M. W. Smith, D. J. Adams, A. L. Cooper, *J. Am. Chem. Soc.* **2012**, *134*, 10741.

[61] S. Dadashi-Silab, H. Bildirir, R. Dawson, A. Thomas, Y. Yagci, *Macromolecules* **2014**, *47*, 4607.

[62] P. M. Budd, B. S. Ghanem, S. Makhseed, N. B. McKeown, K. J. Msayib, C. E. Tattershall, *Chem. Commun.* **2004**, 230.

[63] T. Tozawa, J. T. A. Jones, S. I. Swamy, S. Jiang, D. J. Adams, S. Shakespeare, R. Clowes, D. Bradshaw, T. Hasell, S. Y. Chong, C. Tang, S. Thompson, J. Parker, A. Trewin, J. Bacsa, A. M. Z. Slawin, A. Steiner, A. I. Cooper, *Nat. Mater.* **2009**, *8*, 973.

[64] S.-L. Huang, G.-X. Jin, H.-K. Luo, T. S. A. Hor, *Chemistry – An Asian Journal* **2014**, n/a.

[65] M. Mastalerz, *Chem.-Eur. J.* **2012**, *18*, 10082.

[66] N. B. McKeown, S. Hanif, K. Msayib, C. E. Tattershall, P. M. Budd, *Chem. Commun.* **2002**, 2782.

[67] N. B. McKeown, S. Makhseed, P. M. Budd, *Chem. Commun.* **2002**, 2780.

[68] F. J. Uribe-Romo, J. R. Hunt, H. Furukawa, C. Klock, M. O'Keeffe, O. M. Yaghi, *J. Am. Chem. Soc.* **2009**, *131*, 4570.

[69] K. Oh, K. S. Jeong, J. S. Moore, *J. Org. Chem.* **2003**, *68*, 8397.

[70] T. Ben, H. Ren, S. Q. Ma, D. P. Cao, J. H. Lan, X. F. Jing, W. C. Wang, J. Xu, F. Deng, J. M. Simmons, S. L. Qiu, G. S. Zhu, *Angew. Chem.-Int. Edit.* **2009**, *48*, 9457.

[71] Y. Yuan, F. X. Sun, H. Ren, X. F. Jing, W. Wang, H. P. Ma, H. J. Zhao, G. S. Zhu, *Journal of Materials Chemistry* **2011**, *21*, 13498.

[72] S. Fischer, J. Schmidt, P. Strauch, A. Thomas, *Angew. Chem.-Int. Edit.* **2013**, *52*, 12174.

[73] X. M. Liu, Y. H. Xu, D. L. Jiang, *J. Am. Chem. Soc.* **2012**, *134*, 8738.

[74] R. Dawson, A. Laybourn, R. Clowes, Y. Z. Khimyak, D. J. Adams, A. I. Cooper, *Macromolecules* **2009**, *42*, 8809.

[75] C. Gu, N. Huang, J. Gao, F. Xu, Y. Xu, D. Jiang, *Angewandte Chemie International Edition* **2014**, *53*, 4850.

[76] L. Chen, Y. Honsho, S. Seki, D. L. Jiang, *J. Am. Chem. Soc.* **2010**, *132*, 6742.

[77] L. Chen, Y. Yang, D. L. Jiang, *J. Am. Chem. Soc.* **2010**, *132*, 9138.

[78] H. Bildirir, J. P. Paraknowitsch, A. Thomas, *Chem. - Eur. J.* **2014**, *20*, 9543.

[79] S. Fischer, A. Schimanowitz, R. Dawson, I. Senkovska, S. Kaskel, A. Thomas, *Journal of Materials Chemistry A* **2014**.

[80] J. Schmidt, M. Werner, A. Thomas, *Macromolecules* **2009**, *42*, 4426.

[81] J. Weber, A. Thomas, *J. Am. Chem. Soc.* **2008**, *130*, 6334.

[82] Y. G. Zhang, S. N. Riduan, *Chem. Soc. Rev.* **2012**, *41*, 2083.

[83] X. C. Wang, K. Maeda, A. Thomas, K. Takanabe, G. Xin, J. M. Carlsson, K. Domen, M. Antonietti, *Nat. Mater.* **2009**, *8*, 76.

[84] K. Kailasam, J. Schmidt, H. Bildirir, G. G. Zhang, S. Blechert, X. C. Wang, A. Thomas, *Macromol. Rapid Commun.* **2013**, *34*, 1008.

[85] J. Roeser, K. Kailasam, A. Thomas, *ChemSusChem* **2012**, *5*, 1793.

[86] D. S. Kundu, J. Schmidt, C. Bleschke, A. Thomas, S. Blechert, *Angew. Chem.-Int. Edit.* **2012**, *51*, 5456.

[87] B. Li, Z. Guan, W. Wang, X. Yang, J. Hu, B. Tan, T. Li, *Adv. Mater.* **2012**, *24*, 3390.

[88] J. M. Brunel, *Chem. Rev.* **2005**, *105*, 857.

[89] R. Dawson, A. I. Cooper, D. J. Adams, *Prog. Polym. Sci.* **2012**, *37*, 530.

[90] R. Dawson, D. J. Adams, A. I. Cooper, *Chem. Sci.* **2011**, *2*, 1173.

[91] W. G. Lu, D. Q. Yuan, J. L. Sculley, D. Zhao, R. Krishna, H. C. Zhou, *J. Am. Chem. Soc.* **2011**, *133*, 18126.

[92] J. L. Novotney, W. R. Dichtel, *ACS Macro Letters* **2013**, *2*, 423.

[93] A. Patra, U. Scherf, *Chem.-Eur. J.* **2012**, *18*, 10074.

[94] A. Patra, J.-M. Koenen, U. Scherf, *Chem. Commun.* **2011**, *47*, 9612.

[95] K. Takimiya, I. Osaka, T. Mori, M. Nakano, *Accounts of Chemical Research* **2014**, *47*, 1493.

[96] C. L. Wang, H. L. Dong, W. P. Hu, Y. Q. Liu, D. B. Zhu, *Chem. Rev.* **2012**, *112*, 2208.

[97] A. C. Mayer, S. R. Scully, B. E. Hardin, M. W. Rowell, M. D. McGehee, *Materials Today* **2007**, *10*, 28.

[98] J. S. Yu, Y. F. Zheng, J. Huang, *Polymers* **2014**, *6*, 2473.

[99] H. Sirringhaus, *Adv. Mater.* **2014**, *26*, 1319.

[100] J. Zaumseil, H. Sirringhaus, *Chem. Rev.* **2007**, *107*, 1296.

[101] B. Minaev, G. Baryshnikov, H. Agren, *Phys. Chem. Chem. Phys.* **2014**, *16*, 1719.

[102] S. Mukherjee, P. Thilagar, *Dyes and Pigments* **2014**, *110*, 2.

[103] P. J. Skabara, J.-B. Arlin, Y. H. Geerts, *Adv. Mater.* **2013**, *25*, 1948.

[104] R. Gutzler, D. F. Perepichka, *J. Am. Chem. Soc.* **2013**, *135*, 16585.

[105] C. Gu, Y. Chen, Z. Zhang, S. Xue, S. Sun, K. Zhang, C. Zhong, H. Zhang, Y. Pan, Y. Lv, Y. Yang, F. Li, S. Zhang, F. Huang, Y. Ma, *Adv. Mater.* **2013**, *25*, 3443.

[106] M. Dogru, M. Handloser, F. Auras, T. Kunz, D. Medina, A. Hartschuh, P. Knochel, T. Bein, *Angew. Chem.-Int. Edit.* **2013**, *52*, 2920.

[107] A. Saeki, Y. Koizumi, T. Aida, S. Seki, *Accounts of Chemical Research* **2012**, *45*, 1193.

[108] G. Algara-Siller, N. Severin, S. Y. Chong, T. Bjorkman, R. G. Palgrave, A. Laybourn, M. Antonietti, Y. Z. Khimyak, A. V. Krasheninnikov, J. P. Rabe, U. Kaiser, A. I. Cooper, A. Thomas, M. J. Bojdys, *Angew. Chem.-Int. Edit.* **2014**, *53*, 7450.

[109] S. Lowell, J. Shields, M. Thomas, M. Thommes, in *Characterization of Porous Solids and Powders: Surface Area, Pore Size and Density, Vol. 16*, Springer Netherlands, **2004**, pp. 5.

[110] I. Langmuir, *J. Am. Chem. Soc.* **1916**, *38*, 2221.

[111] S. Brunauer, P. H. Emmett, E. Teller, *J. Am. Chem. Soc.* **1938**, *60*, 309.

[112] S. Lowell, J. Shields, M. Thomas, M. Thommes, in *Characterization of Porous Solids and Powders: Surface Area, Pore Size and Density, Vol. 16*, Springer Netherlands, **2004**, pp. 15.

[113] Micromeritics-INC, *http://www.micromeritics.com/repository/files/gas_sorption.pdf*.

[114] U. H. F. Bunz, K. Seehafer, F. L. Geyer, M. Bender, I. Braun, E. Smarsly, J. Freudenberg, *Macromol. Rapid Commun.* **2014**, *35*, 1466.

[115] K. S. W. Sing, D. H. Everett, R. A. W. Haul, L. Moscou, R. A. Pierotti, J. Rouquerol, T. Siemieniewska, *Pure Appl. Chem.* **1985**, *57*, 603.

[116] K. A. Cychosz, X. Guo, W. Fan, R. Cimino, G. Y. Gor, M. Tsapatsis, A. V. Neimark, M. Thommes, *Langmuir* **2012**, *28*, 12647.

[117] P. I. Ravikovitch, S. C. Odomhnaill, A. V. Neimark, F. Schuth, K. K. Unger, *Langmuir* **1995**, *11*, 4765.

[118] P. I. Ravikovitch, A. V. Neimark, *Colloids and Surfaces a-Physicochemical and Engineering Aspects* **2001**, *187*, 11.

[119] Perkin-Elmer, *http://www.perkinelmer.com/cmsresources/images/44-74668prd_diffusereflectancetransmittance.pdf*.

[120] S. E. Ashbrook, S. Sneddon, *J. Am. Chem. Soc.* **2014**, *136*, 15440.

[121] J. Klinowski, J. Hennel, J. Klinowski, in *New Techniques in Solid-State NMR, Vol. 246*, Springer Berlin Heidelberg, **2005**, pp. 1.

[122] L. Zhang, Z. Liu, Q. Chen, E. W. Hansen, *Macromolecules* **2007**, *40*, 5411.

[123] C. M. Oshiro, in *Other Information: Portions of document are illegible*, **1982**, p. Medium: ED; Size: Pages: 137.

[124] F. Wudl, G. M. Smith, E. J. Hufnagel, *Journal of the Chemical Society D-Chemical Communications* **1970**, 1453.

[125] F. Wudl, Wobschal.D, E. J. Hufnagel, *J. Am. Chem. Soc.* **1972**, *94*, 670.

[126] N. Bashir, J. A. Murphy, *Chem. Commun.* **2000**, 627.

[127] J. O. Jeppesen, M. B. Nielsen, J. Becher, *Chem. Rev.* **2004**, *104*, 5115.

[128] K. B. Simonsen, J. Becher, *Synlett* **1997**, 1211.

[129] J. Lyskawa, F. Le Derf, E. Levillain, M. Mazari, M. Salle, L. Dubois, P. Viel, C. Bureau, S. Palacin, *J. Am. Chem. Soc.* **2004**, *126*, 12194.

[130] J. B. Torrance, B. A. Scott, B. Welber, F. B. Kaufman, P. E. Seiden, *Phys. Rev. B* **1979**, *19*, 730.

[131] E. Ertas, F. B. Kaynak, S. Ozbey, I. Osken, T. Ozturk, *Tetrahedron* **2008**, *64*, 10581.

[132] J. M. Williams, A. M. Kini, H. H. Wang, K. D. Carlson, U. Geiser, L. K. Montgomery, G. J. Pyrka, D. M. Watkins, J. M. Kommers, S. J. Boryschuk, A. V. S. Crouch, W. K. Kwok, J. E. Schirber, D. L. Overmyer, D. Jung, M. H. Whangbo, *Inorg. Chem.* **1990**, *29*, 3272.

[133] J. M. Williams, A. J. Schultz, U. Geiser, K. D. Carlson, A. M. Kini, H. H. Wang, W. K. Kwok, M. H. Whangbo, J. E. Schirber, *Science* **1991**, *252*, 1501.

[134] J. Ferraris, V. Walatka, Perlstei.Jh, D. O. Cowan, *J. Am. Chem. Soc.* **1973**, *95*, 948.

[135] M. R. Bryce, *Adv. Mater.* **1999**, *11*, 11.

[136] H. Kobayashi, A. Kobayashi, H. Tajima, *Chem.-Asian J.* **2011**, *6*, 1688.

[137] Y. Okamoto, H. S. Lee, S. T. Attarwala, *J. Org. Chem.* **1985**, *50*, 2788.

[138] M. Somei, F. Yamada, A. Goto, M. Hayashi, M. Hasegawa, *Heterocycles* **2000**, *53*, 2487.

[139] K. Takimiya, A. Morikami, T. Otsubo, *Synlett* **1997**, 319.

[140] M. Bendikov, F. Wudl, D. F. Perepichka, *Chem. Rev.* **2004**, *104*, 4891.

[141] K. B. Simonsen, N. Svenstrup, J. Lau, O. Simonsen, P. Mork, G. J. Kristensen, J. Becher, *Synthesis* **1996**, 407.

[142] C. S. Wang, A. Ellern, V. Khodorkovsky, J. Bernstein, J. Y. Becker, *J. Chem. Soc.-Chem. Commun.* **1994**, 983.

[143] J. M. Fabre, *Chem. Rev.* **2004**, *104*, 5133.

[144] J. D. Wallis, J. P. Griffiths, *Journal of Materials Chemistry* **2005**, *15*, 347.

[145] E. Ertas, T. Ozturk, *Chem. Commun.* **2000**, 2039.

[146] M. R. Tomcsi, *Tetrathiafulvalene (TTF): Building Block of the Materials Chemist*, **2007**.

[147] T. Anjos, A. Charlton, S. J. Coles, A. K. Croft, M. B. Hursthouse, M. Kalaji, P. J. Murphy, S. J. Roberts-Bleming, *Macromolecules* **2009**, *42*, 2505.

[148] M. Gonzalez, J. L. Segura, C. Seoane, N. Martin, J. Garin, J. Orduna, R. Alcala, B. Villacampa, V. Hernandez, J. T. L. Navarrete, *J. Org. Chem.* **2001**, *66*, 8872.

[149] K. Walzer, B. Maennig, M. Pfeiffer, K. Leo, *Chem. Rev.* **2007**, *107*, 1233.

[150] H. Usta, A. Facchetti, T. J. Marks, *Accounts of Chemical Research* **2011**, *44*, 501.

[151] L. Huchet, S. Akoudad, E. Levillain, J. Roncali, A. Emge, P. Bauerle, *Journal of Physical Chemistry B* **1998**, *102*, 7776.

[152] A. Charlton, A. E. Underhill, G. Williams, M. Kalaji, P. J. Murphy, K. M. A. Malik, M. B. Hursthouse, *J. Org. Chem.* **1997**, *62*, 3098.

[153] P. J. Skabara, K. Mullen, *Synth. Met.* **1997**, *84*, 345.

[154] M. Shao, Y. M. Zhao, *Tetrahedron Lett.* **2009**, *50*, 6897.

[155] E. Ertas, H. Bildirir, O. Sahin, I. Oksen, *Phosphorus Sulfur Silicon Relat. Elem.* **2013**, *188*, 1835.

[156] L. Huchet, S. Akoudad, J. Roncali, *Adv. Mater.* **1998**, *10*, 541.

[157] P. J. Skabara, D. M. Roberts, I. M. Serebryakov, C. Pozo-Gonzalo, *Chem. Commun.* **2000**, 1005.

[158] M. Mas-Torrent, C. Rovira, *Chem. Soc. Rev.* **2008**, *37*, 827.

[159] N. Martin, L. Sanchez, M. A. Herranz, B. Illescas, D. M. Guldi, *Accounts of Chemical Research* **2007**, *40*, 1015.

[160] H. Jiang, X. J. Yang, Z. D. Cui, Y. C. Liu, H. X. Li, W. P. Hu, C. Kloc, *Crystengcomm* **2014**, *16*, 5968.

[161] Y. Takahashi, T. Hasegawa, S. Horiuchi, R. Kumai, Y. Tokura, G. Saito, *Chem. Mat.* **2007**, *19*, 6382.

[162] A. Kumar, A. K. Palai, Y. Dongmyung, C. Sungwoo, P. Seung-un, P. Seungmoon, *J. Phys. D, Appl. Phys.* **2014**, *47*, 355101 (8 pp.).

[163] Y. R. Su, M. Ouyang, P. Y. Liu, Z. Luo, W. G. Xie, J. B. Xu, *Acs Applied Materials & Interfaces* **2013**, *5*, 4960.

[164] F. L. Xue, Y. Su, K. Varahramyan, *IEEE Trans. Electron Devices* **2005**, *52*, 1982.

[165] A. Amacher, C. Y. Yi, J. B. Yang, M. P. Bircher, Y. C. Fu, M. Cascella, M. Gratzel, S. Decurtins, S. X. Liu, *Chem. Commun.* **2014**, *50*, 6540.

[166] J. Liu, Y. Z. Wu, C. J. Qin, X. D. Yang, T. Yasuda, A. Islam, K. Zhang, W. Q. Peng, W. Chen, L. Y. Han, *Energy Environ. Sci.* **2014**, *7*, 2963.

[167] X. Guo, M. Baumgarten, K. Mullen, *Prog. Polym. Sci.* **2013**, *38*, 1832.

[168] A. Facchetti, *Chem. Mat.* **2011**, *23*, 733.

[169] B. Capozzi, E. J. Dell, T. C. Berkelbach, D. R. Reichman, L. Venkataraman, L. M. Campos, *J. Am. Chem. Soc.* **2014**, *136*, 10486.

[170] I. Osken, O. Sahin, A. S. Gundogan, H. Bildirir, A. Capan, E. Ertas, M. S. Eroglu, J. D. Wallis, K. Topal, T. Ozturk, *Tetrahedron* **2012**, *68*, 1216.

[171] A. Mishra, C.-Q. Ma, J. L. Segura, P. Bäuerle, in *Handbook of Thiophene-Based Materials*, John Wiley & Sons, Ltd, **2009**, pp. 1.

[172] K. Meerholz, J. Heinze, *Electrochim. Acta* **1996**, *41*, 1839.

[173] S. J. Wei, J. L. Xia, E. J. Dell, Y. V. Jiang, R. Song, H. Lee, P. Rodenbough, A. L. Briseno, L. M. Campos, *Angew. Chem.-Int. Edit.* **2014**, *53*, 1832.

[174] B. Q. Q. Xu, X. L. L. Li, X. Y. Y. Xiao, H. Sakaguchi, N. J. J. Tao, *Nano Lett.* **2005**, *5*, 1491.

[175] Z. Fei, P. Pattanasattayavong, Y. Han, B. C. Schroeder, F. Yan, R. J. Kline, T. D. Anthopoulos, M. Heeney, *J. Am. Chem. Soc.* **2014**, *136*, 15154.

[176] K. Reuter, S. Kirchmeyer, A. Elschner, in *Handbook of Thiophene-Based Materials*, John Wiley & Sons, Ltd, **2009**, pp. 549.

[177] P. J. Skabara, in *Handbook of Thiophene-Based Materials*, John Wiley & Sons, Ltd, **2009**, pp. 219.

[178] X. N. Zhang, A. P. Cote, A. J. Matzger, *J. Am. Chem. Soc.* **2005**, *127*, 10502.

[179] G. E. Park, J. Shin, D. H. Lee, T. W. Lee, H. Shim, M. J. Cho, S. Pyo, D. H. Choi, *Macromolecules* **2014**, *47*, 3747.

[180] G. Barbarella, M. Melucci, G. Sotgiu, *Adv. Mater.* **2005**, *17*, 1581.

[181] T. Ozturk, E. Ertas, O. Mert, *Tetrahedron* **2005**, *61*, 11055.

[182] A. Capan, H. Veisi, A. C. Goren, T. Ozturk, *Macromolecules* **2012**, *45*, 8228.

[183] S. Holliday, J. E. Donaghey, I. McCulloch, *Chem. Mat.* **2014**, *26*, 647.

[184] Y. Liu, Y. Q. Liu, X. W. Zhan, *Macromol. Chem. Phys.* **2011**, *212*, 428.

[185] P. Leriche, J. M. Raimundo, M. Turbiez, V. Monroche, M. Allain, F. X. Sauvage, J. Roncali, P. Frere, P. J. Skabara, *Journal of Materials Chemistry* **2003**, *13*, 1324.

[186] K. Kyung Hwan, C. Zhenguo, C. Min Ju, J. Jung-Il, C. Mi Yeon, K. Su Jin, J. Jin-soo, C. Dong Hoon, *Chem. Mat.* **2007**, *19*, 4925.

[187] L. San Miguel, W. W. Porter, A. J. Matzger, *Organic Letters* **2007**, *9*, 1005.

[188] S. L. Li, K. J. Jiang, K. F. Shao, L. M. Yang, *Chem. Commun.* **2006**, 2792.

[189] X. W. Zhan, Z. A. Tan, B. Domercq, Z. S. An, X. Zhang, S. Barlow, Y. F. Li, D. B. Zhu, B. Kippelen, S. R. Marder, *J. Am. Chem. Soc.* **2007**, *129*, 7246.

[190] J. A. Schneider, A. Dadvand, W. Wen, D. F. Perepichka, *Macromolecules* **2013**, *46*, 9231.

[191] E. Tedesco, F. Della Sala, L. Favaretto, G. Barbarella, D. Albesa-Jove, D. Pisignano, G. Gigli, R. Cingolani, K. D. M. Harris, *J. Am. Chem. Soc.* **2003**, *125*, 12277.

[192] I. Osken, A. S. Gundogan, E. Tekin, M. S. Eroglu, T. Ozturk, *Macromolecules* **2013**, *46*, 9202.

[193] I. McCulloch, M. Heeney, in *Handbook of Thiophene-Based Materials*, John Wiley & Sons, Ltd, **2009**, pp. 647.

[194] H.-J. Jhuo, P.-N. Yeh, S.-H. Liao, Y.-L. Li, Y.-S. Cheng, S.-A. Chen, *Journal of the Chinese Chemical Society* **2014**, *61*, 115.

[195] I. McCulloch, M. Heeney, C. Bailey, K. Genevicius, I. Macdonald, M. Shkunov, D. Sparrowe, S. Tierney, R. Wagner, W. M. Zhang, M. L. Chabinyc, R. J. Kline, M. D. McGehee, M. F. Toney, *Nat. Mater.* **2006**, *5*, 328.

[196] Y. Liang, Z. Xu, J. Xia, S.-T. Tsai, Y. Wu, G. Li, C. Ray, L. Yu, *Adv. Mater.* **2010**, *22*, E135.

[197] Y. Wu, Z. J. Li, W. Ma, Y. Huang, L. J. Huo, X. Guo, M. J. Zhang, H. Ade, J. H. Hou, *Adv. Mater.* **2013**, *25*, 3449.

[198] J. Hellberg, T. Remonen, *Synth. Met.* **1995**, *70*, 1137.

[199] F. Allared, J. Hellberg, T. Remonen, *Tetrahedron Lett.* **2002**, *43*, 1553.

[200] W. Schroth, E. Hintzsche, H. Jordan, T. Jende, R. Spitzner, I. Thondorf, *Tetrahedron* **1997**, *53*, 7509.

[201] M. M. Krayushkin, F. M. Stoyanovich, O. Y. Zolotarskaya, V. N. Yarovenko, V. N. Bulgakova, I. V. Zavarzin, A. Y. Martynkin, *Russ. Chem. Bull.* **2002**, *51*, 2097.

[202] J. Frey, A. D. Bond, A. B. Holmes, *Chem. Commun.* **2002**, 2424.

[203] E. Ertas, T. Ozturk, *Tetrahedron Lett.* **2004**, *45*, 3405.

[204] M. J. Janssen, F. De Jong, *The Journal of Organic Chemistry* **1971**, *36*, 1645.

[205] Z. Y. Xiao, K. Sun, J. Subbiah, S. M. Ji, D. J. Jones, W. W. H. Wong, *Sci Rep* **2014**, *4*, 7.

[206] J. W. Jung, F. Liu, T. P. Russell, W. H. Jo, *Energy Environ. Sci.* **2012**, *5*, 6857.

[207] A. V. Patil, W. H. Lee, K. Kim, H. Park, I. N. Kang, S. H. Lee, *Polym. Chem.* **2011**, *2*, 2907.

[208] W. P. Wu, Y. Q. Liu, D. B. Zhu, *Chem. Soc. Rev.* **2010**, *39*, 1489.

[209] Y. S. Yang, T. Yasuda, H. Kakizoe, H. Mieno, H. Kino, Y. Tateyama, C. Adachi, *Chem. Commun.* **2013**, *49*, 6483.

[210] X. G. Zhao, L. C. Ma, L. Zhang, Y. G. Wen, J. M. Chen, Z. G. Shuai, Y. Q. Liu, X. W. Zhan, *Macromolecules* **2013**, *46*, 2152.

[211] C. Santato, L. Favaretto, M. Melucci, A. Zanelli, M. Gazzano, M. Monari, D. Isik, D. Banville, S. Bertolazzi, S. Loranger, F. Cicoira, *Journal of Materials Chemistry* **2010**, *20*, 669.

[212] G. Barbarella, L. Favaretto, G. Sotgiu, M. Zambianchi, C. Arbizzani, A. Bongini, M. Mastragostino, *Chem. Mat.* **1999**, *11*, 2533.

[213] G. Barbarella, L. Favaretto, G. Sotgiu, L. Antolini, G. Gigli, R. Cingolani, A. Bongini, *Chem. Mat.* **2001**, *13*, 4112.

[214] F. Della Sala, V. Vitale, M. Mazzeo, R. Cingolani, G. Gigli, L. Favaretto, G. Barbarella, *J. Non-Cryst. Solids* **2006**, *352*, 2461.

[215] M. Mazzeo, V. Vitale, F. Della Sala, M. Anni, G. Barbarella, L. Favaretto, G. Sotgiu, R. Cingolani, G. Gigli, *Adv. Mater.* **2005**, *17*, 34.

[216] Y. Yagci, O. Sahin, T. Ozturk, S. Marchi, S. Grassini, M. Sangermano, *React. Funct. Polym.* **2011**, *71*, 857.

[217] S. Beyazit, B. Aydogan, I. Osken, T. Ozturk, Y. Yagci, *Polym. Chem.* **2011**, *2*, 1185.

[218] B. Aydogan, A. S. Gundogan, T. Ozturk, Y. Yagci, *Chem. Commun.* **2009**, 6300.

[219] Y. Yagci, S. Jockusch, N. J. Turro, *Macromolecules* **2010**, *43*, 6245.

[220] B. Gacal, H. Akat, D. K. Balta, N. Arsu, Y. Yagci, *Macromolecules* **2008**, *41*, 2401.

[221] L. Cokbaglan, N. Arsu, Y. Yagci, S. Jockusch, N. J. Turro, *Macromolecules* **2003**, *36*, 2649.

[222] M. Aydin, N. Arsu, Y. Yagci, *Macromol. Rapid Commun.* **2003**, *24*, 718.

[223] M. Aydin, N. Arsu, Y. Yagci, S. Jockusch, N. J. Turro, *Macromolecules* **2005**, *38*, 4133.

[224] G. Yilmaz, A. Tuzun, Y. Yagci, *J. Polym. Sci., Part A: Polym. Chem.* **2010**, *48*, 5120.

[225] D. K. Balta, N. Arsu, Y. Yagci, S. Jockusch, N. J. Turro, *Macromolecules* **2007**, *40*, 4138.

[226] J. Z. Shao, Y. Huang, Q. U. Fan, *Polym. Chem.* **2014**, *5*, 4195.

[227] G. Yilmaz, B. Aydogan, G. Temel, N. Arsu, N. Moszner, Y. Yagci, *Macromolecules* **2010**, *43*, 4520.

[228] G. Yilmaz, S. Beyazit, Y. Yagci, *J. Polym. Sci. Pol. Chem.* **2011**, *49*, 1591.

[229] M. Calik, F. Auras, L. M. Salonen, K. Bader, I. Grill, M. Handloser, D. D. Medina, M. Dogru, F. LÃ¶bermann, D. Trauner, A. Hartschuh, T. Bein, *J. Am. Chem. Soc.* **2014**, *136*, 17802.

[230] D. Bélanger, in *Handbook of Thiophene-Based Materials*, John Wiley & Sons, Ltd, **2009**, pp. 577.

[231] A. Facchetti, in *Handbook of Thiophene-Based Materials*, John Wiley & Sons, Ltd, **2009**, pp. 595.

[232] S. A. Gevorgyan, F. C. Krebs, in *Handbook of Thiophene-Based Materials*, John Wiley & Sons, Ltd, **2009**, pp. 673.

[233] D. Canevet, M. Salle, G. X. Zhang, D. Q. Zhang, D. B. Zhu, *Chem. Commun.* **2009**, 2245.

[234] H. Ding, Y. Li, H. Hu, Y. Sun, J. Wang, C. Wang, C. Wang, G. Zhang, B. Wang, W. Xu, D. Zhang, *Chem. - Eur. J.* **2014**, *20*, 14614.

[235] S. Jin, T. Sakurai, T. Kowalczyk, S. Dalapati, F. Xu, H. Wei, X. Chen, J. Gao, S. Seki, S. Irle, D. Jiang, *Chem. - Eur. J.* **2014**, *20*, 14608.

[236] S.-L. Cai, Y.-B. Zhang, A. B. Pun, B. He, J. Yang, F. M. Toma, I. D. Sharp, O. M. Yaghi, J. Fan, S.-R. Zheng, W.-G. Zhang, Y. Liu, *Chem. Sci.* **2014**, *5*, 4693.

[237] S. S. Park, E. R. Hontz, L. Sun, C. H. Hendon, A. Walsh, T. Van Voorhis, M. Dinca, *J. Am. Chem. Soc.* **2015**.

[238] T. C. Narayan, T. Miyakai, S. Seki, M. Dinca, *J. Am. Chem. Soc.* **2012**, *134*, 12932.

[239] J. X. Jiang, F. Su, A. Trewin, C. D. Wood, H. Niu, J. T. A. Jones, Y. Z. Khimyak, A. I. Cooper, *J. Am. Chem. Soc.* **2008**, *130*, 7710.

[240] R. Dawson, A. Laybourn, Y. Z. Khimyak, D. J. Adams, A. I. Cooper, *Macromolecules* **2010**, *43*, 8524.

[241] S. J. Ren, R. Dawson, D. J. Adams, A. Cooper, *Polym. Chem.* **2013**, *4*, 5585.

[242] T. Hundertmark, A. F. Littke, S. L. Buchwald, G. C. Fu, *Organic Letters* **2000**, *2*, 1729.

[243] L. L. Hill, J. A. Smith, W. S. Brown, L. R. Moore, P. Guevera, E. S. Pair, J. Porter, J. Chou, C. J. Wolterman, R. Craciun, D. A. Dixon, K. H. Shaughnessy, *Tetrahedron* **2008**, *64*, 6920.

[244] R. Chinchilla, C. Najera, *Chem. Soc. Rev.* **2011**, *40*, 5084.

[245] M. d. Alami, F. Ferri, G. r. Linstrumelle, *Tetrahedron Lett.* **1993**, *34*, 6403.

[246] U. H. F. Bunz, *Chem. Rev.* **2000**, *100*, 1605.

[247] R. Chinchilla, C. Najera, *Chem. Rev.* **2007**, *107*, 874.

[248] G. Cheng, B. Bonillo, R. S. Sprick, D. J. Adams, T. Hasell, A. I. Cooper, *Adv. Funct. Mater.* **2014**, *24*, 5219.

[249] A. Laybourn, R. Dawson, R. Clowes, T. Hasell, A. I. Cooper, Y. Z. Khimyak, D. J. Adams, *Polym. Chem.* **2014**, *5*, 6325.

[250] R. B. Somoano, A. Gupta, V. Hadek, T. Datta, M. Jones, R. Deck, A. M. Hermann, *J. Chem. Phys.* **1975**, *63*, 4970.

[251] Q. Y. Zhu, Y. Liu, W. Lu, Y. Zhang, G. Q. Bian, G. Y. Niu, J. Dai, *Inorg. Chem.* **2007**, *46*, 10065.

[252] A. Coskun, J. M. Spruell, G. Barin, A. C. Fahrenbach, R. S. Forgan, M. T. Colvin, R. Carmieli, D. Benitez, E. Tkatchouk, D. C. Friedman, A. A. Sarjeant, M. R. Wasielewski, W. A. Goddard, J. F. Stoddart, *J. Am. Chem. Soc.* **2011**, *133*, 4538.

[253] E. Gomar-Nadal, J. Veciana, C. Rovira, D. B. Amabilino, *Adv. Mater.* **2005**, *17*, 2095.

[254] R. Andreu, J. Garin, J. Orduna, *Tetrahedron* **2001**, *57*, 7883.

[255] P. R. Ashton, V. Balzani, J. Becher, A. Credi, M. C. T. Fyfe, G. Mattersteig, S. Menzer, M. B. Nielsen, F. i. M. Raymo, J. F. Stoddart, M. Venturi, D. J. Williams, *J. Am. Chem. Soc.* **1999**, *121*, 3951.

[256] J. G. Yang, D. Chen, W. L. Bao, *Tetrahedron Lett.* **2012**, *53*, 3984.

[257] E. Miyazaki, Y. Morita, Y. Yakiyama, S. Maki, Y. Umemoto, M. Ohmoto, K. Nakasuji, *Chem. Lett.* **2007**, *36*, 1102.

[258] A. S. Dhindsa, Y. P. Song, J. P. Badyal, M. R. Bryce, Y. M. Lvov, M. C. Petty, J. Yarwood, *Chem. Mat.* **1992**, *4*, 724.

[259] H. Sakai, M. Mizota, Y. Maeda, *Bull. Chem. Soc. Jpn.* **1986**, *59*, 3417.

[260] M. D. Halling, J. D. Bell, R. J. Pugmire, D. M. Grant, J. S. Miller, *J. Phys. Chem. A* **2010**, *114*, 6622.

[261] J. Casado, V. Hernandez, S. Hotta, J. T. L. Navarrete, *J. Chem. Phys.* **1998**, *109*, 10419.

[262] J. Casado, V. Hernandez, Y. Kanemitsu, J. T. L. Navarrete, *J. Raman Spectrosc.* **2000**, *31*, 565.

[263] B. Barszcz, A. Lapinski, A. Graja, A. M. Flakina, A. N. Chekhlov, R. N. Lyubovskaya, *Chem. Phys.* **2006**, *330*, 486.

[264] L. Gomez, R. Rodriguez-Amaro, *Langmuir* **2009**, *25*, 4799.

[265] C. Coulon, R. Clerac, *Chem. Rev.* **2004**, *104*, 5655.

[266] M. Chiesa, E. Giamello, M. Che, *Chem. Rev.* **2010**, *110*, 1320.

[267] L. Cavara, F. Gerson, D. O. Cowan, K. Lerstrup, *Helv. Chim. Acta* **1986**, *69*, 141.

[268] Y. H. Hou, Y. S. Chen, Q. Lin, M. Yang, X. J. Wan, S. G. Yin, A. Yu, *Macromolecules* **2008**, *41*, 3114.

[269] T. Yamamoto, T. Shimizu, *Journal of Materials Chemistry* **1997**, *7*, 1967.

[270] A. P. Katsoulidis, S. M. Dyar, R. Carmieli, C. D. Malliakas, M. R. Wasielewski, M. G. Kanatzidis, *Journal of Materials Chemistry A* **2013**, *1*, 10465.

[271] S.-L. Cai, Y.-B. Zhang, A. B. Pun, B. He, J. Yang, F. M. Toma, I. D. Sharp, O. M. Yaghi, J. Fan, S.-R. Zheng, W.-G. Zhang, Y. Liu, *Chem. Sci.* **2014**.

[272] T. Yamamoto, I. Yamaguchi, T. Yasuda, in *Poly(Arylene Etynylene)S: from Synthesis to Application, Vol. 177*, **2005**, pp. 181.

[273] T. Mangel, A. Eberhardt, U. Scherf, U. H. F. Bunz, K. Müllen, *Macromol. Rapid Commun.* **1995**, *16*, 571.

[274] C. Y. Jia, Y. N. Chen, J. Q. Zhang, Z. H. Wang, *Synth. Met.* **2012**, *162*, 54.

[275] CNRS, XPS-Database, *lasurface.com*.

[276] A. Chilkoti, B. D. Ratner, *Chem. Mat.* **1993**, *5*, 786.

[277] E. T. Kang, K. G. Neoh, K. L. Tan, *Phys. Rev. B* **1991**, *44*, 10461.

[278] J. D. Comins, T. P. Nguyen, M. A. Pariselle, S. Lefrant, A. M. T. Allen, *Radiation Effects and Defects in Solids* **1995**, *134*, 437.

[279] J. J. Breen, J. S. Tolman, G. W. Flynn, *Appl. Phys. Lett.* **1993**, *62*, 1074.

[280] M. Yudasaka, K. Hironaga, H. Yamochi, G. Saito, *J. Appl. Phys.* **1991**, *70*, 3501.

[281] W. R. Salaneck, H. R. Thomas, R. W. Bigelow, C. B. Duke, E. W. Plummer, A. J. Heeger, A. G. Macdiarmid, *J. Chem. Phys.* **1980**, *72*, 3674.

[282] J. F. Moulder, W. F. Stickle, P. E. Sobol, K. D. Bomben, *Handbook of X-ray Photoelectron Spectroscopy (Ed.: J. Chastain), Perkin-Elmer Corp. (Physical Electronics), Eden Prairie, MN* **1992**.

[283] Z. Juan, T. M. Swager, in *Poly(Arylene Etynylene)S: from Synthesis to Application, Vol. 177*, **2005**, pp. 151.

[284] G. Voskerician, C. Weder, in *Poly(Arylene Etynylene)S: from Synthesis to Application, Vol. 177*, **2005**, pp. 209.

[285] A. I. Kovalev, N. S. Kushakova, A. V. Shapovalov, M. A. Babushkina, I. A. Khotina, *Russian Chemical Reviews* **2014**, *83*, 1062.

[286] Y. Wang, E. Y. Chi, K. S. Schanze, D. G. Whitten, *Soft Matter* **2012**, *8*, 8547.

[287] K. Sonogashira, Y. Tohda, N. Hagihara, *Tetrahedron Lett.* **1975**, *16*, 4467.

[288] U. H. F. Bunz, in *Poly(Arylene Etynylene)S: from Synthesis to Application, Vol. 177*, Springer-Verlag Berlin, Berlin, **2005**, pp. 1.

[289] Q.-S. Hu, in *Synthetic Methods in Step-Growth Polymers*, John Wiley & Sons, Inc., **2003**, pp. 467.

[290] J. Tolosa, C. Kub, U. H. F. Bunz, *Angew. Chem.-Int. Edit.* **2009**, *48*, 4610.

[291] T. Ratvijitvech, R. Dawson, A. Laybourn, Y. Z. Khimyak, D. J. Adams, A. I. Cooper, *Polymer* **2014**, *55*, 321.

[292] W. G. Lu, W. M. Verdegaal, J. M. Yu, P. B. Balbuena, H. K. Jeong, H. C. Zhou, *Energy Environ. Sci.* **2013**, *6*, 3559.

[293] M. Rubina, M. Conley, V. Gevorgyan, *J. Am. Chem. Soc.* **2006**, *128*, 5818.

[294] V. Gevorgyan, U. Radhakrishnan, A. Takeda, M. Rubina, M. Rubin, Y. Yamamoto, *J. Org. Chem.* **2001**, *66*, 2835.

[295] I. J. S. Fairlamb, P. S. Bauerlein, L. R. Marrison, J. M. Dickinson, *Chem. Commun.* **2003**, 632.

[296] A. K. Dash, M. S. Eisen, *Organic Letters* **2000**, *2*, 737.

[297] P. Sun, H. Yan, L. Lu, D. Liu, G. Rong, J. Mao, *Tetrahedron* **2013**, *69*, 6969.

[298] J. X. Jiang, F. Su, H. Niu, C. D. Wood, N. L. Campbell, Y. Z. Khimyak, A. I. Cooper, *Chem. Commun.* **2008**, 486.

[299] G. Zhang, H. Yi, G. Zhang, Y. Deng, R. Bai, H. Zhang, J. T. Miller, A. J. Kropf, E. E. Bunel, A. Lei, *J. Am. Chem. Soc.* **2014**, *136*, 924.

[300] I. F. Perepichka, D. F. Perepichka, H. Meng, in *Handbook of Thiophene-Based Materials*, John Wiley & Sons, Ltd, **2009**, pp. 695.

[301] M. A. Invernale, M. Acik, G. A. Sotzing, in *Handbook of Thiophene-Based Materials*, John Wiley & Sons, Ltd, **2009**, pp. 757.

[302] G. Barbarella, M. Melucci, in *Handbook of Thiophene-Based Materials*, John Wiley & Sons, Ltd, **2009**, pp. 255.

[303] M. Kertesz, S. Yang, Y. Tian, in *Handbook of Thiophene-Based Materials*, John Wiley & Sons, Ltd, **2009**, pp. 341.

[304] L. Ubaghs, D. Sud, N. R. Branda, in *Handbook of Thiophene-Based Materials*, John Wiley & Sons, Ltd, **2009**, pp. 783.

[305] H.-A. Ho, M. Leclerc, in *Handbook of Thiophene-Based Materials*, John Wiley & Sons, Ltd, **2009**, pp. 813.

[306] G. H. V. Bertrand, V. K. Michaelis, T.-C. Ong, R. G. Griffin, M. Dinca, *Proceedings of the National Academy of Sciences of the United States of America* **2013**, *110*, 4923.

[307] M. Ikai, Y. Maegawa, Y. Goto, T. Tani, S. Inagaki, *Journal of Materials Chemistry A* **2014**, *2*, 11857.

[308] M. Ates, N. Eren, I. Osken, S. Baslilar, T. Ozturk, *Journal of Applied Polymer Science* **2014**, *131*, 40061 (9 pp.).

[309] Q. Chen, M. Luo, P. Hammershoj, D. Zhou, Y. Han, B. W. Laursen, C. G. Yan, B. H. Han, *J. Am. Chem. Soc.* **2012**, *134*, 6084.

[310] M. Iyoda, K. Tanaka, H. Shimizu, M. Hasegawa, T. Nishinaga, T. Nishiuchi, Y. Kunugi, T. Ishida, H. Otani, H. Sato, K. Inukai, K. Tahara, Y. Tobe, *J. Am. Chem. Soc.* **2014**, *136*, 2389.

[311] T. Yamamoto, A. Morita, Y. Miyazaki, T. Maruyama, H. Wakayama, Z. Zhou, Y. Nakamura, T. Kanbara, S. Sasaki, K. Kubota, *Macromolecules* **1992**, *25*, 1214.

[312] E. Poverenov, N. Zamoshchik, A. Patra, Y. Ridelman, M. Bendikov, *J. Am. Chem. Soc.* **2014**, *136*, 5138.

[313] P. Pacher, A. Lex, V. Proschek, H. Etschmaier, E. Tchernychova, M. Sezen, U. Scherf, W. Grogger, G. Trimmel, C. Slugovc, E. Zojer, *Adv. Mater.* **2008**, *20*, 3143.

[314] F. Mohammad, *J. Phys. D-Appl. Phys.* **1998**, *31*, 951.

[315] C. L. Jones, S. J. Higgins, P. A. Christensen, *Journal of Materials Chemistry* **2002**, *12*, 758.

[316] A. Szkurlat, B. Palys, J. Mieczkowski, M. Skompska, *Electrochim. Acta* **2003**, *48*, 3665.

[317] G. G. Min, S. J. Choi, S. B. Kim, S. M. Park, *Synth. Met.* **2009**, *159*, 2108.

[318] I. Osken, E. Sezer, E. Ertas, T. Ozturk, *J. Electroanal. Chem.* **2014**, *726*, 36.

[319] G. Sonmez, C. K. F. Shen, Y. Rubin, F. Wudl, *Angew. Chem.-Int. Edit.* **2004**, *43*, 1498.

[320] M. P. Coleman, M. K. Boyd, *J. Org. Chem.* **2002**, *67*, 7641.

[321] P. Xiao, J. Zhang, F. d. r. Dumur, M. A. Tehfe, F. Morlet-Savary, B. Graff, D. Gigmes, J. P. Fouassier, J. LalevÃ©e, *Prog. Polym. Sci.* **2015**, *41*, 32.

[322] Y. H. Xu, L. Chen, Z. Q. Guo, A. Nagai, D. L. Jiang, *J. Am. Chem. Soc.* **2011**, *133*, 17622.

[323] Z. Dogruyol, N. Arsu, S. K. Dogruyol, O. Pekcan, *Prog. Org. Coat.* **2012**, *74*, 181.

[324] E. Andrzejewska, M. Andrzejewski, *Journal of Polymer Science Part A: Polymer Chemistry* **1998**, *36*, 665.

[325] B. Kiskan, M. Antonietti, J. Weber, *Macromolecules* **2012**, *45*, 1356.

[326] Z. J. Wang, K. Landfester, K. A. I. Zhang, *Polym. Chem.* **2014**, *5*, 3559.

[327] G. Yilmaz, B. Iskin, F. Yilmaz, Y. Yagci, *Acs Macro Letters* **2012**, *1*, 1212.

[328] Y. Bi, D. C. Neckers, *Macromolecules* **1994**, *27*, 3683.